Bioorg. Med. Chem. 47 (2021) 116392

Contents lists available at ScienceDirect

Bioorganic & Medicinal Chemistry

journal homepage: www.elsevier.com/locate/bmc

SAR of novel benzothiazoles targeting an allosteric pocket of DENV and ZIKV NS2B/NS3 proteases

Hannah Maus [a,1], Fabian Barthels [a,1], Stefan Josef Hammerschmidt [a], Katja Kopp [b], Benedikt Millies [a], Andrea Gellert [a], Alessia Ruggieri [b], Tanja Schirmeister [a,*]

[a] Institute of Pharmaceutical and Biomedical Sciences, Johannes Gutenberg-University, Staudingerweg 5, 55128 Mainz, Germany
[b] Department of Infectious Diseases, Molecular Virology, Center for Integrative Infectious Disease Research, University of Heidelberg, Im Neuenheimer Feld 344, 69120 Heidelberg, Germany

ARTICLE INFO

Keywords:
SAR
Flaviviruses
Allosteric inhibition
NS2B/NS3 protease

ABSTRACT

In recent years, dengue virus (DENV) and Zika virus (ZIKV), both mosquito-borne members of the *Flaviviridae* family, have emerged as intercontinental health issues since their vectors have spread from their tropical origins to temperate climate zones due to climate change and increasing globalization. DENV and ZIKV are positive-sense, single-stranded RNA viruses, whose genomes consist of three structural (capsid, membrane precursor, envelope) and seven non-structural (NS) proteins, all of which are initially expressed as a single precursor polyprotein. For virus maturation, the polyprotein processing is accomplished by host proteases and the viral NS2B/NS3 protease complex, whose inhibitors have been shown to be effective antiviral agents with loss of viral pathogenicity. In this work, we elucidate new structure–activity relationships of benzo[*d*]thiazole-based allosteric NS2B/NS3 inhibitors. We developed a new series of Y–shaped inhibitors, which, with its larger hydrophobic contact surface, should bind to previously unaddressed regions of the allosteric NS2B/NS3 binding pocket. By scaffold-hopping, we varied the benzo[*d*]thiazole core and identified benzofuran as a new lead scaffold shifting the selectivity of initially ZIKV-targeting inhibitors to higher activities towards the DENV protease. In addition, we were able to increase the ligand efficiency from 0.27 to 0.41 by subsequent inhibitor truncation and identified *N*-(5,6-dihydroxybenzo[*d*]thiazol-2-yl)-4-iodobenzamide as a novel sub-micromolar NS2B/NS3 inhibitor. Utilizing cell-based assays, we could prove the antiviral activity *in cellulo*. Overall, we report new series of sub-micromolar allosteric DENV and ZIKV inhibitors with good efficacy profile in terms of cytotoxicity and protease inhibition selectivity.

1. Introduction

1.1. The global burden

The mosquito-borne dengue virus (DENV) and Zika virus (ZIKV) are major health concerns in the tropical and sub-tropical regions all over the world, putting about half of the world's population at risk. While DENV is endemic in many countries, leading to 100–400 million infections annually, ZIKV is more commonly known for epidemic outbreaks.[1–3] In 2015, Brazil experienced a ZIKV outbreak with about 200,000 reported cases solely in 2016.[4] Both viruses are transmitted by the mosquitoes *Aedes aegypti* and *Aedes albopictus*. In the last decades, these vectors began to spread considerably in temperate climate zones due to increasing globalization and climate change.[5] The appearance of *Aedes albopictus* on the northern side of the Alps recently raised the awareness of this health issue in middle-European countries.[6,7] The first autochthone DENV infections in Europe were reported in 2010 from south France and Croatia.[8,9] In 2012, the first endemic outbreak on the island of Madeira led to > 2,000 documented cases.[10] Now, several European countries report autochthone infections on an annual basis. 2019, the first autochthone ZIKV infections in Europe were reported from the southern French department of Var. Besides the vectorial transmission route, ZIKV was also found to be contracted via unprotected sexual intercourse.[11] This is of particular interest since its emergence in Southern America was correlated with a striking increase of neurological disorders and microcephaly in neonates.[12] Although ZIKV

* Corresponding author.
E-mail address: schirmei@uni-mainz.de (T. Schirmeister).
[1] Authors contributed equally.

https://doi.org/10.1016/j.bmc.2021.116392
Received 27 May 2021; Received in revised form 3 August 2021; Accepted 30 August 2021
Available online 4 September 2021

infections tend to be asymptomatic or accompanied by self-limiting mild symptoms (fever, rash, conjunctivitis), some patients develop severe neurological conditions such as the Guillain-Barré syndrome.[13–15] Typical DENV infections show the very unpleasant symptoms of dengue fever. It is characterized by high fever and flu-like symptoms that are usually self-limiting. Some patients, however, develop severe dengue syndrome. Respiratory distress, fluid accumulation, plasma leaking, severe bleedings, and organ impairments can lead to a potentially fatal outcome. Although there is a vaccination against DENV available, the antibody-dependent enhancement of recurring DENV infections increases the risk for severe courses if a vaccinated patient gets infected by another DENV serotype. Hence, the approval of this vaccination is limited to people who have already recovered from dengue infection.[16–18] To date, there is no approved causative treatment for patients, suffering DENV or ZIKV infections, making it inevitable to pursue further research on small molecule drugs against these diseases.[19]

1.2. Functions of NS2B/NS3 in viral replication

Amongst others, the five serotypes of dengue virus (DENV1–5) and ZIKV belong to the family of *Flaviviridae*, genus flavivirus.[20,21] Their whole genome is a single-stranded (+)-sense RNA, which is translated into a single precursor polyprotein, consisting of the structural proteins capsid, membrane, and envelope, that are components of the virion, and the seven non-structural (NS) proteins involved in viral replication and maturation. The functional proteins are released after processing by the host proteases furin and signalase as well as the viral NS2B/NS3 protease.[22–26] On top of this essential role, the NS2B/NS3 protease was also found to modulate the human immune system by cleaving the stimulator of interferon genes (STING).[27] Based on these functions, the NS2B/NS3 protease is considered a promising target for developing specific anti-flaviviral therapeutics.[28–31]

1.3. Structure of NS2B/NS3

The NS3 protein consists of two domains. The *N*-terminal serine protease domain ($NS3_{pro}$) and the *C*-terminal helicase ($NS3_{hel}$). For its proteolytic activity, $NS3_{pro}$ requires NS2B as its cofactor which is composed of a transmembrane region, anchoring the protease to the endoplasmic reticulum, and its *C*-terminal cofactor region ($NS2B_{cf}$), essential for proper folding of the $NS3_{pro}$ catalytic domain.[32,33] Crystallography of the flaviviral $NS2B_{cf}$-$NS3_{pro}$ revealed the existence of at least two distinct conformations.[28,34,35] The catalytically active conformation is known as the *closed* conformation with $NS2B_{cf}$ wrapped around the protease domain forming a β-turn with its *C*-terminus contributing to the formation of the S2- and S3-binding pockets.[35,36] Besides that, an inactive *open* conformation was identified, in which $NS2B_{cf}$ is loosely bound to $NS3_{pro}$.[35] In solution, an equilibrium between these conformations could be observed, whereas an increased proportion of the closed conformation was achieved by the addition of substrate or active site-directed inhibitors via conformational selection or induced fit mechanisms.[28,33,86] An allosteric binding pocket around Ala125 was first identified with surface cysteine mutagenesis and cysteine reactive probes.[37] It was proposed, that binding to this site may rearrange the 120 s loop, thus locking the protein in its open conformation.[38]

1.4. Obstacles in inhibitor development

To achieve protease inhibition, developing substrate analogous inhibitors is a reasonable approach.[39,40] In the case of the flaviviral NS2B/NS3 protease, however, such inhibitors may feature poor pharmacological properties due to the substrate preferences for dibasic residues in *P*1 and *P*2 amino acids (AA). Inhibitor development is also hindered by the shallow and charged nature of the active site. Therefore, it is comprehensible that, although some substrate competitive inhibitors display high-affinity binding properties, their efficacy in cell-based assays stayed far behind expectations due to poor membrane permeability.[34,41,42] Some recent research efforts, however, did overcome these issues.[30,43,44]

In our group, we focused on inhibitor design by addressing the allosteric site. Previous docking studies of our inhibitors suggested the allosteric binding site to be located close to Asn152. Since Asn152 was found to be addressable from both the active and the allosteric site, this residue was referred to as a "molecular switch" between the open and closed conformation.[37,45] The allosteric binding mode of our inhibitors was perfectly demonstrated by their non-competitive behavior as well as by single cysteine mutagenesis studies.[37,46]

Based on these previously reported inhibitors including the lead structures **1a,b**, **2**, and **3a,b** (Figure 1), we synthesized and tested new series of inhibitors to explore further structure–activity relationships (SAR).[37] A second objective was to optimize the inhibitors in terms of their ligand efficacy (LE), generating an improved starting point for following drug development.

2. Results and discussion

The individual moieties of the lead structures **1a,b**, **2**, and **3a,b**, namely AA linker, sulfonamide/amide connector, and heteroaromatic system, were systematically varied to investigate SAR.

Since the exchange of the (*R/S*)-proline moiety in **1a,b** to pipecolic acid in **3a,b** led to an improved inhibition of the NS2B/NS3 protease, further AA exchanges were explored in this work. Previously, the exchange of the sulfonamide moiety in **1a** to an amide linker in compound **2** resulted in modest changes of inhibitory potency so that both linking groups were used here depending on the synthetic context. A second approach was based on docking and molecular dynamics studies of the enantiomers **1a** and **1b** which are predicted to bind with their tosyl moieties in opposing subsites (Figure 2). Consequently, Y-shaped inhibitors were designed to combine both binding modes into one molecule. A third series of compounds was designed to increase the ligand efficacy by truncating previous full-scale inhibitors to a smaller scaffold consisting of only the 5,6-dihydroxybenzo[*d*]thiazole fragment, which was previously identified as the important pharmacophore, attached to different aromatic residues. Last, a scaffold hopping strategy was evaluated, for which the benzo[*d*]thiazole itself was exchanged to different (hetero)aromatic structures.

2.1. Chemistry

For the first SAR strategy, inhibitors based on different AA were synthesized according to a previously published route.[37] 2-Amino-5,6-dimethoxybenzo[*d*]thiazole **5** was coupled with different Boc-protected AA **4a–f** mediated by 2-(1*H*-benzotriazole-1-yl)-1,1,3,3-tetramethylaminium tetrafluoroborate (TBTU), followed by BBr_3-deprotection of the Boc- and methoxy-groups to yield the corresponding hydrobromide salts **7a–f**. The sulfonamides **8a–f** were obtained by reaction of the deprotected amines with *p*-tosyl chloride (Scheme 1**A**).

For synthetic stability reasons, the tyrosine derivative **12a**, the aspartic acid derivative **12b** (Scheme 1**B**), and the β-alanine derivative **17** (Scheme 1**C**) were synthesized with an amide linker instead of a sulfonamide linking group. As shown in previous work, the exchange between sulfonamides and amides in these structures did not significantly influence the IC_{50} values of the inhibitors.[37] For compounds **12a, b**, the Boc- and benzyl-protected AA were reacted with **5** to form the precursor amides **9a,b**. The Boc group was removed with HCl in dioxane to give **10a,b**, followed by benzoylation to yield the dimethoxy derivates **11a,b**. Deprotection with BBr_3 gave the final compound **12a**. For the deprotection of **11b**, BBr_3-deprotection led to unwanted side reactions, hence, $EtSH/AlCl_3$ was used instead for deprotection of the methoxy and benzyl groups to obtain **12b**. The β-alanine derivative **17** was obtained

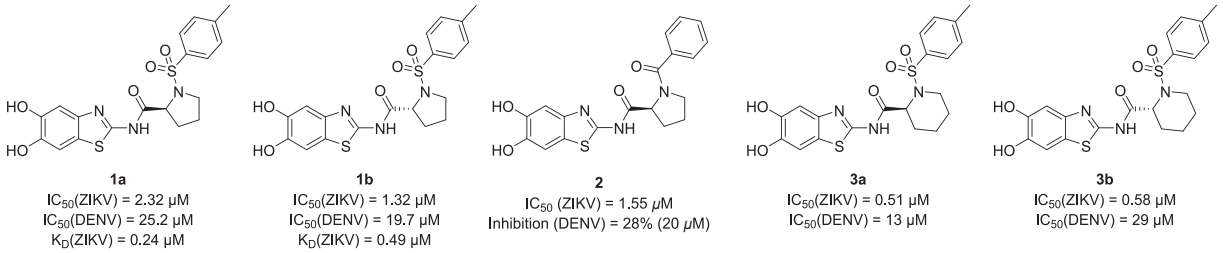

Fig. 1. Structures of previously reported benzo[*d*]thiazole-based inhibitors **1a,b**, **2** and **3a,b**.[37]

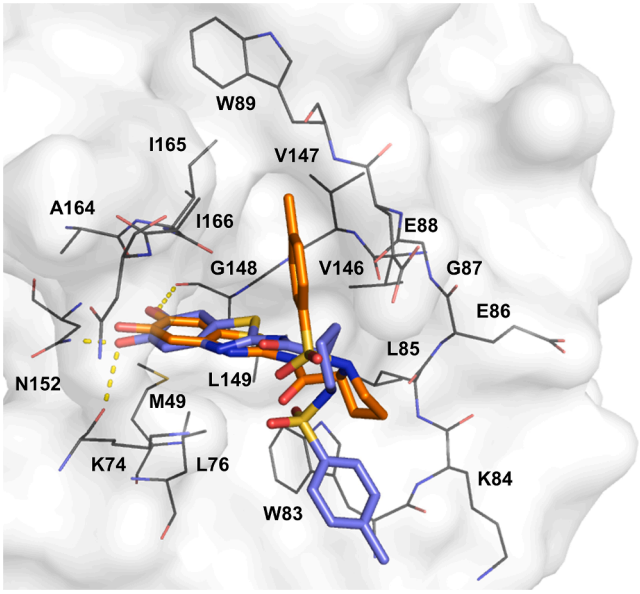

Fig. 2. Predicted binding modes of the previously investigated enantiomeric proline derivates **1a** (orange) and **1b** (purple) in the DENV2 allosteric binding site (pdb: 2FOM).[35,37] The catechol fragment shows conserved interactions with Lys74, Gly148, and Asn152 for both (*R*)- and (*S*)-enantiomers, while the aromatic *para*-tosyl moieties interact with distinct hydrophobic subsites. The design of inhibitors with an enlarged interaction surface targeting both subsites may lead to the generation of more potent inhibitors. (For interpretation of the references to colour in this figure legend, the reader is referred to the web version of this article.)

by TBTU-mediated coupling of **5** to Boc-protected *β*-alanine. After Boc-deprotection by HCl in dioxane and benzoylation, the dimethoxy derivative **16** was obtained. Subsequently, BBr_3-deprotection gave the final product **17** (Scheme 1**C**).

Initial Y-shaped inhibitors designed to bind to the two subsites addressed by **1a** and **1b** were synthesized based on the aspartic acid compound **12b**. Hence, asparagine-derivates **20a,b** were synthesized starting from **11b** by hydrolysis of the benzyl ester to yield the carboxylic acid **18**. Coupling to *N,N*-diethyl amine and aniline led to the dimethoxy precursors **19a,b**, followed by deprotection to yield the final compounds **20a,b** (Scheme 2**A**). Furthermore, Y–shaped inhibitors **23a–d** were obtained by the synthesis of different carboxylic acids **21a–d**.[47–49] Subsequent coupling with **5** and deprotection with BBr_3 yielded the final compounds **23a–d** (Scheme 2**B**).

To increase the ligand efficiency of parent compounds **1a,b**, truncated inhibitors, consisting of only a benzo[*d*]thiazole fragment and substituted benzoic acids, were synthesized. By amide coupling between the benzo[*d*]thiazoles **5** or **26** and the corresponding benzoic acids with TBTU or the respective benzoyl chlorides, the dimethoxy derivates **24a–f** were obtained (Scheme 3**A**). The 6-nitrobenzo[*d*]thiazole derivates **27** and **28** were synthesized accordingly (Scheme 3**B**). Methoxy derivatives **24a–f** were deprotected by BBr_3, to obtain the final compounds **25a–f** with free hydroxy groups (Scheme 3**A**).

In order to vary and optimize the benzo[*d*]thiazole core fragment, a scaffold hopping strategy was evaluated for the synthesis of different heterocyclic systems. Since various heteroaromatics were synthetically more accessible as carboxylic acid derivatives than as amines, the amide bond was inverted compared to the previously described compounds. The corresponding (hetero)aromatic carboxylic acids **32a–m** were synthesized according to literature procedures.[50–59] In this way, a variety of different amides **33a–k** and **35a–n** could be synthesized by TBTU-mediated coupling of the (hetero)aromatic carboxylic acids with either aniline, *p*-iodoaniline (Scheme 4**B**), prolyl anilide **31a** or pipecolyl anilide **31b** (Scheme 4**C**). The latter were synthesized from Boc-protected proline or pipecolic acid **29a,b**, and aniline via condensation catalyzed by triethylamine and ethyl chloroformate (Scheme 4**A**).[60] Subsequent deprotection of the dimethoxy compounds **33a–k** and **35a–n** by BBr_3 yielded the catechols **34a–k** and **36a–n** (Scheme 4**B,C**). Inhibitor **34l** was obtained by reducing the nitro group of compound **34j** using tin chloride.

2.2. Structure–activity relationships

To evaluate the inhibition potency of all final compounds, these were evaluated by means of fluorometric enzyme assays with recombinantly expressed DENV and ZIKV NS2B/NS3 protease and Boc-Gly-Arg-Arg-AMC as substrate.[61,62] Starting from parent compounds **1a,b**, **2**, and **3a,b**, which previously showed sub-micromolar IC_{50} values on the ZIKV protease, inhibitors containing a variety of AA were synthesized and tested for inhibition against DENV2 and ZIKV NS2B/NS3 proteases (Table 1).

The most potent amino acid-based inhibitors were found to have IC_{50} values in the low micromolar range, however, none of the inhibitors showed improved inhibition compared to the previously published parent compounds. Inhibition selectivity towards the ZIKV protease was consistent for all tested inhibitors **8a–17**, as they caused a maximum of 63% inhibition at an inhibitor concentration of 20 μM for the homologous DENV2 protease. A significant SAR was observed for the alanine derivatives **8a,b**. The (*S*)-derivative **8a** showed inhibition in the low micromolar range (6.48 μM), while the (*R*)-enantiomer **8b** inhibited ZIKV protease only to 26% at 20 μM. The other compounds of this series, which were based on hydrophobic (*S*)-AA (isoleucine **8c**, *tert*-leucine **8d**, and phenylalanine **8e**), showed similar IC_{50} values ranging from 3.66 to 5.74 μM. Compound **8f** that was based on an *S*-benzyl-modified cysteine residue, displayed the lowest IC_{50} of this compound series (2.13 μM). Moderate polar decoration, like the introduction of a hydroxyl group, yielded the tyrosine-based inhibitor **12a** and did not significantly change inhibition potency compared to the phenylalanine-based derivate **8e** (4.59 μM).

However, this trend was reversed for more polar substituents. The aspartic acid-based inhibitor **12b** showed only 45% inhibition of the ZIKV protease at 20 μM. Therefore, we concluded that the allosteric binding pocket may tolerate hydrophobic residues of different sizes, but anionic substituents potentially abolish the inhibition due to non-beneficial interactions with the pocket-determining non-polar (Trp83, Leu85, V147) and acidic residues (Glu86, Glu88). Lengthening of the AA

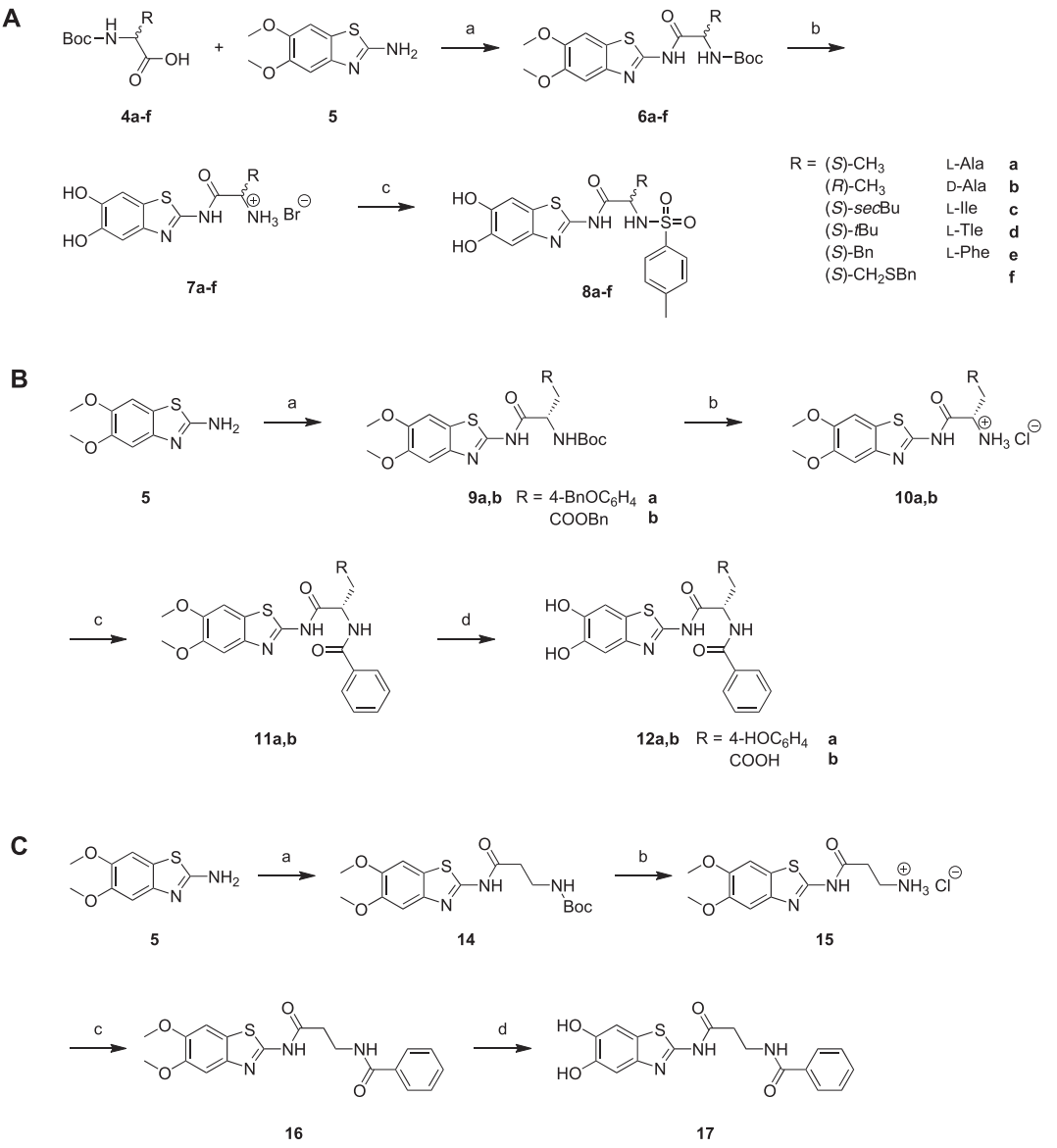

Scheme 1. Synthesis of the AA-based compounds **8a–f**, **12a,b**, and **17**. (**A**) Synthesis of sulfonamides **8a–f**. Reagents and conditions: a) TBTU, HOBt, DIPEA, DMF, 2 d, 34–82%. b) BBr_3, DCM, –78 °C to r.t., 16 h, 66–99%. c) *p*-TsCl, pyridine, 16 h, 32–70%. (**B**) Synthesis of the tyrosine- (**12a**) and aspartate-based inhibitor **12b**. Reagents and conditions: a) TBTU, HOBt, DIPEA, DMF, 2 d, 95–97%. b) HCl, dioxane, r.t., 30 min, 87–95%. c) PhCOCl, NEt_3, DCM, 16 h, 71–76%. d) BBr_3, DCM, –78 °C to r.t., 16 h, 77% or $AlCl_3$, EtSH, DCM, 0 °C to r.t., 16 h, 87%. (**C**) Synthesis of the *β*-alanine derivative **17**. Reagents and conditions: a) Boc-*β*-Ala-OH, TBTU, HOBt, DIPEA, DMF, 3 d, 78%. b) HCl, dioxane, r.t., 30 min, 70%. c) PhCOCl, NEt_3, DCM, 16 h, 40%. d) BBr_3, DCM, –78 °C to r.t., 16 h, 87%.

linker by one methylene unit from (*S*)-alanine **8a** to *β*-alanine **17** resulted in a strong decrease of inhibition, demonstrating the importance of the distance between the benzo[*d*]thiazole unit and the aromatic group for binding into the allosteric binding pocket.

To increase the affinity of the benzo[*d*]thiazole inhibitors, a second strategy was applied to optimize the hydrophobic interaction surface of the inhibitor while maintaining the core benzo[*d*]thiazole pharmacophore. Previous docking and molecular dynamics studies of **1a** and **1b** proposed that *p*-tosyl moieties bind to opposing subsites corresponding to the orientation of the proline stereoisomers (Figure 2). Thus, Y-shaped inhibitors were designed to address both subsites and to increase the overall inhibition potency.[37] Due to the observation that mainly hydrophobic AA lead to potent inhibition, we decided to functionalize the aspartic acid-based inhibitor **12b** at the carboxyl group by hydrophobic substituents. In addition to the resulting asparagine-based inhibitors (**20a,b**), diphenyl-derived Y-shaped compounds (**23a–d**) were also designed and evaluated for their inhibition (Table 2).

The asparagine-based inhibitor **20a**, which includes an *N,N*-diethyl amide substitution, showed very low inhibition at 20 μM (13%). On the other hand, the corresponding aniline substituted derivate **20b** showed a significantly improved IC_{50} value of 5.48 μM for the ZIKV protease and 9.95 μM for the DENV2 protease. From these results, the hydrophobic yet structurally circumscribed binding region of the allosteric binding pocket becomes apparent. Increasing the inhibition strength seems to depend on the hydrophobic contact area as well as on the relative orientation of the Y-shape arms, and thus, should be an optimizable parameter.

Aromatic structures appear to be favored in this process, hence, four additional structures **23a–d** with diphenyl-derived Y-shapes were investigated. Inhibitor **23a**, incorporating a rigid *N*-phenyl peptoid-structure, led to a slight decrease of affinity (2.07 μM) compared to the proline amide derivative **2** (1.55 μM). The 2,2-diphenylacetic acid derivate **23b** showed the lowest IC_{50} value of this series (0.95 μM), albeit with no increased inhibition for the DENV2 protease (11.12 μM).

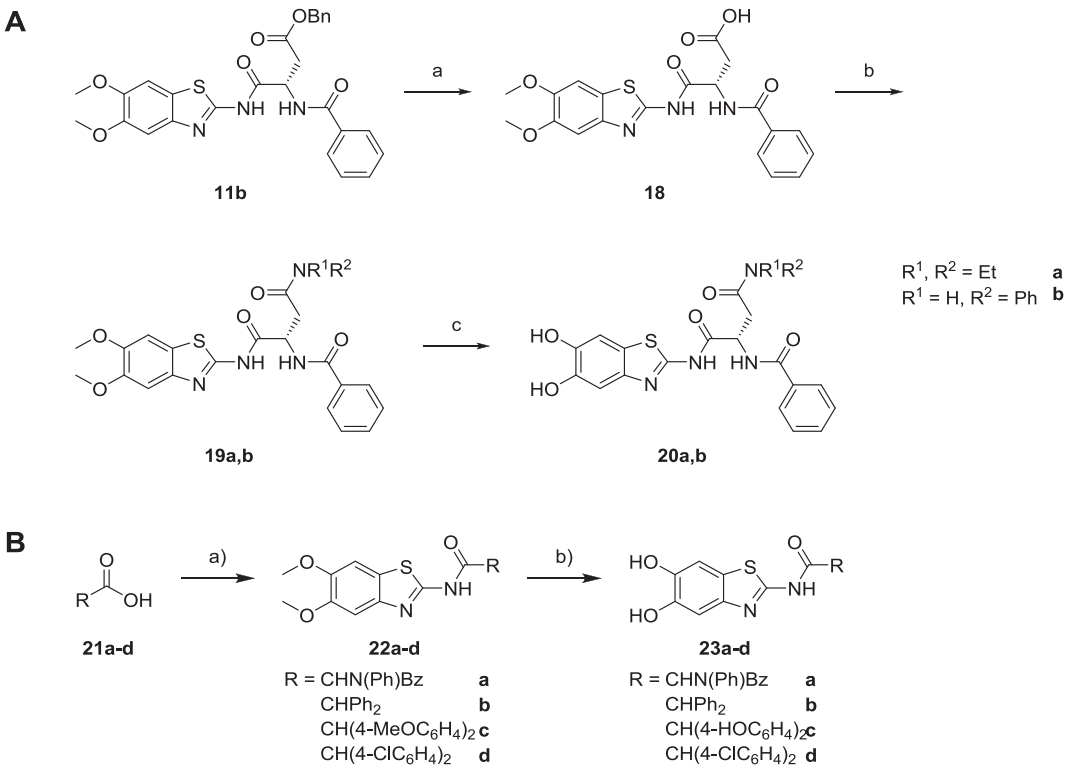

Scheme 2. Synthesis of Y-shaped inhibitors. (**A**) Synthesis of asparagine-based Y-shaped inhibitors **20a,b**. Reagents and conditions: a) LiOH, THF, H_2O, 1 h, 98%. b) TBTU, HOBt, DIPEA, DMF, 2 d, 35–65%. c) BBr_3, DCM, –78 °C to r.t., 16 h, 44–85%. (**B**) Synthesis of Y-shaped inhibitors **23a–d**. Reagents and conditions: a) **5**, TBTU, HOBt, DIPEA, DMF, 2 d, 29–68%. b) BBr_3, DCM, –78 °C to r.t., 16 h, 50–85%.

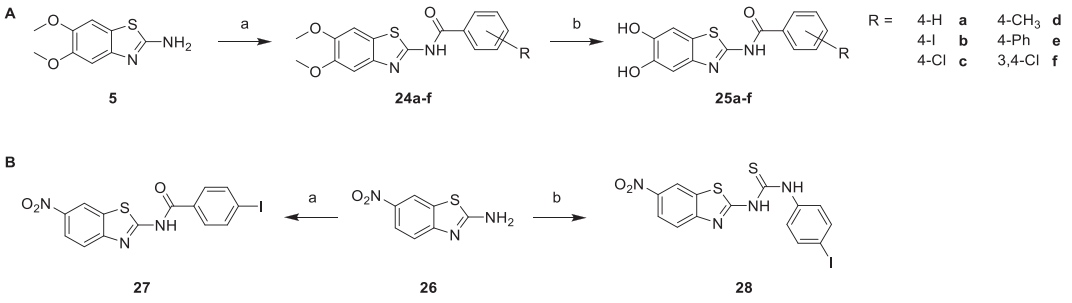

Scheme 3. Synthesis of truncated inhibitors. (**A**) Synthesis of catechol derivatives **25a–f**. Reagents and conditions: a) R-PhCOOH, TBTU, HOBt, DIPEA, DMF, 2 d, 24–99% or PhCOCl, NEt_3, DCM, 16 h, 72%. b) BBr_3, DCM, –78 °C to r.t., 16 h, 29–99%. (**B**) Synthesis of the 6-nitrobenzo[*d*]thiazole derivative **27** and **28**. Reagents and conditions: a) 4-iodobenzoic acid, TBTU, DMF, 2 d, 74%. b) 4-iodophenyl isothiocyanate, DBU, DCM, r.t., 7 d, 68%.

However, the improvement in inhibitory strength is not yet optimal related to the increase in molecular weight, as the ligand efficiency between parent compound **1a** and Y-shape inhibitors changed only marginally from 0.27 to 0.21–0.31 (**23a–d**). To improve the inhibition potency, the hypothesis was pursued to rationally address the polar residues Glu86/Glu88 of the allosteric binding pocket. For this purpose, similar to tyrosine derivative **12a**, two hydroxyl groups were introduced as *para*-decoration substituents. However, the resulting tetrahydroxy derivate **23c** led to a significant decrease in inhibitory potency (54%). Calculation of the protonation state revealed that one of the two additional hydroxyl groups forms a negatively charged phenolate under assay conditions, possibly leading to repulsion of Glu86/Glu88 and low inhibition as for aspartic acid derivative **12b**. In contrast, the dichloro derivative **23d** did not show increased activity compared with the undecorated analog **23b**, so we suggest that 2,2-diphenylacetic acid derivatives cannot be further improved by substitution. With the derivatives **20b** and **23a,b** we were able to show that the Y-shape strategy is successful and is a promising idea in future structure-based inhibitor designs.

To increase the ligand efficiency at the same or smaller molecular size, the synthesis and evaluation of truncated inhibitors was performed as a third SAR strategy. In this series, truncated inhibitors consisting only of a benzo[*d*]thiazole scaffold and a substituted benzoic acid were evaluated for their inhibition potency (Table 3). Root compound **25a** *N*-(5,6-dihydroxybenzo[*d*]thiazol-2-yl) benzamide showed an IC_{50} of 9.19 μM for the ZIKV protease and 26.95 μM for the DENV protease. Thus, the starting point of this SAR series was an inhibitor about 2–3 times weaker than the parent compounds **1a,b**. Subsequentially, the *para*-substituent of the benzamide was varied to modulate the structure.

Exemplary, the introduction of a halogen atom in the *para*-position, was accompanied by an improved IC_{50} for DENV2 protease as demonstrated for iodine **25b** (4.38 μM) or chlorine substituents **25c** (5.97 μM). Other derivates bearing a *para*-methyl group (**25d**), a *para*-phenyl substituent (**25e**), or two chlorine atoms in *meta* and *para* positions (**25f**), inhibited the DENV2 protease, with IC_{50} value of 4.86–7.80 μM, in the similar range. For ZIKV, however, the iodine derivate **25b** displayed a

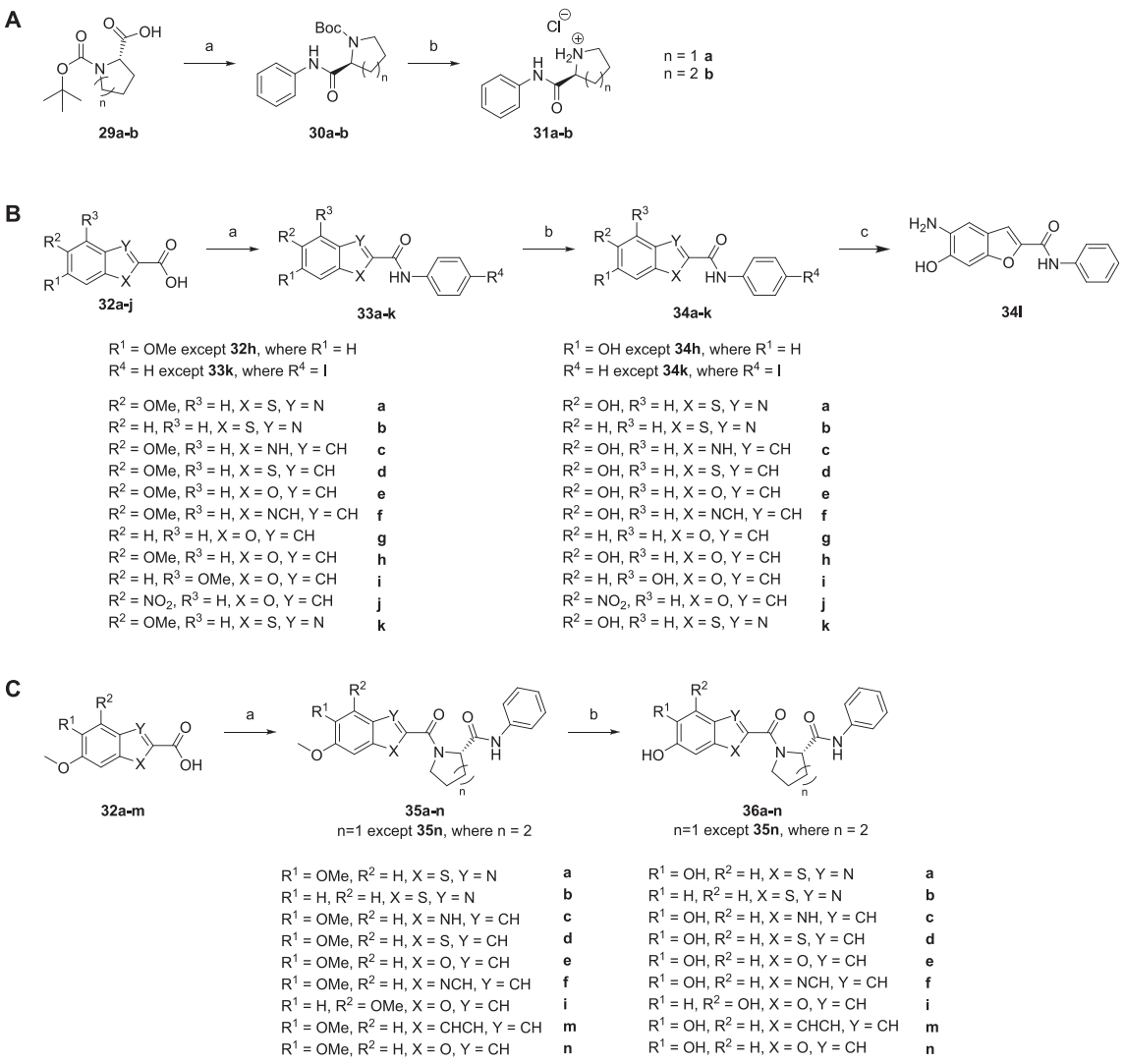

Scheme 4. Synthesis of inhibitors with different (hetero)aromatic moieties. (**A**) Reagents and conditions: a) aniline, ethyl chloroformate, triethylamine, THF, 0 °C to 70 °C, 20 h, 89–90%. b) HCl in dioxane, r.t., 15 h, quantitative. (**B**) Reagents and conditions: a) aniline, TBTU, HOBt, DIPEA, EtOAc, 0 °C to r.t., 3 d, 66%–quantitative. b) BBr_3, DCM, –78 °C to r.t., 16 h, 20%–quantitative. c) $SnCl_2$, HCl, r.t. to 70 °C, 16 h, 56%. (**C**) Reagents and conditions: a) **31a** or **31b**, TBTU, HOBt, DIPEA, EtOAc, 0 °C to r.t., 3 d, 55%–quantitative. b) BBr_3, DCM, –78 °C to r.t., 16 h, 13–96%.

Table 1
Inhibition of the DENV2 and ZIKV NS2B/NS3 proteases by amino acid-based inhibitors.[a]

Compound	Included AA	ZIKV	DENV2
		IC_{50} [μM]/%	IC_{50} [μM]/%
8a	(*S*)-Ala	6.48 ± 1.41	39%
8b	(*R*)-Ala	26%	14%
8c	(*S*)-Ile	5.35 ± 0.33	33%
8d	(*S*)-*tert*-Leu	5.74 ± 0.79	44%
8e	(*S*)-Phe	3.66 ± 0.49	33%
8f	(*S*)-Cys(SBn)	2.13 ± 0.11	57%
12a	(*S*)-Tyr	4.59 ± 0.50	63%
12b	(*S*)-Asp	45%	32%
17	β-Ala	38%	23%

[a] IC_{50} values are indicated by mean ± standard deviation from at least three independent measurements. Percentage inhibition was determined at 20 μM inhibitor concentration.

significantly higher potency (0.67 μM) than the unsubstituted derivate **25a** (9.19 μM) which makes **25b** the best inhibitor of this series. Exemplarily, the substrate conversion plot in the presence of inhibitor **25b** is showing sub-micromolar inhibition (Figure 3).

For the other substituted benzamides, no clear structural trend was recognized for ZIKV protease inhibition. Wherein the *para*-chlorine (**25c**, 6.66 μM) and *para*-phenyl (**25e**, 1.22 μM) derivatives showed improved inhibition, the inhibition was decreased for the *para*-methyl (**25d**, 15.40 μM) and the 3,4-dichloro derivative (**25f**, 39%) compared to the root compound **25a**. To follow up the best inhibitor **25b**, two additional *para*-iodine substituted inhibitors were synthesized. Derivate **27** harbors a nitro-benzothiazole fragment instead of the catechol-benzo[*d*]thiazole motif. **27** inhibits both proteases at lower potencies (49% for ZIKV and 36% for DENV2). Compared to compound **27**, compound **28** incorporates a thiourea linker instead of an amide linker. The replacement of the linker is accompanied by a significant increase in inhibition (IC_{50} = 6.51 μM for ZIKV and 11.21 μM for DENV2).

In summary, by shortening the inhibitor scaffold, the ligand efficacy of the compounds was increased from 0.27 resp. 0.28 for the parent compounds **1a,b** to 0.41 for the iodine-substituted inhibitor **25b**. In contrast, the ligand efficacy for the best Y-shape inhibitor **23b** could be increased to only 0.31, illustrating that optimizing the root scaffold is more effective than increasing the hydrophobic contact area of the inhibitor.

As the fourth SAR optimization strategy, the core benzo[*d*]thiazole

Table 2
Inhibition of the DENV2 and ZIKV NS2B/NS3 proteases by inhibitors with a Y-shaped structure.[a]

Compound	Structure	ZIKV IC_{50} [μM]/%	DENV2 IC_{50} [μM]/%
20a	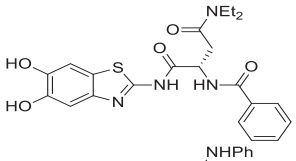	13%	16%
20b	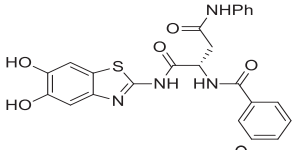	5.48 ± 0.35	9.95 ± 0.34
23a	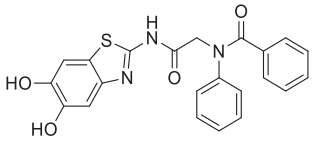	2.07 ± 0.16	56%
23b	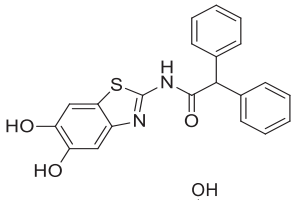	0.95 ± 0.13	11.12 ± 0.49
23c	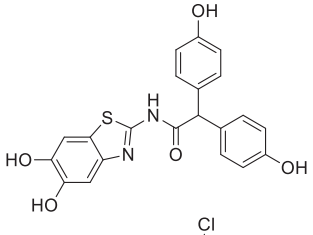	54%	45%
23d	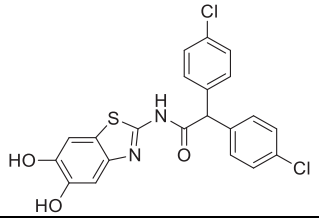	0.96 ± 0.12	58%

[a] IC_{50} values are indicated by mean ± standard deviation from at least three independent measurements. Percentage inhibition was determined at 20 μM inhibitor concentration.

itself was varied by scaffold hopping alterations, leading to a variety of inhibitors with (hetero)cyclic structures that were evaluated for their inhibition towards the NS2B/NS3 proteases (Table 4). Since various heteroaromatics were synthetically more accessible as carboxylic acid derivatives than as amines, the amide bond was inverted compared to the previously described compounds. Therefore, an amide-inverted prototype scaffold **36a**, analogously to parent compound **2**, was first synthesized and tested. This root compound **36a**, based on a benzo[*d*]thiazole, showed a similar IC_{50} value (4.00 μM) on the ZIKV protease compared to the inhibitor with inverted amide bonds **2** (1.55 μM, Figure 1). Furthermore, the inhibition of DENV2 protease could even be significantly increased by the inversion of the amide bond (**36a** IC_{50} = 11.59 μM, **2** 28% at 20 μM).

Subsequently, two series of heteroaromatic scaffold hops were evaluated: 1) those (**36a–n**) containing a proline linker and derived from parent compound **2** and 2) those (**34a–l**) derived from the truncated benzamide derivatives **25a** and lacking a proline linker. An overview of all derivatives can be found in Table 4 and Scheme 4.

Table 3
Inhibition of the DENV2 and ZIKV NS2B/NS3 proteases by differently substituted truncated inhibitors.[a]

Compound	Structure	ZIKV IC_{50} [μM]/%	DENV2 IC_{50} [μM]/%
25a	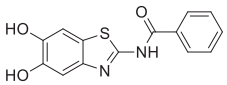	9.19 ± 0.33	26.95 ± 1.61
25b	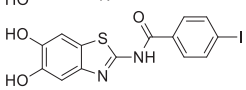	0.67 ± 0.32	4.38 ± 0.38
25c	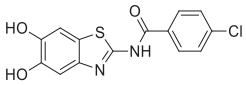	6.66 ± 0.41	5.97 ± 0.50
25d	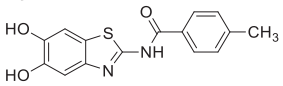	15.40 ± 4.70	6.39 ± 0.20
25e	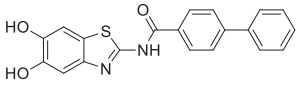	1.22 ± 0.13	7.80 ± 0.89
25f	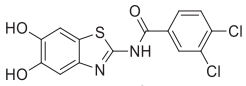	39%	4.86 ± 0.33
27	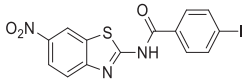	49%	36%
28	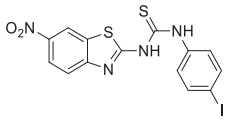	6.51 ± 0.44	11.21 ± 0.87

[a] IC_{50} values are indicated by mean ± standard deviation from at least three independent measurements. Percentage inhibition was determined at 20 μM inhibitor concentration.

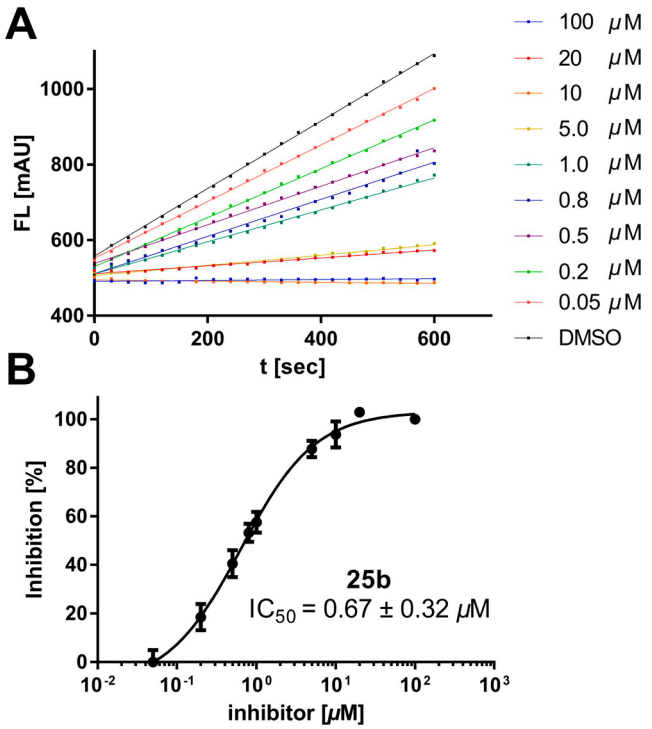

Fig. 3. (**A**) Fluorometric assay with top inhibitor **25b** showing enzyme inhibition from linear substrate conversion plots. (**B**) Determination of IC_{50} values [μM] for compound **25b** by regression to the four-parameter Hill equation.

Table 4
Inhibition of the DENV2 and ZIKV NS2B/NS3 proteases by inhibitors with different (hetero)aromatic scaffolds.[a]

Compound	Heterocycle—C(=O)—Linker—NHPh: (Hetero)cycle	Linker	ZIKV IC_{50} [μM]/%	DENV2 IC_{50} [μM]/%
36a	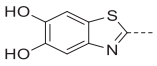	(*S*)-proline	4.00 ± 0.34	11.59 ± 0.90
34a		none	9.19 ± 0.33	26.95 ± 1.60
36b	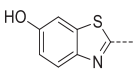	(*S*)-proline	19% at 20 μM	47% at 20 μM
34b		none	25% at 20 μM	20% at 20 μM
36c	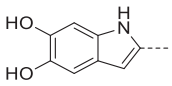	(*S*)-proline	44% at 20 μM	36% at 20 μM
34c		none	3.44 ± 1.21	6.90 ± 2.30
36d	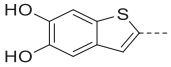	(*S*)-proline	3.43 ± 0.14	4.01 ± 0.47
34d		none	1.59 ± 0.08	2.73 ± 0.90
36e	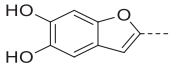	(*S*)-proline	2.43 ± 0.28	6.43 ± 0.76
34e		none	1.04 ± 0.26	0.69 ± 0.16
36n		(*S*)-pipecolic acid	2.90 ± 0.04	4.73 ± 0.28
36f	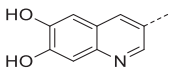	(*S*)-proline	44% at 20 μM	23% at 20 μM
34f		none	6.38 ± 0.50	3.63 ± 0.21
36m	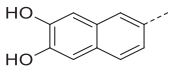	(*S*)-proline	42% at 20 μM	9% at 20 μM
34g	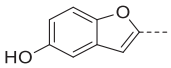	none	n. i.	n. i.
34h	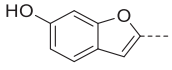	none	n. i.	n. i.
36i	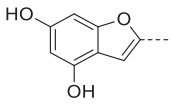	(*S*)-proline	20.13 ± 3.48	27.69 ± 2.82
34i		none	62% at 100 μM	51% at 100 μM
34j	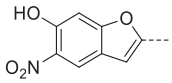	none	48% at 200 μM	19% at 200 μM
34k	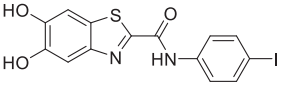		1.30 ± 0.08	2.48 ± 0.16
34l	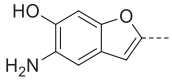	none	52% at 200 μM	34% at 200 μM

[a] IC_{50} values are indicated by mean ± standard deviation from at least three independent measurements. Percentage inhibition was determined at 20 μM, 100 μM, 200 μM inhibitor concentration. n. i.: no inhibition at an inhibitor concentration of 200 μM

Truncated benzo[*d*]thiazole derivate **34a** (without proline linker) exhibited comparable activities compared to the inverted-amide derivate **25a**, thus, it was proven for both **36a** and **34a** that the orientation of the amide bonds does not influence the NS2B/NS3 inhibition. In the series of heterocycles containing only one heteroatom **34c–f** and **36c–f**, the benzofuran derivate **34e** showed with IC_{50} values of 0.69 μM for DENV2 and 1.04 μM for ZIKV the best inhibition profile of the whole series. Remarkably, the benzofuran derivative **34e** showed an abrogation of the previously observed inhibition selectivity, which was manifested by the fact that benzo[*d*]thiazole inhibitors inhibited ZIKV protease by a factor of 2–10 better than the DENV2 protease.

Besides this observation, the benzo[*d*]thiazole and benzofuran derivates **34b**, **36b**, **34g**, and **34h** contained only one single 5′- or 6′-hydroxyl group, and consequently, these derivates displayed reduced inhibition compared to their corresponding catechol analogs **34a**, **36a**, and **34e**. This confirms the previously shown trend that both hydroxyl groups are necessary for effective inhibition potency.[46] For benzofurans **34i** and **36i**, the hydroxyl groups were arranged in *meta*-positions instead of the conserved *ortho*-configuration (**34e** and **36e**) resulting in loss of inhibition potency with IC_{50} values for **36i** of 20.13 μM for ZIKV and 27.69 μM for DENV2. For the other modifications, the exchange of a hydroxyl group for nitro or amine substituents also resulted in a partial loss of inhibitory activity as can be seen for compounds **34j** and **34l**. Quinoline **36f** as a core scaffold led to significantly decreased inhibition, as well as the naphthalene derivative **36m**. Based on these results, it can be hypothesized that one heteroatom is necessary for the core scaffold and that scaffolds containing five-membered rings are superior to scaffolds with six-membered rings such as quinolines or naphthalenes. Similar to the transformation from **1** to **3**, the replacement of (*S*)-proline by pipecolic acid resulted in a slight improvement of the DENV2 IC_{50} values of proline derivate **36e** (6.43 μM) compared to pipecolyl derivate **36n** (4.73 μM). In analogy to the improvement of inhibition of the DENV2 protease upon the inversion of the amide bond (**25a** (26.95 μM) vs. **34a** (11.59 μM)), amide inversion of the iodinated top inhibitor **25b** (4.38 μM) also resulted in an improvement of DENV2 inhibition (**34k**, 2.48 μM). In summary, besides the original benzo[*d*]thiazole scaffold, benzo[*b*]thiophenes (**34d** and **36d**) and benzofurans (**34e** and **36e**) were identified as promising scaffolds for the synthesis of allosteric DENV2 and ZIKV inhibitors.

To validate our hypothesis of allosteric inhibition, IC_{50} values were determined for the top inhibitor **25b** at various substrate concentrations (50–200 μM). Evaluation by Dixon plot analysis revealed that the inhibition is not substrate competitive, supporting our hypothesis of an allosteric binding (**SI** Figure 5**A**). The apparent K_i was determined to be 7.67 μM and thus lies in the same range as the determined IC_{50} for **25b**. In a previous work, we showed by single-site cysteine mutagenesis and subsequent maleimide blockage that the lead structure **1b** binds into an allosteric binding pocket.[37] Here, we have also applied this assay to the top inhibitors of this work (**23b**, **25b**, and **34e**). Thus, the IC_{50} values of compounds **23b**, **25b**, and **34e** were compared for the DENV2 wild-type protease, the T122C mutant protease, and the T122C mutant protease after incubation with *N*-benzylmaleimide (BMI, 250 nM). For all three inhibitors, significantly higher IC_{50} values were measured for the BMI pre-incubated protease in comparison to the native T122C protease (**23b**: 5.14 μM/50.80 μM, **25b**: 1.60 μM/25.12 μM, **34e**: 1.22 μM/2.22 μM, **SI** Figure 5**B**) suggesting that the inhibitors in this work also bind near the allosteric Thr122 residue and that this binding interferes with the sterically demanding BMI label.

2.3. Off-target selectivity

To investigate how the benzo[*d*]thiazole and benzofuran inhibitors affect the activity of other serine and cysteine proteases, a selectivity panel was constructed from a matrix of seven NS2B/NS3 inhibitors and seven different proteases. A representative set of compounds for each SAR optimization series was tested for their selectivity against various in-house serine (trypsin, thrombin, α-chymotrypsin, and urokinase plasminogen activator (uPA)) and cysteine proteases (rhodesain, *Staphylococcus aureus* sortase A, SARS-CoV-2 M^{pro}). The serine protease NS2B/NS3 is structurally most related to trypsin, but the latter does not have an NS2B cofactor and thus does not feature an allosteric binding pocket. Neither trypsin nor any of the other proteases showed appreciable inhibition at an inhibitor concentration of 20 μM. The results of the inhibition data are summarized in Table 5.

Table 5
Protease inhibition selectivity of representative compounds towards various serine and cysteine proteases.[a]

	Residual Enzyme Activity in [%] at 20 μM						
Compound	Trypsin	Thrombin	Chymotrypsin	uPA	SARS-CoV-2 M^{pro}	Rhodesain	Sortase A
1b	96 ± 4	97 ± 3	100 ± 7	100 ± 0	94 ± 1	93 ± 6	83 ± 4
23b	85 ± 6	95 ± 2	96 ± 2	62 ± 4	77 ± 6	86 ± 0	73 ± 0
25a	80 ± 6	75 ± 0.3	77 ± 1	100 ± 15	90 ± 1	91 ± 6	57 ± 1
25b	94 ± 5	65 ± 3	79 ± 7	100 ± 10	89 ± 4	77 ± 4	74 ± 1
34e	88 ± 2	81 ± 2	78 ± 7	82 ± 4	99 ± 2	93 ± 2	81 ± 11
36e	96 ± 1	97 ± 3	58 ± 2	91 ± 5	52 ± 6	93 ± 4	64 ± 0
36n	95 ± 3	93 ± 1	77 ± 4	94 ± 8	57 ± 10	90 ± 3	74 ± 2

[a] Residual enzyme activities at 20 μM of corresponding compound are indicated by mean ± standard deviation from at least three independent measurements. The residual enzyme activity is expressed relative to the DMSO control in [%].

2.4. Inhibitor stability

Due to the known susceptibility of phenolic compounds to oxidation, selected compounds (**23b**, **25a**, **25b**, **34a**, **34e**, **36e**) were tested for their chemical stability in the assay buffer (Tris pH 9.0) and under cell culture conditions (HEPES pH 7.4). For this purpose, the conditions of the respective assay were simulated, and the stability was determined by HPLC/MS after 15 min, 90 min, and 20 h of incubation time. The stability was interpreted as the integral of the corresponding compound in the 210 nm UV trace as a proportion of the total integral.

Except for compound **25a** (recovery of the compound after 15 min, 90 min, 20 h: 67%, 61%, 0%), all substances that were active in the fluorometric enzyme assay showed sufficient stability in the assay buffer for the duration of the assay (Tris pH 9.0, 83–100%). Under cell-assay conditions (HEPES pH 7.4), the stability of the compounds was even significantly increased due to the lower pH value (95–100%). The inversion of the amide bond increased the stability of the oxidation-labile dihydroxy group (compare **25a** with **34a**: 95%, 94%, 88% after 15 min, 90 min, 20 h in Tris buffer), which means that the new benzofuran derivatives are not only more potent than the previous derivatives, but also have higher stability.[63]

2.5. Docking studies

Until now, no crystal structure of the flaviviral NS2B/NS3 protease in complex with a benzo[*d*]thiazole inhibitor was solved. However, previously a specific allosteric binding site for non-competitive benzo[*d*]thiazole inhibitors of the NS2B/NS3 protease had been proposed by biochemical and computational investigations.[37,38,46,64,65] This prominent cavity is located on the back side of the protein as viewed from the active site (Ser135, Asp175, and His51) and is formed by the AAs Met49, Lys74, Leu76, Trp83, Lys84, Leu85, Glu86, Gly87, Glu88, Trp89, Val146, Vak147, Gly148, Leu149, Asn152, Ala164, Ile165, and Ile166.

The allosteric binding site was shown to be existing for both the open and closed conformations of the DENV2 and ZIKV NS2B/NS3.[32,38] However, the most stable predicted binding modes of benzo[*d*]thiazole ligands were previously found for the open conformation of the DENV2 protease (PDB code: 2FOM).[35,37] Hence, molecular docking studies of a comprehensive set of inhibitors were performed to the 2FOM-protein receptor by FlexX docking within the LeadIT worksuite.[66]

The key interactions between the NS2B/NS3 protein and the respective ligands are exemplarily shown for a representative top inhibitor from each investigated SAR series **8e**, **23b**, **25b**, and **34e** (Figure 4). The docking of the non-covalently bound ligands resulted in conformations that aligned well with the docking poses obtained in our previous study.[37] When docked into the allosteric site the benzo[*d*]thiazole moiety was inserted into the lipophilic sub-pocket generated by the residues Leu76, Gly148, and Ile165. Here, the catechol motif of all four ligands forms a hydrogen-bonding network to the residues Asn152, Lys74, and Gly148.

In their docking pose, the two Y-shaped inhibitors **8e** and **23b** show beneficial interactions with the two spatially separated hydrophobic subsites (Figure 4 **A,B**). One arm of each inhibitor interacts hydrophobically with the subsite determining residues Trp89/Ala166 resp. Val146/147 analogously to the overlay of the two proline-derived parent compounds (Figure 2).

However, compared to the linear truncated inhibitor **25b**, the catechol motif in the Y-shape inhibitors is slightly twisted because the sterically demanding Y-shape substituent exerts a geometric constraint on the benzothiazole moiety (Figure 4**C**). This could be the reason why there was only a slight increase in inhibitory potency with the Y-shaped structures despite the increased hydrophobic contact area: The selected Y-shape geometry does not yet optimally fit the binding pocket. Of note, the connector moiety (AA resp. sulfonamide) showed only few interactions with the protein (Lys74, Trp84, and Asn167) indicating that the type of connector is of minor importance if the hydrophobic moieties can find one of the hydrophobic subsites.

The truncated inhibitor **25b** incorporates an aromatic iodine substituent oriented toward the acidic residues Glu86/Glu88. A favorable carboxylate-halogen interaction could determine the reason for the high inhibitory potency of this compound despite its small size.[67] The inhibitors **8e**, **23b**, and **25b** have higher inhibitory potency for the ZIKV

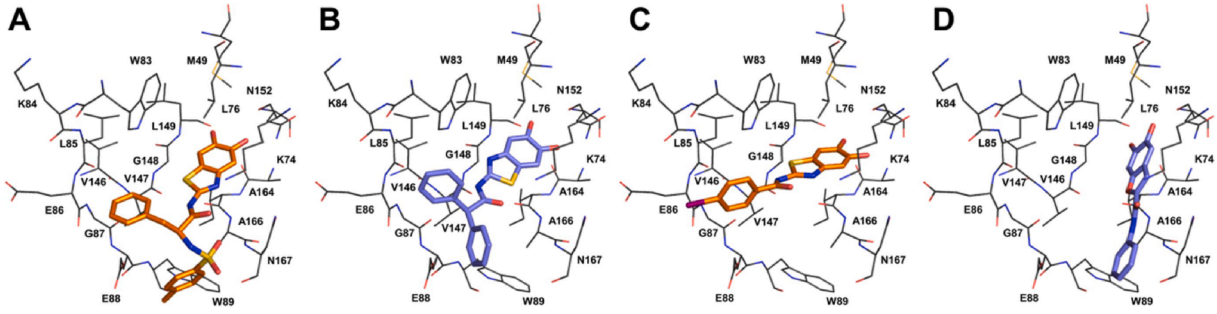

Fig. 4. Docking poses of each top inhibitor from the respective SAR series in complex with the DENV2 NS2B/NS3 protease (PDB: 2FOM) highlighting the proposed interaction features upon allosteric binding. (**A**) Docking pose for phenylalanine-derived inhibitor **8e**. (**B**) Docking pose for Y-shaped inhibitor **23b**. (**C**) Docking pose for truncated inhibitor **25b**. (**D**) Docking pose for benzofuran-derived inhibitor **34e**.

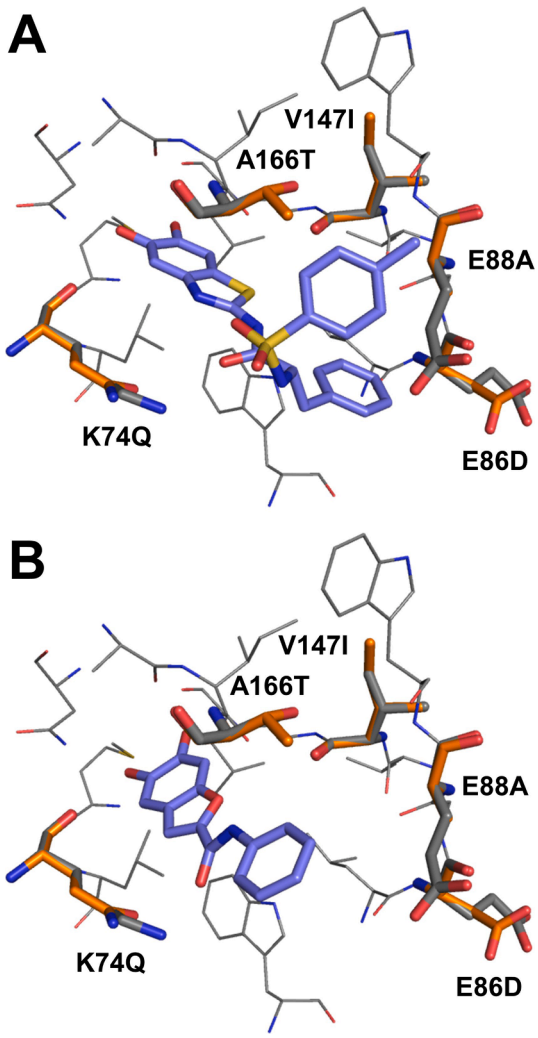

Fig. 5. Residue differences between DENV2 (grey) and ZIKV (orange) NS2B/NS3 within the allosteric binding site explaining the protease inhibitor selectivity by five differences in AA composition (K74Q, G87A, E88A, V147I, and A166T). (**A**) Docking pose for phenylalanine-derived inhibitor **8e**. (**B**) Docking pose for benzofuran-derived inhibitor **34e**. (For interpretation of the references to colour in this figure legend, the reader is referred to the web version of this article.)

protease than for the DENV2 homolog, while this trend is reversed for the benzofuran derivative **34e**, which preferentially inhibits the DENV2 NS2B/NS3. The differences in inhibitory potencies may be explained by the binding mode of the inhibitors. The benzofuran motif has a slightly tilted binding mode compared to the benzothiazole fragment, which allows better interaction of the amide carbonyl atom with Lys74 in the DENV2 protease (Figure 4**D**). This residue is replaced in the ZIKV protease by a K74Q exchange, by which the positive charge at the pocket entry is lost and might explain the inverse selectivity of the benzofuran inhibitors for the DENV2 protease (Figure 5**B**).

In a sequence-based alignment between DENV2 (pdb: 2FOM) and ZIKV (pdb: 5GXJ) proteases, five core residue differences of the allosteric binding pocket were identified (K74Q, G87A, E88A, V147I, and A166T), which might explain the protease selectivity. The superior inhibitory potency of large and hydrophobic Y-shaped structures for the ZIKV protease might be explained by an $Glu88_{DENV2}$ to $Ala88_{ZIKV}$ exchange, which reduces the polarity of the respective DENV2 subsite and further enhances the space for hydrophobic substituents in the ZIKV protease as shown for the phenylalanine derivate **8e** (Figure 5**A**).

2.6. Antiviral activity

To determine the antiviral activity of NS2B/NS3 inhibitors in a cellular context, we studied the suppression of viral replication by a luciferase replication assay. Briefly, Huh7 cells were transfected by electroporation of DENV2 (strain New Guinea C, NGC) or ZIKV (strain H/PF/2013) subgenomic luciferase reporter replicon RNAs, expressing the luciferase gene and all NS genes to monitor viral replication.[68,69] After 4 h, 10 μM of the respective inhibitor was added. As a quantity for the determination of viral replication, luciferase activity was measured at 24, 48, 72, and 96 h after electroporation. A depiction of the DENV2/ZIKV RNA replication time curves for active compounds can be found in **SI** Figure 1.

Prior to viral replication analyses, the effect of inhibitors on mammalian cell integrity, potential cytotoxicity was determined by luminescent cell viability assay at varying compound concentrations. While most of the compounds had no measurable effects on Huh7 cell viability at concentrations between 1.25 and 10 μM, only the dimethoxy derivate **24b** showed cytotoxic effect by a reduction of substrate turnover at concentrations $\geq$ 5 μM (**SI** Figure 2). Therefore, the measured decrease in RNA replication of **24b** (Figure 6**A**) is probably not solely due to the antiviral properties of this compound but is caused by its cytotoxicity, which is why this compound was not used for further investigations.

The effect on DENV2 replication was tested for the top inhibitors of

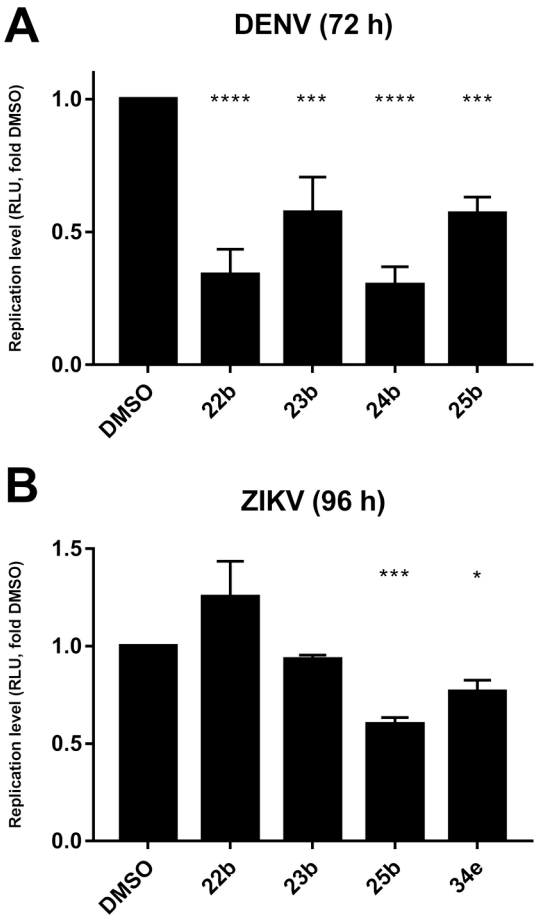

Fig. 6. ZIKV and DENV2 RNA replication quantified by luciferase activity assays. (**A**) Inhibition of DENV2 NGC replication by the most potent compounds (10 μM) 72 h after electroporation. (**B**) Inhibition of ZIKV HPF replication by the most potent compounds (10 μM) 96 h after electroporation. Shown are means ± standard deviation (n = 3). ****, $P < 0.0001$; ***, $P < 0.001$; *, $P < 0.05$. Statistical significance was calculated by using one-way ANOVA.

each SAR optimization series (Tables 1–4): Truncated *para*-iodine derivate **25b**, Y-shaped 2,2-diphenylacetic acid inhibitor **23b**, truncated benzofuran inhibitor **34e**, proline-containing benzofuran inhibitor **36e**, and pipecolic acid-containing benzofuran inhibitor **36n**. In addition, the corresponding dimethoxy derivates **24b**, **22b**, **33e**, **35e**, and **35n** were also tested for their effect on DENV2 replication since it was shown in our previous work that the dimethoxy compounds can act as prodrugs. After enzymatic metabolization, the corresponding dihydroxy derivatives are released.[37] At a concentration of 10 μM, both the *para*-iodine derivate **25b** and the Y-shaped 2,2-diphenylacetic acid inhibitor **23b** showed a significant decrease in RNA copies of DENV2 replication after 72 h (Figure 6**A**). Furthermore, the attenuation of viral replication was even more pronounced for the corresponding dimethoxy derivates **24b** and **22b**, which agrees with our previous study. The increased activity can probably be attributed to a higher membrane permeability of these prodrugs. However, the other benzofuran-consisting inhibitors tested for DENV2 inhibition showed no significant reduction of viral replication. The reason for this could not be conclusively elucidated here, as these had even shown a selectivity shift towards better inhibition of DENV2 protease in the fluorometric enzyme assay (Table 4).

To further investigate the DENV2 insusceptibility to the benzofuran-based inhibitors, sequence analysis was performed to identify possible amino acid differences between the recombinantly expressed NS2B/NS3 protease and DENV2 NGC protease (**SI** Figure 3). The protein construct used in the fluorometric assay in fact showed two point mutations near the allosteric pocket (T120A, N167Q). To study the activity and inhibition of the native cellular protease sequence in the context of the fluorometric assay, a double mutant of our NS2B/NS3 protease was recombinantly expressed by site-directed mutagenesis and tested for both protease activity compared to the wildtype and inhibition by selected compounds. The activity of the DENV2 protease T120A/N167Q-mutant appears to be slightly decreased compared with the wild type (**SI** Figure 4, wildtype: $k_{cat} = 0.709 \pm 0.039$ mAU s^{-1}; T120A/N167Q: $k_{cat} = 0.447 \pm 0.003$ mAU s^{-1}). Inhibition by benzofuran inhibitor **34e** and *para*-iodine derivative **25b** was evaluated for the T120A/N167Q-mutant by determination of the IC_{50} values (**34e:** 0.73 ± 0.015 μM, **25b**: 8.01 ± 1.25 μM). Since neither the activities nor the inhibition rates did severely differ, it can be assumed that the two mutations have only minimal influence on the inhibition of the compounds, and insusceptibility to benzofurans is most likely due to cellular causes (metabolism, permeability, etc.).

Besides DENV2 replication inhibition, ZIKV H/PF/2013 reporter virus replication was analyzed by a luciferase assay for the benzofuran inhibitor **34e**, the *para*-iodine derivate **25b**, the 2,2-diphenylacetic acid inhibitor **23b**, and its corresponding dimethoxy derivate **22b**, which showed efficient reduction of DENV2 replication. Luciferase activity was significantly reduced by 10 μM of benzofuran inhibitor **34e** and *para*-iodine derivate **25b** after 96 h. Compounds **22b** and **23b**, on the other hand, showed no significant effect on ZIKV replication. That our inhibitors have a generally lower efficiency to inhibit ZIKV replication compared to DENV2 inhibition could be since ZIKV replication factories are additionally surrounded by intermediate filaments in cage-like structures. This could lead to stronger protection of the ZIKV protease from inhibitors compared to DENV2.[70]

3. Conclusions

In this work, we have optimized allosteric inhibitors for the DENV2 and ZIKV NS2B/NS3 proteases. Hereby, we found new lead structures with good inhibitory properties. By exchanging the individual moieties of the lead structures **1a,b**, different series of inhibitors were synthesized and investigated regarding their inhibitory effects on the NS2B/NS3 proteases of DENV2 and ZIKV. Replacing the amino acid linker with (*R/S*)-alanine (**8a,b**), isoleucine (**8c**), *tert*-leucine (**8d**), phenylalanine (**8e**), tyrosine (**12a**), and aspartic acid (**12b**) did not significantly improve the inhibitory effect. Nevertheless, the ZIKV protease was inhibited by the compounds **8a–f** and **12a** in the low micromolar range (IC_{50} = 2.13–6.48 μM). In the series of newly designed Y-shaped inhibitors (Table 2), 2,2-diphenylacetic acid derivate **23b** was the most promising compound with a sub-micromolar IC_{50} for ZIKV (0.95 μM). Y-shaped compounds **23b** and **20b** as well as AA-based compounds with hydrophobic side chains **8c–f** demonstrated with IC_{50} values in the low micromolar range that addressing both binding subsites with Y-shaped inhibitors is a promising strategy for further improvement. By truncating the inhibitor scaffold (Table 3), we were able for the first time to achieve inhibition in the low micromolar range for the DENV2 protease and simultaneously increased the ligand efficacy to obtain new starting points for further DENV2 drug discovery. The iodine-substituted inhibitor **25b** was the most promising compound of this series with an IC_{50} of 4.38 μM for DENV2 and a sub-micromolar IC_{50} of 0.67 μM for ZIKV, respectively. By exchanging the benzo[*d*]thiazole core heterocycle, we could show that other heteroaromatic systems can serve as scaffolds besides benzo[*d*]thiazoles. In this SAR series, the benzofuran derivate **34e** showed the best inhibitory properties (IC_{50}(DENV2) = 0.69 μM, IC_{50}(ZIKV) = 1.04 μM). In contrast to the benzo[*d*]thiazole-based compounds, **34e** inhibits both the ZIKV and the DENV2 NS2B/NS3 proteases in the same order of magnitude. Screening of selected compounds against various serine and cysteine proteases demonstrated excellent off-target selectivity of our inhibitors. The most potent inhibitors and their respective methoxy prodrugs were administered in a cell-based assay for their antiviral potential to interfere with DENV2 and ZIKV replication. The compounds **22b**, **23b**, and **25b** highlighted their antiviral potential by significantly attenuating DENV2 replication, whereas **25b** and **34e** showed reduced ZIKV replication. In summary, we identified two promising compounds that resemble suitable starting points for upcoming drug development. First, *N*-(5,6-dihydroxybenzo[*d*]thiazol-2-yl)-4-iodobenzamide (**25b**) and second, 5,6-dihydroxy-*N*-phenylbenzofuran-2-carboxamide (**34e**), both of them containing only 20 and 21 heavy atoms, respectively, and with ligand efficiencies above 0.4 are good starting points for further NS2B/NS3 inhibitor development.

4. Experimental section

4.1. Expression constructs

A pET15b expression vector, harboring a thrombin-cleavable *N*-terminal hexahistidine-tagged DENV2 NS2B cofactor domain covalently linked to the NS3 protease domain *via* a $Gly_4SerGly_4$-linker (GenBank ID: AY037116.1) with two point mutations in the NS3 region (I30A and L31A for better solubility, herein referred to as WT), was kindly provided by the group of W. Diederich (University of Marburg, Germany).[71] The pET11a vector, containing the sequence of the French Polynesia ZIKV strain (GenBank ID: KJ776791.1) protease was used as described previously.[37,61,72] To abolish autocatalytic cleavage of the covalently linked construct, a point mutation (R95A) was introduced. The construct contains a *N*-terminal hexahistidine tag provided with a tobacco etch virus (TEV) protease cleavage site. The DENV2 T120A-N167Q mutant for validation of antiviral activity measurements and the DENV2 T122C mutant suitable for maleimide coupling based binding site verification were generated using the Kapa HiFi PCR kit (Kapa Biosystems) and the following primers:

(i) T120A: 5′–GACCAAT**GCG**GGTACCATTGGCG–3′ and 5′–GGTACC**CGC**ATTGGTCTTAAACAGGC–3′,
(ii) N167Q: 5′–CGATTGCC**CAG**ACGGAAAAGTCCATTGAAGATAACC–3′ and 5′–CTTTTCCGT**CTG**GGCAATCGCGGACACGTAG–3′,
(iii) T122C: 5′-CAATACGGGT**TGC**ATTGGCGCGGTTAGCCTGG–3′ and 5′–CGCCAAT**GCA**ACCCGTATTGGTCTTAAACAGGCCC–3′.

4.2. Protein preparation

The DENV2 and ZIKV proteases were expressed in *E. coli* BL21-Gold (DE3) (Agilent Technologies) cells according to the literature.[61] Briefly, cells were grown in LB media with the presence of 100 μg/mL ampicillin at 37 °C. Overexpression was induced by the addition of 1 mM IPTG at an OD_{600} nm of ~0.8 and incubated at 20 °C for 16 h. Cells were harvested by centrifugation, shock frozen in liquid nitrogen, and stored at –20 °C until further use. For purification, cells were resuspended in lysis buffer (20 mM Tris-HCl pH 8, 300 mM NaCl, 2 mM imidazole, 0.1% (v/v) $Triton_{X\text{-}100}$, RNase, lysozyme) and lysed by sonication (Sonopuls, Bandelin). Cell debris was removed by centrifugation and the supernatant was subjected to affinity chromatography using a HisTrap HP column (GE Healthcare, Chicago, USA). Histidine-rich proteins and other impurities were removed by subsequent increasing amounts of elution buffer (20 mM Tris-HCl pH 8, 300 mM NaCl, 250 mM imidazole). Eluted fractions were further purified by size exclusion chromatography (*SEC*) using a HiLoad 16/600 Superdex 75 pg (GE Healthcare, Chicago, USA) and eluted in *SEC* buffer (20 mM Tris-HCl pH 8, 150 mM NaCl). Prior to storage at –80 °C, proteins were concentrated, and flash-frozen with liquid nitrogen.

4.3. Molecular Modeling

Docking calculations were performed applying the FlexX algorithm as implemented in LeadIT.[73] The non-covalent mode was started from the program GUI with advanced settings. A standardized ligand preparation protocol was executed with MOE2020 prior docking. Ligand minimization was performed using the MMFF94x force field.[74] 3D coordinates of minimized structures were exported from MOE as single libraries in SDF file format to be imported to LeadIT. Modeling the putative binding mode of inhibitors to the allosteric pocket of DENV2 NS2B/NS3 protease was done using the crystal structure in the open conformation thereof (pdb entry: 2FOM). The binding site was defined as 11 Å shell around the core residue K73 including 24 receptor defining residues in the NS2B-protein chain: K73, K74, L76, W83, L85, E86, G87, E88, W89, T118, T120, I123, V146, V147, G148, L149, Y150, G151, N152, V154, A164, I165, A166, and N167. Chemical receptor properties were kept in FlexX default settings: No alternate protonation states from ligand preparation; Ligand binding driven by entropy and enthalpy (hybrid approach); Full score contribution threshold = 0.3; No score contribution threshold = 0.7; Consider *R/S* stereo mode during docking; Maximum allowed overlap volume = 2.9 $Å^3$; Clash factor = 0.6; Consider hydrogens in internal clash tests; Maximum number of solutions per iteration = 500; Maximum number of solutions per fragmentation = 500, Number of poses to keep = Top 10. A torsion subgraph was defined to force the thiazole-attached amide bond to be restricted in a planar constitution with the aromatic system as determined by QM-calculations.[37]

4.4. Fluorometric assays

The determination of the inhibitory activity of the compounds against the proteases was performed with an assay based on the fluorogenic substrates or FRET-based substrates. The inhibitors and the substrate were prepared as stock solutions in DMSO. The fluorescence was measured in white flat-bottom 96-well microtiter plates from Greiner Bio-One using a Tecan Infinite F2000 PRO plate reader. Measurements were performed in at least three independent experiments. In each well a total volume of 200 μL was used, consisting of 180 μL buffer, 5 μL enzyme solution, 10 μL inhibitor in DMSO or pure DMSO as control, and 5 μL solution of the corresponding substrate. Initial screenings were performed at inhibitor concentrations of 20 μM. IC_{50} values were determined with dilution series between 0.01 μM and 100 μM. The fluorescence was measured every 30 s for 10 min at 25 °C with the corresponding excitation and emission wavelengths. IC_{50} values were calculated with GraFit (Version 6.0.12; Erithacus Software Limited, East Grinstead, West Sussex, UK)[75] by fitting the remaining enzymatic activity to the four-parameter IC_{50} equation

$$Y = \frac{Y_{max} - Y_{min}}{1 + \left(\frac{[I]}{IC_{50}}\right)^{s}} + Y_{min}$$

with Y [ΔF/min] as the substrate hydrolysis rate, Y_{max} as the maximum value of the dose–response curve, measured at inhibitor concentrations of [I] = 0 μM, Y_{min} as the minimum value, obtained at high inhibitor concentrations, and s as the Hill coefficient.[76]

Buffers and Substrates. Rhodesain (50 mM Na-acetate pH 5.5, 5 mM EDTA, 200 mM NaCl, 5 mM DTT, 10 μM Z-Phe-Arg-AMC),[77] SARS-CoV-2 M^{pro} (20 mM Tris pH 7.5, 0,1 mM EDTA, 200 mM NaCl, 1 mM DTT, 50 μM Dabcyl-KTSAVLQ|SGFRKME-Edans),[78] DENV2 and ZIKV NS2B/NS3 (50 mM Tris pH 9.0, 20% (v/v) Glycerol, 1 mM Chaps, 100 μM Boc-Gly-Arg-Arg-AMC),[62] urokinase plasminogen activator (50 mM Tris pH 7.4, 50 mM NaCl, 0.5 mM EDTA, 240 μM Z-Gly-Gly-Arg-AMC),[79] *Staphylococcus aureus* sortase A (50 mM Tris pH 7.5, 150 mM NaCl, 5 mM $CaCl_2$,0.5 mM Gly_4, 25 μM Abz-LPETG-Dap(dnp)–OH),[80] thrombin (50 mM Tris pH 8.0, 100 mM NaCl, 5 mM $CaCl_2$, 0.01% Tween-20, 200 μM Z-Gly-Gly-Arg-AMC), trypsin (50 mM Tris pH 8.0, 100 mM NaCl, 5 mM EDTA, 40 μM Z-Phe-Arg-AMC), and α-chymotrypsin (50 mM Tris pH 8.0, 100 mM NaCl, 5 mM EDTA, 75 μM Succ-Leu-Tyr-AMC).[81]

4.5. Antiviral activity and cytotoxicity

4.5.1. Cell culture

Huh7 cells were maintained in Dulbecco's modified Eagle's medium (DMEM) supplemented with 2 mM L–glutamine, 1x non-essential AA, 100 U/mL penicillin, 100 μg/mL streptomycin (all from GIBCO, Life Technologies), and 10% fetal calf serum (Capricorn).

4.5.2. Plasmids

Plasmids encoding the wildtype ZIKV H/PF/2013 sub-genomic replicon expressing a *Renilla* luciferase gene (pFK-sgR2A-H/PF/2013) as well as the replication-defective mutant (pFK-sgR2A-H/PF/2013-GAA) were previously described.[69] Plasmid encoding the DENV2 strain New Guinea C (NGC) sub-genomic replicon expressing a *Firefly* luciferase gene (pDVWSK601ΔCprME-LucUbi) were also described previously.[68] Plasmids were kindly provided by R. Bartenschlager (Heidelberg).

4.5.3. *In vitro* transcription

10 μg plasmid were linearized by restriction using *Xho*I and *Xba*I for ZIKV-based and DENV2-based plasmids, respectively. Linearized plasmid was purified using the Nucleospin Extract II kit (Macherey-Nagel). *In vitro* transcription reactions were carried out in 100 μL final volume containing the linearized plasmid DNA in transcription buffer containing 80 mM HEPES pH 7.5, 12 mM $MgCl_2$, 2 mM spermidine, 40 mM dithiothreitol (DTT), 3.125 mM of ATP, CTP, and UTP, 1.5625 mM GTP (all from Roche), 100 U RNAsin ribonuclease inhibitor (Promega), and 1 mM cap structure analog. For DENV2 transcripts, m7G(5′)ppp(5′)G RNA cap structure analog (New England Biolabs) was used. For ZIKV transcripts, 3́-O-Me-m7G(5′)ppp(5′)G RNA cap structure analog (New England Biolabs). Reactions were supplemented with 80 U T7 RNA polymerase (Promega). After incubation for 3 h at 37 °C, 80 U T7 RNA polymerase was added and transcription was carried out for another 3 h. Transcription was terminated by the addition of 10 U RQ1 RNase-free DNase (Promega) and incubation at 37 °C for 30 min. RNA was purified using phenol:chloroform:isoamyl alcohol (25:24:1) (Applichem), precipitated with isopropanol, and the RNA pellet was dissolved in RNase-free water. RNA integrity was determined by using agarose gel electrophoresis and concentration was determined by measuring optical density at 260 nm.

4.5.4. Replication analysis and luciferase assays

Quantification of luciferase activity was used to determine ZIKV and DENV2 RNA replication as described previously.[68,69] In brief, single-cell suspensions of Huh7 cells were prepared by trypsinization and washed once with phosphate-buffered saline. Cells were resuspended at a concentration of 1×10^7 cells per mL in Cytomix containing 2 mM ATP and 5 mM glutathione. 10 µg of *in vitro* transcribed RNA was mixed with 400 µL of the cell suspension ($4x10^6$ cells) and transfected by electroporation using a Gene Pulser system (Bio-Rad) in a cuvette with a gap width of 0.4 cm (Bio-Rad) at 975 µF and 270 V.[82] Cells were resuspended in 15 mL culture medium. Cells were seeded in duplicate wells in a 12-well plate: 500 µL for the time points 4 h and 24 h and 1 mL for the time points 48 h, 72 h, and 96 h. 4 h after electroporation, cells were treated with 10 µM compound or an equivalent volume of DMSO, as vehicle control, in culture medium supplemented with 15 mM HEPES (Gibco, Life technologies). Compound- or DMSO-containing culture medium was replenished after 48 h. Cells were lysed at 4, 24, 48, 72, and 96 h after electroporation by addition of 250 µL luciferase lysis buffer (0.1% (v/v) $Triton_{X\text{-}100}$, 25 mM glycylglycine, 15 mM $MgSO_4$, 15 mM K_3PO_4 pH 7.8, 4 mM EGTA, 10% (v/v) glycerol, and 1 mM DTT). For detection of *Renilla* luciferase activity, 100 µL lysate was mixed with 200 µL luciferase assay buffer (25 mM glycylglycine, 15 mM $MgSO_4$, 15 mM K_3PO_4 pH 7.8, and 4 mM EGTA) supplemented with 14 or 28 nM coelanterazine (P.J.K). For detection of firefly luciferase activity, 100 µL lysate was mixed with 350 µL luciferase assay buffer freshly supplemented with 1 mM DTT and 2 mM ATP, and D-luciferin substrate (200 µM D-Luciferin, P.J.K.) in 25 mM glycylglycine. All measurements were done in duplicates by using a tube luminometer (Berthold Technologies). Replication efficiency was determined relative to the 4 h values, which reflect input transcript levels.

4.5.5. Cell viability assay

To determine the impact of compound treatment on cell viability, Huh7 cells were seeded at a density of $4x10^3$ cells per well in white-walled 96-well plates (Greiner Bio-One) and one day after seeding cells were treated with 1.25, 2.5, 5, 10, 20, and 40 µM compound or equivalent volumes of DMSO for 96 h. Cell viability was measured using the CellTiter-Glo Luminescent Cell Viability Assay (Promega) following manufacturer instructions. Cell viability was determined by measurement with a plate luminometer (Berthold Technologies) and values normalized to untreated cells.

4.5.6. Statistical significance

Statistical analysis was performed by using the GraphPad Prism.[83] Statistical significance was calculated by using one-way ANOVA for single time points and by using 2way ANOVA for replication curves. ****, $p < 0.0001$; ***, $p < 0.001$; **, $p < 0.01$; *, $p < 0.05$.

4.6. Chemistry

All reagents and solvents were of analytical grade quality and purchased from Sigma-Aldrich, Carbolution, BLDpharmatech, or FisherScientific. Chemicals were used without further purification. Solvents were purified by distillation and desiccated by standard methods if necessary. ^1H and ^{13}C spectra were recorded on a *Bruker* Fourier 300 using DMSO-d_6, $CDCl_3$, MeOD-d_4 as solvent. Chemical shifts δ are given in parts per million (ppm) using residual proton peaks of the solvent as internal standard. HPLC and mass spectra were obtained by LC-MS consisting of a 1100 series HPLC system from *Agilent* with an *Agilent* Poroshell 120 EC-C_{18} 150 × 2.10 mm, 4 μm column. Detection wavelength was 254 nm. The purities of the inhibitors were higher than 95% in all cases. The molecular mass was detected by an *Agilent* 1100 series LC/MSD Trap with electron spray ionization (ESI) in positive mode. Column chromatography was performed with silica gel (0.06–0.02 mm) obtained from *Carl Roth*. All reactions were monitored by thin-layer chromatography using *Macherey-Nagel* ALUGRAM Xtra SIL G/UV254 silica gel 60 plates for detection at 254 nm. Melting points (uncorrected) were determined in open capillaries using a Schorpp MPM-H3 melting point device. Specific rotations $[\alpha]_D^{20}$ were measured on a P3000 polarimeter from Krüss and are reported in $cm^3\ g^{-1}\ dm^{-1}$.

***2-Amino-5,6-dimethoxybenzo[d]thiazole* (5)**: was prepared according to the literature.[84]

(Hetero)aromatic carboxylic acids (32a–l): were prepared according to literature procedures.

5,6-Dimethoxybenzo[d]thiazole-2-carboxylic acid ***(32a)***:[52] 400 mg, 1.65 mmol, yield: 89%. mp: 140–142 °C. ^1H NMR: (300 MHz, DMSO-d_6) δ = 7.73 (s, 1H), 7.67 (s, 1H), 3.87 (s, 6H) ppm. ^{13}C NMR: (75 MHz, DMSO-d_6) δ = 161.6, 150.3, 149.9, 147.4, 129.4, 105.5, 103.4, 103.2, 56.0, 55.8 ppm.

6-Methoxybenzo[d]thiazole-2-carboxylic acid ***(32b)***:[52] 360 mg, 1.72 mmol, yield: 82%. mp: 120–122 °C. ^1H NMR: (300 MHz, DMSO-d_6) δ = 9.17 (s, 1H), 8.06 (d, J = 9.0 Hz, 1H), 7.76 (d, J = 2.5 Hz, 1H), 7.22 (dd, J = 9.0, 2.5 Hz, 1H), 3.86 (s, 3H) ppm. ^{13}C NMR: (75 MHz, DMSO-d_6) δ = 157.6, 153.5, 147.6, 135.2, 123.5, 115.8, 104.8, 55.8 ppm.

5,6-Dimethoxy-1H-indole-2-carboxylic acid ***(32c)***:[53,54] 330 mg, 1.49 mmol, yield: 99%. mp: decomp. > 205 °C. ^1H NMR: (300 MHz, DMSO-d_6) δ = 11.45 (s, 1H), 7.07 (s, 1H), 6.96 (d, J = 2.1 Hz, 1H), 6.89 (s, 1H), 3.77 (s, 3H), 3.74 (s, 3H) ppm. ^{13}C NMR: (75 MHz, DMSO-d_6) δ = 162.7, 149.2, 145.6, 132.5, 126.6, 119.9, 107.7, 102.7, 94.5, 55.7, 55.5 ppm.

5,6-Dimethoxybenzo[b]thiophene-2-carboxylic acid ***(32d)***:[55] 320 mg, 1.34 mmol, yield: 94%. mp: 256–258 °C. ^1H NMR: (300 MHz, DMSO-d_6) δ = 7.94 (s, 1H), 7.55 (s, 1H), 7.45 (s, 1H), 3.84 (s, 3H), 3.81 (s, 3H) ppm. ^{13}C NMR: (75 MHz, DMSO-d_6) δ = 163.7, 150.4, 148.5, 135.2, 132.3, 132.0, 130.1, 106.3, 104.2, 55.9, 55.6 ppm.

5,6-Dimethoxybenzofuran-2-carboxylic acid ***(32e)***:[56,57] 220 mg, 1.00 mmol, yield: 99%. mp: decomp. > 250 °C. ^1H NMR: (300 MHz, DMSO-d_6) δ = 7.52 (s, 1H), 7.31 (s, 1H), 7.21 (s, 1H), 3.83 (s, 3H), 3.79 (s, 3H) ppm. ^{13}C NMR: (75 MHz, DMSO-d_6) δ = 160.0, 150.7, 150.5, 147.2, 145.0, 118.6, 114.1, 103.2, 95.6, 56.0, 55.9 ppm.

6,7-Dimethoxyquinoline-3-carboxylic acid ***(32f)***:[58] 390 mg, 1.67 mmol, yield: 99%. mp: 265–267 °C. ^1H NMR: (300 MHz, DMSO-d_6) δ = 9.10 (s, 1H), 8.72 (s, 1H), 7.52 (s, 1H), 7.43 (s, 1H), 3.96 (s, 3H), 3.92 (s, 3H) ppm. ^{13}C NMR: (75 MHz, DMSO-d_6) δ = 166.9, 153.9, 149.9, 147.7, 146.6, 136.1, 122.4, 122.3, 107.5, 106.7, 55.9, 55.8 ppm.

5-Methoxybenzofuran-2-carboxylic acid ***(32g)***: 160 mg, 0.83 mmol, yield: 91%. mp: 217–219 °C. ^1H NMR: (300 MHz, DMSO-d_6) δ = 7.61–7.59 (m, 1H), 7.58 (s, 1H), 7.26 (d, J = 2.6 Hz, 2H), 7.08 (dd, J = 9.0, 2.6 Hz, 2H), 3.79 (s, 3H) ppm. ^{13}C NMR: (75 MHz, DMSO-d_6) δ = 160.1, 156.1, 150.1, 146.8, 127.5, 117.2, 113.7, 112.8, 104.3, 55.7 ppm.

6-Methoxybenzofuran-2-carboxylic acid ***(32h)***: 190 mg, 0.99 mmol, yield: 87%. mp: 211–213 °C. ^1H NMR: (300 MHz, DMSO-d_6) δ = 7.64 (d, J = 8.7 Hz, 1H), 7.58 (d, J = 1.0 Hz, 1H), 7.28 (dd, J = 2.3, 1.0 Hz, 1H), 6.97 (dd, J = 8.7, 2.3 Hz, 1H), 3.83 (s, 3H) ppm. ^{13}C NMR: (75 MHz, DMSO-d_6) δ = 160.1, 160.1, 156.5, 145.3, 123.4, 120.0, 113.9, 113.8, 95.9, 55.8 ppm.

4,6-Dimethoxybenzofuran-2-carboxylic acid ***(32i)***: 530 mg, 2,39 mmol, yield: 99%. mp: 235–237 °C. ^1H NMR: (300 MHz, DMSO-d_6) δ = 7.45 (d, J = 1.0 Hz, 1H), 6.85 (dd, J = 1.9, 1.0 Hz, 1H), 6.44 (d, J = 1.9 Hz, 1H), 3.87 (s, 3H), 3.81 (s, 3H) ppm. ^{13}C NMR: (75 MHz, DMSO-d_6): δ = 161.6, 160.0, 157.2, 154.4, 144.2, 111.1, 111.0, 95.3, 88.5, 56.0, 55.9 ppm.

6-Methoxy-5-nitrobenzofuran-2-carboxylic acid ***(32j)***: 590 mg, 2.5 mmol, yield: 75%. decomp. > 250 °C. ^1H NMR: (300 MHz, DMSO-d_6) δ = 8.34 (s, 1H), 7.69 (dd, J = 9.1, 1.0 Hz, 2H), 3.98 (s, 3H) ppm. ^{13}C NMR: (75 MHz, DMSO-d_6) δ = 159.5, 157.2, 152.5, 147.7, 138.0, 120.0, 119.0, 113.9, 97.7, 57.3 ppm.

6,7-Dimethoxy-2-naphthoic acid ***(32m)***:[50,51] 500 mg, 2.17 mmol, yield: 99%. mp: 245–247 °C. ^1H NMR: (300 MHz, $CDCl_3$) δ = 12.80 (s, 1H), 8.44 (s, 1H), 7.80 (s, 2H), 7.49 (s, 1H), 7.36 (s, 1H), 3.91 (s, 3H), 3.89 (s, 3H) ppm. ^{13}C NMR: (75 MHz, $CDCl_3$) δ = 167.8, 151.1, 149.8,

131.5, 128.9, 128.0, 126.4, 126.0, 123.5, 107.7, 106.3, 55.6 ppm.

***tert*-Butyl (*S*)-2-(phenylcarbamoyl)pyrrolidine-1-carboxylate (30a)**: was prepared according to the literature.[60] 1.80 g, 6.20 mmol, yield: 89%. mp: 187–189 °C. R_f = 0.37 (CH/EtOAc 2:1). $[\alpha]_D^{20}$ = –80 (*c* = 5 in MeCN). ^{1}H NMR: (300 MHz, DMSO-d_6) δ = 9.96 (s, 1H), 7.59 (d, *J* = 7.6 Hz, 2H), 7.30 (t, *J* = 7.6 Hz, 2H), 7.03 (t, *J* = 7.6 Hz, 1H), 4.27–4.17 (m, 1H), 3.46–3.29 (m, 2H), 2.28–2.09 (m, 1H), 1.97–1.72 (m, 3H), 1.39 (s, 3H), 1.27 (s, 6H) ppm. ^{13}C NMR: (75 MHz, DMSO-d_6) δ = 171.5, 153.2, 139.1, 128.7, 123.2, 119.2, 119.0, 78.5, 60.4, 46.6, 31.0, 28.2, 28.0, 23.4 ppm.

***tert*-Butyl (*S*)-2-(phenylcarbamoyl)piperidine-1-carboxylate (30b)**: was prepared according to the literature.[60] 355 mg, 1.47 mmol, yield: 90%. mp: 183–185 °C. R_f = 0.66 (CH/EtOAc 2:1). $[\alpha]_D^{20}$ = –131 (*c* = 10 in $CHCl_3$). ^{1}H NMR: (300 MHz, DMSO-d_6) δ = 9.89 (s, 1H), 7.58 (d, *J* = 7.7 Hz, 2H), 7.29 (t, *J* = 7.7 Hz, 2H), 7.03 (t, *J* = 7.7 Hz, 1H), 4.65 (s, 1H), 3.94–3.69 (m, 1H), 3.34 (s, 2H), 2.17–1.99 (m, 1H), 1.80–1.50 (m, 4H), 1.36 (s, 11*H*) ppm. ^{13}C NMR: (75 MHz, DMSO-d_6) δ = 170.8, 155.3, 139.0, 128.7, 123.2, 119.3, 78.9, 28.0, 27.5, 24.2, 19.6 ppm.

(*S*)-*S*-Benzyl-*N*-(*tert*-butoxycarbonyl)cysteine (4f): was prepared according to the literature.[85] 1100 mg, 3.31 mmol, yield: 81%. mp: 76 °C. R_f = 0.48 (CH/EtOAc 1:1). $[\alpha]_D^{20}$ = –44 (*c* = 10 in MeOH). ^{1}H NMR: (300 MHz, DMSO-d_6) δ = 7.35–7.27 (m, 5H), 4.18–4.05 (m, 1H), 3.75 (s, 2H), 2.89–2.57 (m, 2H), 1.39 (s, 9H) ppm. ^{13}C NMR: (75 MHz, DMSO-d_6) δ = 172.5, 155.3, 138.3, 128.8, 128.3, 126.8, 78.2, 53.2, 35.2, 32.4, 28.2 ppm.

***N*-Benzoyl-*N*-phenylglycine (21a)**: was prepared according to the literature.[47] 826 mg, 3.24 mmol, yield: 81%. mp: 160 °C. R_f = 0.43 (CH/EtOAc 1:1). ^{1}H NMR: (300 MHz, DMSO-d_6) δ = 12.77 (s, 1H), 7.32–7.09 (m, 10*H*), 4.49 (s, 2H) ppm. ^{13}C NMR: (75 MHz, DMSO-d_6) δ = 170.6, 169.8, 143.9, 135.8, 129.2, 128.8, 128.5, 128.1, 127.6, 126.8, 52.1 ppm.

2,2-Diphenylacetic acid (21b): was prepared according to the literature.[48] 1060 mg, 5.00 mmol, yield: 99%. mp: 146 °C. R_f = 0.80 (CH/EtOAc). ^{1}H NMR: (300 MHz, DMSO-d_6) δ = 12.71 (s, 1H), 7.32 (s, 8H), 7.28–7.19 (m, 2H), 5.06 (s, 1H) ppm. ^{13}C NMR: (75 MHz, DMSO-d_6) δ = 173.3, 139.5, 128.4, 128.3, 126.8, 56.2 ppm.

2,2-Bis-(4-methoxyphenyl)acetic acid (21c): was prepared according to the literature.[49] 568 mg, 2.09 mmol, yield: 95%. mp: 107 °C. R_f = 0.64 (CH/EtOAc 1:1). ^{1}H NMR: (300 MHz, DMSO-d_6) δ = 12.48 (s, 1H), 7.24–7.17 (m, 4H), 6.90–6.83 (m, 4H), 4.90 (s, 1H), 3.71 (s, 6H) ppm. ^{13}C NMR: (75 MHz, DMSO-d_6) δ = 173.9, 158.0, 131.9, 129.4, 113.7, 55.0, 54.6 ppm.

1-(4-Iodophenyl)-3-(6-Nitrobenzo[*d*]thiazol-2-yl)thiourea (28): A mixture of 2-amino-6-nitrobenzo[*d*]thiazole (195 mg, 1.0 mmol, 1.1 eq.), 4–iodophenyl isothiocyanate (234 mg, 0.9 mmol, 1.0 eq.), and DBU (179 µL, 1.2 mmol, 1.33 eq.) in DCM (5 mL) was stirred at room temperature for 7 d. The mixture was evaporated and conc. HCl (5 mL) was added. The crude product was filtrated and washed with HCl (3x 10 mL) and pentane (3x 10 mL) to yield **28** (280 mg, 0.61 mmol, yield: 68%). mp: 231 °C. R_f = 0.20 (EtOAc). ^{1}H NMR: (300 MHz, DMSO-d_6) δ = 11.22 (s, 1H), 8.87 (d, *J* = 2.4 Hz, 1H), 8.26 (dd, *J* = 8.8, 2.4 Hz, 1H), 7.74–7.63 (m, 3H), 7.54 (d, *J* = 8.8 Hz, 2H) ppm. ^{13}C NMR: (75 MHz, DMSO-d_6) δ = 166.8, 164.5, 153.5, 151.5, 143.0, 142.6, 138.9, 138.2, 137.7, 137.3, 132.2, 125.1, 122.6, 120.9, 119.6, 119.2 ppm. MS (ESI) *m/z* [M + H$^+$] calcd for $C_{14}H_9IN_4O_2S_2$ 456.92 (100%), 457.92 (15.1%), 458.92 (9.0%), found 456.89 (100%), 457.87 (16.3%), 458.88 (8.0%); purity (HPLC) = 96%.

General procedure for the amide bond formation mediated by TBTU

The respective carboxylic acid (1.0 eq.), TBTU (1.1 eq.), and HOBt were dissolved in dry DMF and DIPEA (4.0 eq.) was added while cooling with an ice-water bath. The corresponding amine (1.0 eq.) was added after 30 min and the solution was stirred for 2 d at r.t. Water and EtOAc were added and the aqueous phase was extracted three times with EtOAc and the combined organic phases were washed with 2 M HCl, saturated $NaHCO_3$-solution, and saturated NaCl-solution three times each. The organic phase was dried with $MgSO_4$ and the solvent was evaporated under reduced pressure.

(*S*)-2-(*tert*-Butoxycarbonylamino)-*N*-(5,6-dimethoxybenzo[*d*]thiazol-2-yl)propionamide (6a): 864 mg, 2.27 mmol, yield: 48%. mp: 93–100 °C. R_f = 0.37 (CH/EtOAc 2:1). $[\alpha]_D^{20}$ = –39 (*c* = 10 in EtOAc). ^{1}H NMR: (300 MHz, $CDCl_3$) δ = 7.31 (s, 1H), 7.23 (s, 1H), 4.01–3.81 (m, 7H), 1.56–1.34 (m, 12H) ppm. ^{13}C NMR: (75 MHz, $CDCl_3$) δ = 171.8, 157.3, 155.8, 149.7, 147.9, 141.3, 123.3, 103.0, 102.9, 80.9, 56.5, 56.3, 50.6, 28.4, 18.1 ppm.

(*R*)-2-(*tert*-Butoxycarbonylamino)-*N*-(5,6-dimethoxybenzo[*d*]thiazol-2-yl)propionamide (6b): 561 mg, 1.47 mmol, yield: 77%. mp: 83–85 °C. R_f = 0.37 (CH/EtOAc 2:1). $[\alpha]_D^{20}$ = +43 (*c* = 10 in EtOAc). ^{1}H NMR: (300 MHz, $CDCl_3$) δ = 7.31 (s, 1H), 7.23 (s, 1H), 4.01–3.81 (m, 7H), 1.56–1.34 (m, 12H) ppm. ^{13}C NMR: (75 MHz, $CDCl_3$) δ = 171.8, 157.3, 155.8, 149.7, 147.9, 141.3, 123.3, 103.0, 102.9, 80.9, 56.5, 56.3, 50.6, 28.4, 18.1 ppm.

(*S*),(*S*)-2-(*tert*-Butoxycarbonylamino)-*N*-(5,6-dihydroxybenzo[*d*]thiazol-2-yl)-3-methylpentanoicamide (6c): 308 mg, 0.82 mmol, yield: 99%. mp = 99–103 °C. R_f = 0.47 (CH/EtOAc 1:1). $[\alpha]_D^{20}$ = –14 (*c* = 10 in EtOAc). ^{1}H NMR: (300 MHz, $CDCl_3$) δ = 7.39 (s, 1H), 7.17 (s, 1H), 4.40–4.25 (m, 1H), 3.89 (s, 3H), 3.89 (s, 3H), 1.83–1.68 (m, 1H), 1.46–1.27 (m, 10*H*), 1.05–0.83 (m, 1H), 0.78–0.58 (m, 6H) ppm. ^{13}C NMR: (75 MHz, $CDCl_3$) δ = 171.5, 157.9, 156.0, 149.9, 148.0, 140.5, 122.8, 102.9, 102.7, 80.4, 59.4, 56.5, 56.4, 37.6, 28.4, 24.7, 15.5, 11.1 ppm.

(*S*)-2-(*tert*-Butoxycarbonylamino)-*N*-(5,6-dimethoxybenzo[*d*]thiazol-2-yl)-3,3-dimethylbutyramide (6d): 1500 mg, 3.55 mmol, yield: 82%. mp = 185–195 °C. R_f = 0.51 (CH/EtOAc 1:1). $[\alpha]_D^{20}$ = +9 (*c* = 10 in DCM). ^{1}H NMR: (300 MHz, DMSO-d_6) δ = 7.54 (s, 1H), 7.29 (s, 1H), 4.22 (d, *J* = 8.6 Hz, 1H), 3.82 (s, 3H), 3.80 (s, 3H), 1.37 (s, 9H), 0.96 (s, 9H) ppm. ^{13}C NMR: (75 MHz, DMSO-d_6) δ = 170.9, 170.4, 155.9, 148.9, 147.0, 142.5, 122.9, 103.7, 103.5, 78.4, 62.1, 56.0, 55.7, 34.0, 28.2, 26.5 ppm.

(*S*)-2-(*tert*-Butoxycarbonylamino)-*N*-(5,6-dimethoxybenzo[*d*]thiazol-2-yl)-3-phenylpropionamide (6e): 370 mg, 0.81 mmol, yield: 72%. mp: 96–98 °C. R_f = 0.70 (CH/EtOAc 1:1). $[\alpha]_D^{20}$ = +24 (*c* = 10 in EtOAc). ^{1}H NMR: (300 MHz, $CDCl_3$) δ = 7.32 (s, 1H), 7.24 (s, 1H), 7.21–7.14 (m, 3H), 7.09–6.98 (m, 2H), 4.87–4.60 (m, 1H), 3.96 (s, 3H), 3.90 (s, 3H), 3.26–2.99 (m, 2H), 1.39 (s, 9H) ppm. ^{13}C NMR: (75 MHz, $CDCl_3$) δ = 170.9, 157.8, 155.6, 150.0, 148.1, 139.8, 135.7, 129.2, 128.8, 127.3, 122.6, 102.8, 102.6, 77.4, 56.5, 56.4, 56.1, 38.3, 28.3 ppm.

***tert*-Butyl (*S*)-(3-(benzylthio)-1-((5,6-dimethoxybenzo[*d*]thiazol-2-yl)amino)-1-oxopropan-2-yl)carbamate (6f)**: 305 mg, 0.60 mmol, yield: 34%. mp: 99 °C. R_f = 0.51 (CH/EtOAc 1:1). $[\alpha]_D^{20}$ = –61 (*c* = 5 in MeOH). ^{1}H NMR: (300 MHz, DMSO-d_6) δ = 12.46 (s, 1H), 7.56 (s, 1H), 7.37–7.17 (m, 6H), 4.64–4.42 (m, 1H), 3.93–3.72 (m, 8H), 2.87–2.58 (m, 2H), 1.40 (s, 9H) ppm. ^{13}C NMR: (75 MHz, DMSO-d_6) δ = 170.3, 155.2, 154.0, 148.9, 147.0, 142.5, 138.2, 128.9, 128.3, 126.9, 122.9, 103.7, 103.5, 78.5, 55.9, 55.74, 54.3, 35.0, 32.6, 28.1 ppm.

(*S*)-3-(4-(Benzyloxy)phenyl)-2-(*tert*-butoxycarbonylamino)-*N*-(5,6-dimethoxybenzo[*d*]thiazol-2-yl)propionamide (9a): 1039 mg, 1.84 mmol, yield: 97%. mp: 86–88 °C. R_f = 0.59 (CH/EtOAc 1:1). $[\alpha]_D^{20}$ = –38 (*c* = 10 in DCM). ^{1}H NMR: (300 MHz, $CDCl_3$) δ = 7.46–7.23 (m, 7H), 6.87 (d, *J* = 8.3 Hz, 2H), 6.75 (d, *J* = 8.3 Hz, 2H), 4.95 (s, 2H), 4.81–4.63 (m, 1H), 3.96 (s, 3H), 3.91 (s, 3H), 3.18–2.86 (m, 2H), 1.40 (s, 9H) ppm. ^{13}C NMR: (75 MHz, $CDCl_3$) δ = 170.9, 157.9, 157.3, 155.6, 149.7, 147.8, 142.0, 137.0, 130.2, 128.6, 128.0, 127.9, 127.6, 123.5, 115.0, 103.4, 102.8, 70.0, 69.9, 56.5, 56.3, 38.7, 37.6, 28.4 ppm.

Benzyl (*S*)-3-((*tert*-butoxycarbonyl)amino)-4-((5,6-dimethoxybenzo[*d*]thiazol-2-yl)amino)-4-oxobutanoate (9b): 604 mg, 1.17 mmol, yield: 95%. mp = 73–75 °C. R_f = 0.36 (CH/EtOAc 1:2). $[\alpha]_D^{20}$ = –17 (*c* = 10 in DCM). ^{1}H NMR: (300 MHz, $CDCl_3$) δ = 7.35–7.30 (m, 5H), 7.29 (s, 1H), 7.22 (s, 1H), 4.91–4,69 (m, 1H), 5.14 (d, *J* = 2.2 Hz, 2H) 3.94 (s, 3H), 3.93 (s, 3H), 3.20 (dd, *J* = 17.5, 4.6 Hz, 1H), 2.87 (dd, *J* = 17.5, 5.6 Hz, 1H), 1.47 (s, 9H) ppm. ^{13}C NMR: (75 MHz, $CDCl_3$) δ =

171.3, 169.1, 155.9, 155.6, 149.4, 147.7, 142.4, 135.1, 128.6, 128.5, 128.3, 123.8, 103.5, 102.7, 81.5, 67.2, 56.4, 56.2, 51.3, 35.7, 28.3 ppm.

3-(*tert*-Butoxycarbonylamino)-*N*-(5,6-dimethoxybenzo [*d*] thiazol-2-yl)propionamide (14): 1.58 g, 4.10 mmol, yield: 78%. mp: 130–135 °C. $R_f = 0.23$ (CH/EtOAc 1:1). ^{1}H NMR: (300 MHz, DMSO-d_6) $\delta = 7.53$ (s, 1H), 7.28 (s, 1H), 3.82 (s, 3H), 3.80 (s, 3H), 3.30–3.19 (m, 2H), 2.63 (t, $J = 6.8$ Hz, 2H), 1.36 (s, 9H) ppm. ^{13}C NMR: (75 MHz, DMSO-d_6) $\delta = 170.0$, 156.3, 155.5, 148.9, 146.9, 142.5, 122.8, 103.7, 103.5, 77.7, 55.9, 55.7, 36.0, 35.6, 28.2 ppm.

(*S*)-2-benzamido-*N*^{1}-(5,6-dimethoxybenzo [*d*] thiazol-2-yl)-*N*^{4}, *N*^{4}-diethylsuccinamide (19a): 200 mg, 0.41 mmol, yield: 35%. mp: 121–123 °C. $R_f = 0.32$ (CH/EtOAc 1:1). $[\alpha]_D{}^{20} = +2$ ($c = 10$ in DCM). ^{1}H NMR: (300 MHz, $CDCl_3$) $\delta = 7.90$ (d, $J = 7.2$ Hz, 1H), 7.59–7.39 (m, 3H), 7.29 (s, 1H), 7.19 (s, 1H), 5.28 (td, $J = 6.8$, 3.0 Hz, 1H), 3.93 (s, 3H), 3.92 (s, 3H), 3.54–3.24 (m, 5H), 2.84–2.63 (m, 1H), 1.28–1.19 (m, 6H) ppm. ^{13}C NMR: (75 MHz, $CDCl_3$) $\delta = 170.3$, 169.6, 167.4, 156.4, 149.5, 147.7, 141.6, 133.0, 132.2, 128.7, 127.4, 123.2, 103.2, 102.6, 56.4, 56.1, 50.6, 42.6, 40.8, 34.4, 14.1, 13.0 ppm.

(*S*)-2-Benzamido-*N*^{1}-(5,6-dimethoxybenzo [*d*] thiazol-2-yl)-*N*^{4}-phenylsuccinamide (19b): 88 mg, 0.18 mmol, yield: 65%. mp: 205–208 °C. $R_f = 0.17$ (CH/EtOAc 1:1). $[\alpha]_D{}^{20} = +3$ ($c = 10$ in DCM). ^{1}H NMR: (300 MHz, DMSO-d_6) $\delta = 7.93$ (d, $J = 7.5$ Hz, 2H), 7.65 (d, $J = 8.0$ Hz, 2H), 7.57–7.42 (m, 4H), 7.35–7.23 (m, 3H), 7.05 (t, $J = 7.4$ Hz, 1H), 5.14–5.01 (m, 1H), 3.82 (s, 3H), 3.80 (s, 3H), 3.22–3.01 (m, 2H) ppm. ^{13}C NMR: (75 MHz, DMSO-d_6) $\delta = 170.0$, 169.3, 166.9, 156.7, 149.4, 147.4, 143.0, 139.5, 134.3, 131.9, 129.1, 128.7, 128.0, 123.8, 123.3, 119.8, 104.2, 104.0, 56.5, 56.2, 51.5, 37.5 ppm.

(2-((5,6-Dimethoxybenzo [*d*] thiazol-2-yl)amino)-2-oxoethyl)-*N*-phenylbenzamide (22a): 300 mg, 0.67 mmol, yield: 52%. mp: 231 °C. $R_f = 0.61$ (CH/EtOAc 1:1). ^{1}H NMR: (300 MHz, DMSO-d_6) $\delta =$ 12.41 (s, 1H), 7.53 (s, 1H), 7.32 (d, $J = 4.8$ Hz, 1H), 7.31–7.09 (m, 10*H*), 4.80 (s, 2H), 4.01–3.87 (m, 6H) ppm. ^{13}C NMR: (75 MHz, DMSO-d_6) $\delta =$ 169.7, 167.6, 156.1, 148.9, 147.0, 143.8, 142.5, 135.4, 129.8, 128.8, 128.4, 127.8, 127.5, 126.6, 122.8, 103.7, 103.6, 55.9, 55.7, 53.1 ppm.

***N*-(5,6-Dimethoxybenzo [*d*] thiazol-2-yl)-2,2-diphenylacetamide (22b)**: 550 mg, 136 mmol, yield: 68%. mp: 234 °C. $R_f = 0.59$ (CH/EtOAc 1:1). ^{1}H NMR: (300 MHz, DMSO-d_6) $\delta = 12.69$ (s, 1H), 7.54 (s, 1H), 7.40–7.24 (m, 11*H*), 5.40 (s, 1H), 4.04–3.85 (m, 6H) ppm. ^{13}C NMR: (75 MHz, DMSO-d_6) $\delta = 170.3$, 156.2, 148.9, 147.0, 142.4, 138.9, 128.5, 128.5, 127.1, 122.8, 103.6, 103.5, 59.7, 55.9, 55.7 ppm. MS (ESI) m/z [M + H$^+$] calcd for $C_{23}H_{20}N_2O_3S$ 405.12 (100%), 406.12 (24.9%), 407.12 (4.5%), found 405.23 (100%), 406.19 (24.8%), 407.15 (4.0%); purity (HPLC) = 99%.

***N*-(5,6-Dimethoxybenzo [*d*] thiazol-2-yl)-2,2-bis-(4-methoxyphenyl)acetamide (22c)**: 120 mg, 0.25 mmol, yield: 25%. mp: 242 °C. $R_f = 0.40$ (CH/EtOAc 1:1). ^{1}H NMR: (300 MHz, DMSO-d_6) $\delta = 12.52$ (s, 1H), 7.53 (s, 1H), 7.31–7.17 (m, 5H), 6.91 (d, $J = 8.4$ Hz, 4H), 5.25 (s, 1H), 4.00–3.84 (m, 6H), 3.72 (s, 6H) ppm. ^{13}C NMR: (75 MHz, DMSO-d_6) $\delta = 172.0$, 158.3, 156.3, 148.9, 147.0, 142.5, 131.3, 129.5, 122.8, 113.9, 103.6, 103.5, 55.9, 55.7, 55.1, 54.4 ppm.

***N*-(5,6-Dimethoxybenzo [*d*] thiazol-2-yl)-2,2-bis-(4-chlorophenyl)acetamide (22d)**: 230 mg, 0.48 mmol, yield: 54%. mp: 251 °C. $R_f = 0.48$ (CH/EtOAc 1:1). ^{1}H NMR: (300 MHz, DMSO-d_6) $\delta =$ 7.54 (s, 1H), 7.46–7.27 (m, 9H), 5.47 (s, 1H), 3.81 (d, $J = 4.4$ Hz, 6H) ppm. ^{13}C NMR: (75 MHz, DMSO-d_6) $\delta = 169.8$, 156.0, 148.9, 147.1, 142.4, 137.5, 132.0, 130.4, 128.6, 122.8, 103.6, 103.5, 56.0, 55.7, 54.5 ppm.

***N*-(5,6-Dimethoxybenzo [*d*] thiazol-2-yl)-4-iodobenzamide (24b)**: 223 mg, 0.51 mmol, yield 51%. mp: 298 °C. $R_f = 0.66$ (CH/EtOAc 1:1). ^{1}H NMR: (300 MHz, DMSO-d_6) $\delta = 12.81$ (s, 1H), 7.95 (d, $J = 8.6$ Hz, 2H), 7.88 (d, $J = 8.6$ Hz, 2H), 7.59 (s, 1H), 7.30 (s, 1H), 4.06–3.82 (m, 6H) ppm. ^{13}C NMR: (75 MHz, DMSO-d_6) $\delta = 172.5$, 158.7, 149.0, 147.2, 137.5, 137.0, 131.6, 130.1, 129.4, 122.9, 103.7, 100.9, 56.0, 55.6 ppm. MS (ESI) m/z [M + H$^+$] calcd for $C_{16}H_{13}IN_2O_3S$ 440.97 (100%), 441.97 (17.3%), 442.97 (4.5%), found 441.05 (100%), 442.05 (16.3%), 443.00 (4.3%); purity (HPLC) = 97%.

4-Chloro-*N*-(5,6-dimethoxybenzo [*d*] thiazol-2-yl)benzamide (24c): 378 mg, 1.08 mmol, yield: 85%. mp: 254 °C. $R_f = 0.30$ (DCM/MeOH 49:1). ^{1}H NMR: (300 MHz, DMSO-d_6): $\delta = 7.89$ (d, $J = 8.3$ Hz, 2H), 7.38 (d, $J = 8.3$ Hz, 2H), 7.34 (s, 1H), 7.07 (s, 1H) 3.90–3.76 (m, 6H) ppm. ^{13}C NMR: (75 MHz, DMSO-d_6): $\delta = 165.1$, 157.8, 149.5, 147.6, 142.4, 138.0, 131.4, 130.7, 129.2, 123.3, 104.2, 103.6, 56.4, 56.2 ppm.

4-Methyl-*N*-(5,6-dimethoxybenzothiazol-2-yl)benzamide (24d): 502 mg, 1.53 mmol yield: 99%. mp: 254 °C. $R_f = 0.30$ (DCM/MeOH 49:1). ^{1}H NMR: (300 MHz, DMSO-d_6): $\delta = 8.02$ (d, $J = 7.8$ Hz, 2H), 7.57 (s, 1H), 7.35 (d, $J = 7.8$ Hz, 2H), 7.30 (s, 1H), 3.82 (s, 6H), 2.38 (s, 3H) ppm. ^{13}C NMR: (75 MHz, DMSO-d_6): $\delta = 165.8$, 157.8, 149.4, 147.5, 143.5, 142.7, 123.4, 129.7, 129.6, 128.7, 104.2, 103.7, 56.4, 56.2, 21.6 ppm.

***N*-(5,6-dimethoxybenzo [*d*] thiazol-2-yl)- [1,1́-biphenyl] -4-carboxamide (24e)**: 295 mg, 0.75 mmol, yield: 75%. mp: 273 °C. $R_f = 0.70$ (CH/EtOAc 1:1). ^{1}H NMR: (300 MHz, DMSO-d_6) $\delta = 12.71$ (s, 1H), 8.27–8.19 (m, 2H), 7.87 (d, $J = 8.2$ Hz, 2H), 7.79 (d, $J = 7.6$ Hz, 2H), 7.58–7.48 (m, 4H), 7.32 (s, 1H), 3.88–3.81 (m, 6H) ppm. ^{13}C NMR: (75 MHz, DMSO-d_6) $\delta = 170.4$, 157.1, 149.0, 147.1, 138.8, 144.3, 139.1, 129.9, 129.6, 128.9, 128.1, 126.9, 126.7, 126.7, 107.4, 106.4, 98.9, 59.7, 55.9 ppm.

3,4-Dichloro-*N*-(5,6-dimethoxybenzo [*d*] thiazol-2-yl)benzamide (24f): 95 mg, 0.29 mmol, yield: 24%. mp: 150 °C. $R_f = 0.30$ (DCM/MeOH 49:1). ^{1}H NMR: (300 MHz, DMSO-d_6): $\delta = 8.43$ (s, 1H), 8.12 (d, $J =$ 8.5 Hz, 1H), 7.89 (d, $J = 8.5$ Hz, 1H), 7.64 (s, 1H), 7.36 (s, 1H), 4.00–3.84 (m, 6H) ppm. ^{13}C NMR: (75 MHz, DMSO-d_6): $\delta =$ 172.5, 164.1, 149.5, 147.7, 142.2, 135.8, 133.2, 131.4, 130.7, 129.0, 123.4, 104.2, 103.5, 56.44, 56.2 ppm.

4-Iodo-*N*-(6-nitrobenzo [*d*] thiazol-2-yl) benzamide (27): 171 mg, 0.30 mmol, yield: 74%. mp: 211 °C. $R_f = 0.21$ (CH/EtOAc 3:1). ^{1}H NMR: (300 MHz, DMSO-d_6) $\delta = 13.34$ (s, 1H), 9.10 (d, $J = 2.4$ Hz, 1H), 8.31 (dd, $J = 9.0$, 2.4 Hz, 1H), 8.01–7.88 (m, 5H) ppm. ^{13}C NMR: (75 MHz, DMSO-d_6) $\delta = 177.6$, 165.8, 150.4, 143.1, 138.3, 137.6, 130.2, 121.8, 119.1, 101.7 ppm. MS (ESI) m/z [M + H$^+$] calcd for $C_{14}H_8IN_3O_3S$ 425.93 (100%), 426.94 (15.1%), 427.93 (4.5%), found 425.88 (100%), 426.91 (14.6%), 427.90 (2.0%); purity (HPLC) = 97%.

5,6-Dimethoxy-*N*-phenylbenzo [*d*] thiazole-2-carboxamide (33a): 180 mg, 0.57 mmol, yield: 90%. mp: 205–207 °C. $R_f = 0.76$ (CH/EtOAc 1:2). ^{1}H NMR: (300 MHz, DMSO-d_6): $\delta = 10.87$ (s, 1H), 7.89 (d, J = 7.4 Hz, 2H), 7.79 (s, 1H), 7.59 (s, 1H), 7.38 (t, $J = 7.4$ Hz, 2H), 7.15 (t, $J = 7.4$ Hz, 1H), 3.90 (s, 3H), 3.89 (s, 3H) ppm. ^{13}C NMR: (75 MHz, DMSO-d_6): $\delta = 161.8$, 158.3, 149.9, 147.0, 138.0, 129.4, 128.8, 124.3, 120.6, 104.9, 103.6, 56.0, 55.8 ppm. MS (ESI) m/z [M + H$^+$] calcd for $C_{16}H_{14}N_2O_3S$ 315.1, found 315.2.

6-Methoxy-*N*-phenylbenzo [*d*] thiazole-2-carboxamide (33b): 180 mg, 0.63 mmol, yield: 88%. mp: 163–165 °C. $R_f = 0.67$ (CH/EtOAc 2:1). ^{1}H NMR: (300 MHz, DMSO-d_6): $\delta = 10.99$ (s, 1H), 8.08 (d, $J = 9.1$ Hz, 1H), 7.96–7.85 (m, 2H), 7.81 (d, $J = 2.6$ Hz, 1H), 7.44–7.31 (m, 2H), 7.24 (dd, $J = 9.1$, 2.6 Hz, 1H), 7.21–7.09 (m, 1H), 3.88 (s, 3H) ppm. ^{13}C NMR: (75 MHz, DMSO-d_6): $\delta = 161.8$, 158.7, 158.3, 147.1, 138.3, 138.0, 128.7, 124.8, 124.4, 120.7, 117.4, 104.8, 55.9 ppm. MS (ESI) m/z [M + H$^+$] calcd for $C_{15}H_{12}N_2O_2S$ 285.1, found 285.1.

5,6-Dimethoxy-*N*-phenyl-1*H*-indole-2-carboxamide (33c): 140 mg, 0.47 mmol, yield: 69%. mp: decomp. > 215 °C. $R_f = 0.23$ (CH/EtOAc 2:1). ^{1}H NMR: (300 MHz, DMSO-d_6): $\delta = 11.44$ (s, 1H), 10.02 (s, 1H), 7.84–7.67 (m, 2H), 7.55–7.27 (m, 3H), 7.16–7.02 (m, 2H), 6.93 (s, 1H), 3.79 (s, 3H), 3.78 (s, 3H) ppm. ^{13}C NMR: (75 MHz, DMSO-d_6): $\delta =$ 159.7, 148.8, 145.5, 139.2, 132.0, 129.7, 128.7, 123.3, 120.1, 119.9, 104.1, 102.8, 94.6, 55.8, 55.5 ppm. MS (ESI) m/z [M + H$^+$] calcd for $C_{17}H_{16}N_2O_3$ 297.1, found 297.2.

5,6-Dimethoxy-*N*-phenylbenzo [*b*] thiophene-2-carboxamide (33d): 160 mg, 0.50 mmol, yield: 99%. mp: 204–206 °C. $R_f = 0.36$ (CH/EtOAc 2:1). ^{1}H NMR: (300 MHz, DMSO-d_6): $\delta = 10.38$ (s, 1H), 8.19 (s, 1H), 7.75 (d, $J = 7.7$ Hz, 2H), 7.59 (s, 1H), 7.44 (s, 1H), 7.36 (t, $J = 7.7$ Hz, 2H), 7.11 (t, $J = 7.7$ Hz, 1H), 3.86 (s, 6H) ppm. ^{13}C NMR: (75 MHz, DMSO-d_6): $\delta = 160.5$, 149.9, 148.5, 138.8, 137.5, 134.3, 132.5, 128.8,

125.7, 123.8, 120.4, 106.2, 104.3, 55.9 ppm. MS (ESI) *m/z* [M + H^+] calcd for $C_{17}H_{15}NO_3S$ 314.1, found 314.2.

5,6-Dimethoxy-*N*-phenylbenzofuran-2-carboxamide (33e): 180 mg, 0.61 mmol, yield: 90%. mp: 187–189 °C. R_f = 0.37 (CH/EtOAc 2:1). ^{1}H NMR: (300 MHz, DMSO-d_6): δ = 10.33 (s, 1H), 7.81 (d, J = 7.7 Hz, 2H), 7.67 (s, 1H), 7.36 (t, J = 7.7 Hz, 2H), 7.32–7.24 (m, 2H), 7.11 (d, J = 7.7 Hz, 1H), 3.86 (s, 3H), 3.82 (s, 3H) ppm. ^{13}C NMR: (75 MHz, DMSO-d_6): δ = 156.7, 150.3, 149.8, 147.7, 147.2, 138.6, 128.7, 123.8, 120.4, 118.9, 111.1, 103.3, 95.5, 56.0, 55.9 ppm. MS (ESI) *m/z* [M + H^+] calcd for $C_{17}H_{15}NO_4$ 298.10 (100%), 299.10 (18.4%), 300.11 (1.6%), found 298.18 (100%), 299.18 (16.7%), 300.17 (1.0%); purity (HPLC) = 99%.

6,7-Dimethoxy-*N*-phenylquinoline-3-carboxamide (33f): 140 mg, 0.45 mmol, yield: 70%. mp: 201–203 °C. R_f = 0.53 (DCM/MeOH 19:1). ^{1}H NMR: (300 MHz, DMSO-d_6): δ = 10.48 (s, 1H), 9.17 (d, J = 2.2 Hz, 1H), 8.74 (d, J = 2.2 Hz, 1H), 7.82 (d, J = 7.7 Hz, 2H), 7.49 (s, 1H), 7.47 (s, 1H), 7.38 (t, J = 7.7 Hz, 2H), 7.13 (t, J = 7.7 Hz, 1H), 3.98 (s, 3H), 3.94 (s, 3H) ppm. ^{13}C NMR: (75 MHz, DMSO-d_6): δ = 164.4, 153.6, 150.0, 146.5, 146.1, 139.1, 134.1, 128.7, 125.8, 123.8, 122.1, 120.3, 107.5, 106.4, 55.9, 55.8 ppm. MS (ESI) *m/z* [M + H^+] calcd for $C_{17}H_{15}NO_4$ 298.1, found 298.2.

5-Methoxy-*N*-phenylbenzofuran-2-carboxamide (33g): 170 mg, 0.64 mmol, yield: 94%. mp: 168–170 °C. R_f = 0.40 (CH/EtOAc 4:1). ^{1}H NMR: (300 MHz, DMSO-d_6) δ = 10.48 (s, 1H), 7.87–7.77 (m, 2H), 7.73–7.66 (m, 3H), 7.62 (d, J = 9.1 Hz, 1H), 7.42–7.33 (m, 2H), 7.34–7.27 (m, 2H), 7.18–7.04 (m, 2H), 3.81 (s, 3H) ppm. ^{13}C NMR: (75 MHz, DMSO-d_6) δ = 156.7, 156.1, 149.4, 138.4, 128.7, 127.8, 124.1, 120.5, 116.5, 112.6, 110.8, 104.2, 55.6 ppm.

6-Methoxy-*N*-phenylbenzofuran-2-carboxamide (33h): 165 mg, 0.62 mmol, yield: 91%. mp: 134–136 °C. R_f = 0.4 (CH/EtOAc 4:1). ^{1}H NMR: (300 MHz, DMSO-d_6) δ = 10.37 (s, 1H), 7.86–7.76 (m, 2H), 7.74–7.64 (m, 2H), 7.36 (dd, J = 8.6, 7.3 Hz, 2H), 7.30–7.23 (m, 1H), 7.17–7.06 (m, 1H), 6.99 (dd, J = 8.6, 2.3 Hz, 1H), 3.85 (s, 3H) ppm. ^{13}C NMR: (75 MHz, DMSO-d_6) δ = 159.7, 156.7, 155.8, 148.0, 138.5, 128.7, 123.9, 123.2, 120.4, 120.3, 113.4, 110.8, 95.9, 55.7 ppm.

4,6-Dimethoxy-*N*-phenylbenzofuran-2-carboxamide (33i): 160 mg, 0.54 mmol, yield: 79%. mp: 144–146 °C. R_f = 0.25 (CH/EtOAc 4:1). ^{1}H NMR: (300 MHz, DMSO-d_6) δ = 10.25 (s, 1H), 7.84–7.75 (m, 2H), 7.76–7.70 (m, 2H), 7.41–7.30 (m, 2H), 7.16–7.05 (m, 1H), 6.89–6.83 (m, 2H), 6.49 (d, J = 1.9 Hz, 1H), 3.91 (s, 3H), 3.84 (s, 3H) ppm. ^{13}C NMR: (75 MHz, DMSO-d_6) δ = 161.2, 156.6, 154.2, 146.6, 138.6, 128.7, 123.8, 120.3, 111.1, 108.1, 95.2, 88.5, 55.9, 55.8, 52.8 ppm.

6-Methoxy-5-nitro-*N*-phenylbenzofuran-2-carboxamide (33j): 760 mg, 2.4 mmol, yield: 97%. mp: 184–186 °C. R_f = 0.44 (CH/EtOAc 2:1). ^{1}H NMR: (300 MHz, DMSO-d_6): δ = 10.51 (s, 1H), 8.44 (s, 1H), 7.85 (d, J = 0.9 Hz, 1H), 7.81–7.73 (m, 2H), 7.67 (d, J = 0.9 Hz, 1H), 7.43–7.32 (m, 2H), 7.20–7.08 (m, 1H), 4.00 (s, 3H) ppm. ^{13}C NMR: (75 MHz, DMSO-d_6): δ = 157.2, 156.5, 152.7, 150.6, 138.7, 138.5, 129.2, 124.7, 121.0, 120.4, 119.8, 111.3, 98.0, 57.8 ppm.

5,6-Dimethoxy-*N*-(4-iodophenyl)benzo [*d*] thiazole-2-carboxamide (33k): 230 mg, 0.52 mmol, yield: 76%. mp: 181–185 °C. R_f = 0.55 (CH/EtOAc 2:1). ^{1}H NMR: (300 MHz, DMSO-d_6): δ = 10.96 (s, 1H), 7.78–7.67 (m, 5H), 7.57 (s, 1H), 3.89 (d, J = 2.0 Hz, 6H) ppm. ^{13}C NMR: (75 MHz, DMSO-d_6): δ = 161.4, 158.4, 150.0, 150.0, 146.9, 137.9, 137.4, 129.5, 122.7, 104.9, 103.5, 88.3, 56.0, 55.8 ppm.

(*S*)-1-(5,6-Dimethoxybenzo [*d*] thiazole-2-carbonyl)-*N*-phenylpyrrolidine-2-carboxamide (35a): 210 mg, 0.51 mmol, yield: 81%. mp: 237–239 °C. R_f = 0.47 (CH/EtOAc 1:2). $[\alpha]_D^{20}$ = –10 (c = 5 in DMSO). ^{1}H NMR: (300 MHz, DMSO-d_6): δ = 10.2 (s, 1H), 7.74–7.52 (m, 3H), 7.38–7.20 (m, 3H), 7.11–6.39 (m, 1H), 4.76–4.56 (m, 1H), 4.36–4.23 (m, 1H), 3.88 (s, 3H), 3.82 (s, 3H), 3.79–3.72 (m, 1H), 2.37–1.82 (m, 4H) ppm. ^{13}C NMR: (75 MHz, DMSO-d_6): δ = 171.2, 169.0, 159.0, 149.9, 149.7, 147.5, 139.5, 128.7, 128.5, 123.3, 119.2, 105.5, 103.2, 62.3, 55.9, 55.5, 48.7, 32.1, 21.8 ppm. MS (ESI) *m/z* [M + H^+] calcd for $C_{21}H_{21}N_3O_4S$ 412.1, found 412.1.

(*S*)-1-(6-Methoxybenzo [*d*] thiazole-2-carbonyl)-*N*-phenylpyrrolidine-2-carboxamide (35b): 150 mg, 0.39 mmol, yield: 54%. mp: 209–211 °C. R_f = 0.28 (CH/EtOAc 2:1). $[\alpha]_D^{20}$ = –6 (c = 5 in DMSO). ^{1}H NMR: (300 MHz, DMSO-d_6): δ = 10.21 (s, 1H), 8.05 (d, J = 9.0 Hz, 1H), 7.78–7.57 (m, 2H), 7.55–7.48 (m, 1H), 7.34–7.17 (m, 3), 7.14–6.95 (m, 1H), 5.58–5.39 (m, 1H), 4.34–4.17 (m, 1H), 3.84 (s, 3H), 3.78–3.64 (m, 1H), 2.47–1.85 (m, 4H) ppm. ^{13}C NMR: (75 MHz, DMSO-d_6): δ = 170.9, 169.9, 159.0, 147.6, 147.2, 139.3, 128.7, 125.3, 124.8, 123.3, 119.3, 117.0, 104.3, 62.2, 55.8, 49.6, 32.2, 21.7 ppm. MS (ESI) *m/z* [M + H^+] calcd for $C_{20}H_{19}N_3O_3S$ 382.1, found 382.1.

(*S*)-1-(5,6-Dimethoxy-1*H*-indole-2-carbonyl)-*N*-phenylpyrrolidine-2-carboxamide (35c): 250 mg, 0.63 mmol, yield: 93%. mp: 113–115 °C. R_f = 0.33 (CH/EtOAc 1:2). $[\alpha]_D^{20}$ = –62 (c = 5 in DMSO). ^{1}H NMR: (300 MHz, DMSO-d_6): δ = 11.26 (s, 1H), 10.10 (s, 1H), 7.71–7.53 (m, 2H), 7.36–7.24 (m, 2H), 7.14–7.00 (m, 2H), 6.96–6.88 (m, 2H), 4.74–4.64 (m, 1H), 4.09–3.85 (m, 2H), 3.40 (s, 6H), 2.31–2.06 (m, 1H), 2.06–1.89 (m, 3H) ppm. ^{13}C NMR: (75 MHz, DMSO-d_6): δ = 170.8, 160,4, 148.7, 145.3, 139.3, 131.1, 129.0, 128.7, 123.2, 120.2, 119.2, 105.4, 102.8, 94.5, 61.7, 55.7, 55.4, 48.8, 29.1, 25.1 ppm. MS (ESI) *m/z* [M + H^+] calcd for $C_{22}H_{23}N_3O_4$ 394.2, found 394.2.

(*S*)-1-(5,6-Dimethoxybenzo [*b*] thiophene-2-carbonyl)-*N*-phenylpyrrolidine-2-carboxamide (35d): 210 mg, 0.50 mmol, yield: 99%. mp: 95–97 °C. R_f = 0.13 (CH/EtOAc 2:1). $[\alpha]_D^{20}$ = –16 (c = 5 in MeCN). ^{1}H NMR: (300 MHz, DMSO-d_6): δ = 10.10 (s, 1H), 7.90 (s, 1H), 7.62 (d, J = 7.7 Hz, 2H), 7.55 (s, 1H), 7.45 (s, 1H), 7.30 (d, J = 7.7 Hz, 2H), 7.04 (t, J = 7.7 Hz, 1H), 4.70–4.60 (m, 1H), 4.04–3.92 (m, 2H), 3.84 (s, 3H), 3.83 (s, 3H), 2.33–2.22 (m, 1H), 2.18–2.06 (m, 1H), 2.05–1.89 (m, 2H) ppm. ^{13}C NMR: (75 MHz, DMSO-d_6): δ = 170.4, 161.1, 149.8, 148.3, 139.2, 136.9, 133.5, 132.8, 128.7, 126.8, 123.2, 119.2, 106.3, 103.9, 62.0, 55.8, 55.6, 49.4, 29.2, 25.2 ppm. MS (ESI) *m/z* [M + H^+] calcd for $C_{22}H_{22}N_2O_4S$ 411.1, found 411.2.

(*S*)-1-(5,6-Dimethoxybenzofuran-2-carbonyl)-*N*-phenylpyrrolidine-2-carboxamide (35e): 250 mg, 0.63 mmol, yield: 93%. mp: 184–186 °C. R_f = 0.17 (CH/EtOAc 1:2). $[\alpha]_D^{20}$ = –80 (c = 5 in MeCN). ^{1}H NMR: (300 MHz, DMSO-d_6): δ = 10.11 (s, 1H), 7.67–7.55 (m, 2H), 7.44 (s, 1H), 7.36–7.24 (m, 3H), 7.15 (s, 1H), 7.01–6.98 (m, 1H), 4.72–4.62 (m, 1H), 4.05–3.97 (m, 2H), 3.84 (s, 3H), 3.80 (s, 3H), 2.33–2.18 (m, 1H), 2.16–1.83 (m, 3H) ppm. ^{13}C NMR: (75 MHz, DMSO-d_6): δ = 170.4, 157.6, 150.1, 149.5, 147.8, 147.1, 139.2, 128.7, 123.2, 119.2, 118.6, 112.5, 103.1, 95.5, 61.6, 61.3, 59.8, 56.0, 55.8, 48.6, 48.1, 32.3, 29.0, 25.0, 21.7, 20.7, 14.1 ppm. MS (ESI) *m/z* [M + H^+] calcd for $C_{22}H_{22}N_2O_5$ 395.15 (100%), 396.16 (23.8%), 397.16 (2.7%), found 395.20 (100%), 396.17 (26.7%), 397.16 (2.4%); purity (HPLC) = 99%.

(*S*)-1-(6,7-Dimethoxyquinoline-3-carbonyl)-*N*-phenylpyrrolidine-2-carboxamide (35f): 30 mg, 0.57 mmol, yield: 89%. mp: 112–114 °C. R_f = 0.18 (DCM/MeOH 49:1). $[\alpha]_D^{20}$ = –44 (c = 5 in MeCN). ^{1}H NMR: (300 MHz, DMSO-d_6): δ = 10.13 (s, 1H), 8.83 (d, J = 2.1 Hz, 1H), 8.46 (d, J = 2.1 Hz), 7.65 (t, J = 7.8 Hz, 2H), 7.48 (s, 1H), 7.42 (s, 1H), 7.32 (t, J = 7.8 Hz, 2H), 7.05 (t, J = 7.8 Hz, 1H), 4.73–4.62 (m, 1H), 3.96 (s, 3H), 3.92 (s, 3H), 3.74–3.60 (m, 2H), 2.38–2.25 (m, 1H), 2.38–2.04 (m, 3H) ppm. ^{13}C NMR: (75 MHz, DMSO-d_6): δ = 170.4, 166.7, 153.3, 150.0, 146.3, 145.2, 139.2, 133.2, 128.7, 127.2, 123.2, 122.0, 119.2, 107.4, 106.3, 61.0, 55.8, 54.9, 29.8, 25.2. MS (ESI) *m/z* [M + H^+] calcd for $C_{23}H_{23}N_3O_4$ 406.2, found 406.2.

(*S*)-1-(4,6-Dimethoxybenzofuran-2-carbonyl)-*N*-phenylpyrrolidine-2-carboxamide (35i): 260 mg, 0.67 mmol, yield: 98%. mp: 125–128 °C. R_f = 0.43 (CH/EtOAc 1:2). $[\alpha]_D^{20}$ = –50 (c = 5 in MeOH). ^{1}H NMR: (300 MHz, DMSO-d_6): δ = ^{1}H NMR: (300 MHz, DMSO-d_6) δ = 10.36–9.96 (m, 1H), 7.66–7.52 (m, 2H), 7.41–7.23 (m, 3H), 7.09–6.99 (m, 1H), 6.88 (s, 1H), 6.50–6.35 (m, 1H), 5.14–4.59 (m, 1H), 4.09–3.94 (m, 1H), 3.93–3.63 (m, 6H), 2.46–1.82 (m, 4H) ppm. ^{13}C NMR: (75 MHz, DMSO-d_6): δ = 170.3, 161.0, 157.4, 156.2, 154.1, 146.7, 139.1, 128.7, 123.2, 119.3, 119.2, 110.8, 109.2, 95.1, 88.3, 61.6, 61.3, 55.9, 55.7, 48.6, 48.2, 32.3, 29.0, 25.0, 21.7 ppm.

(*S*)-1-(6,7-Dimethoxy-2-naphthoyl)-*N*-phenylpyrrolidine-2-carboxamide (35m): 150 mg, 0.37 mmol, yield: 86%. mp: 173–175 °C. R_f

= 0.33 (CH/EtOAc 1:2). ^{1}H NMR: (300 MHz, DMSO-d_6): δ = 10.10 (s, 1H), 8.01 (s, 1H), 7.79 (d, J = 8.3 Hz, 1H), 7.72 (s, 1H), 7.65 (d, J = 8.3 Hz, 1H), 7.52–7.41 (m, 2H), 7.39–7.19 (m, 3H), 7.11–6.99 (m, 1H), 4.70–4.59 (m, 1H), 3.93–3.82 (m, 6H), 3.73–3.55 (m, 2H), 2.35–2.24 (m, 1H), 2.04–1.80 (m, 3H) ppm. ^{13}C NMR: (75 MHz, DMSO-d_6): δ = 170.7, 168.6, 150.3, 149.8, 139.2, 131.7, 129.6, 128.7, 127.9, 126.1, 125.6, 123.2, 122.7, 119.2, 107.1, 106.3, 60.8, 55.5, 50.2, 29.8, 25.2 ppm. MS (ESI) *m/z* [M + H$^+$] calcd for $C_{24}H_{24}N_2O_4$ 405.2, found 405.2.

(*S*)-1-(5,6-Dimethoxybenzofuran-2-carbonyl)-*N*-phenylpiperidine-2-carboxamide (35n): 155 mg, 0.38 mmol, yield: 56%. mp: 104–106 °C. R_f = 0.22 (CH/EtOAc 2:1). $[\alpha]_D^{20}$ = –148 (c = 10 in MeCN). ^{1}H NMR: (300 MHz, DMSO-d_6) δ = 10.01 (s, 1H), 7.67–7.57 (m, 2H), 7.37–7.26 (m, 3H), 7.21 (s, 1H), 7.12–7.01 (m, 1H), 5.15 (d, J = 3.9 Hz, 1H), 4.36 (d, J = 12.8 Hz, 1H), 3.92–3.70 (m, 6H), 2.23 (d, J = 14.0 Hz, 1H), 1.91–1.63 (m, 3H), 1.61–1.37 (m, 3H) ppm. ^{13}C NMR: (75 MHz, DMSO-d_6) δ = 169.8, 160.6, 149.8, 149.1, 147.5, 147.0, 138.9, 128.7, 123.5, 119.7, 118.4, 103.1, 95.5, 55.9, 55.9, 28.1, 27.8, 24.7, 20.2 ppm. MS (ESI) *m/z* [M + Na$^+$] calcd for $C_{23}H_{24}N_2O_5$ 431.16 (100%), 432.16 (24.9%), 433.17 (2.7%), found 431.30 (100%), 432.30 (26.0%), 433.26 (2.4%); purity (HPLC) = 99%.

General procedure for the deprotection of Boc-groups by HCl

The Boc-protected amide was placed in a round-bottom flask and dissolved in HCl (4 M in dioxane). After stirring for 30 min at room temperature, crystallization was induced by the addition of pentane and the product was obtained by filtration.

(*S*)-2-Amino-*N*-(5,6-dimethoxybenzo[*d*]thiazol-2-yl)-3-(4-benzoxyphenyl)propionamide hydrochloride (10a): 387 mg, 0.77 mmol, yield: 87%. mp: 215–219 °C. $[\alpha]_D^{20}$ = +46 (c = 10 in DMSO). ^{1}H NMR: (300 MHz, DMSO-d_6) δ = 7.58 (s, 1H), 7.47–7.25 (m, 6H), 7.26–7.11 (m, 2H), 7.01–6.86 (m, 2H), 5.07 (s, 1H), 5.03 (s, 1H), 4.43–4.33 (m, 1H), 3.85–3.76 (m, 6H), 3.24–3.05 (m, 2H) ppm. ^{13}C NMR: (75 MHz, DMSO-d_6) δ = 170.3, 157.6, 155.4, 149.1, 147.3, 142.3, 137.1, 130.7, 128.4, 127.8, 127.7, 127.0, 123.0, 114.8, 103.8, 103.7, 69.2, 56.0, 55.8, 53.3, 35.8 ppm.

(*S*)-Benzyl 3-amino-4-((5,6-dimethoxybenzo[*d*]thiazol-2-yl)amino)-4-oxobutanoate hydrochloride (10b): 414 mg, 0.92 mmol, yield: 95%. mp: 178–180 °C. $[\alpha]_D^{20}$ = +35 (c = 10 in H_2O). ^{1}H NMR: (300 MHz, DMSO-d_6) δ = 7.58 (s, 1H), 7.38–7.23 (m, 6H), 5.13 (s, 2H), 4.55–4.42 (m, 1H), 3.83 (s, 3H), 3.81 (s, 3H), 3.20 (d, J = 6.2 Hz, 2H) ppm. ^{13}C NMR: (75 MHz, DMSO–d_6) δ = 168.8, 167.0, 156.1, 149.1, 147.3, 141.9, 135.6, 128.4, 128.2, 128.1, 122.9, 103.8, 103.4, 66.4, 56.0, 55.8, 49.2, 34.8 ppm.

3-Amino-*N*-(5,6-dimethoxybenzo[*d*]thiazol-2-yl)propionamide hydrochloride (15): 291 mg, 0.92 mmol, yield: 70%. mp: 225–235 °C. ^{1}H NMR: (300 MHz, DMSO-d_6) δ = 7.54 (s, 1H), 7.29 (s, 1H), 3.81 (s, 3H), 3.79 (s, 3H), 3.18–3.03 (m, 2H), 2.98–2.86 (m, 2H) ppm. ^{13}C NMR: (75 MHz, DMSO-d_6) δ = 169.1, 156.1, 149.0, 147.0, 142.5, 122.8, 103.8, 103.6, 56.0, 55.8, 34.3, 32.5 ppm.

(*S*)-*N*-Phenylpyrrolidine-2-carboxamide hydrochloride (31a): 310 mg, 1.38 mmol, yield: 99%. mp: 237–239 °C. $[\alpha]_D^{25}$ = –36 (*S*, c = 5 in DMSO). ^{1}H NMR: (300 MHz, DMSO-d_6) δ = 11.02 (s, 1H), 10.19 (s, 1H), 8.66 (s, 1H), 7.65 (d, J = 7.7 Hz, 2H), 7.34 (t, J = 7.7 Hz, 2H), 7.10 (t, J = 7.7 Hz, 1H), 4.47–4.35 (m, 1H), 3.33–3.19 (m, 2H), 2.47–2.36 (m, 1H), 2.04–1.84 (m, 3H) ppm. ^{13}C NMR: (75 MHz, DMSO–d_6) δ = 166.8, 138.3, 128.9, 124.1, 119.5, 59.5, 45.6, 29.8, 23.7 ppm.

(*S*)-*N*-Phenylpiperidine-2-carboxamide hydrochloride (31b): 355 mg, 1.47 mmol, yield: 90%. decomp. > 270 °C. $[\alpha]_D^{20}$ = +3 (c = 3 in MeOH). ^{1}H NMR: (300 MHz, DMSO-d_6) δ = 11.09 (s, 1H), 9.64 (d, J = 9.4 Hz, 1H), 8.83 (d, J = 10.9 Hz, 1H), 7.74–7.56 (m, 2H), 7.42–7.24 (m, 2H), 7.16–6.96 (m, 1H), 4.11–3.89 (m, 1H), 3.31–3.17 (m, 1H), 2.97–2.82 (m, 1H), 2.34–2.22 (m, 1H), 1.86–1.42 (m, 5H) ppm. ^{13}C NMR: (75 MHz, DMSO–d_6) δ = 167.3, 138.4, 128.8, 123.9, 119.4, 57.6, 43.3, 27.1, 21.7, 21.2 ppm.

4.7. General procedure for the formation of amides by acid chlorides

The respective amine or the corresponding hydrochloride (1.0 eq.) was dissolved in dichloromethane and triethylamine (1.1 eq., in the case of the hydrochlorides 2.1 eq.) was added, followed by the addition of the acyl chloride (1.1 eq.) while cooling the reaction mixture with an ice-water bath. The cooling bath was removed, and the mixture was stirred for 16 h. After removal of the solvent under reduced pressure, the residue was purified by silica column chromatography.

(*S*)-*N*-(3-(4-(benzyloxy)phenyl)-1-((5,6-dimethoxybenzo[*d*]thiazol-2-yl)amino)-1-oxopropan-2-yl)benzamide (11a): 241 mg, 0.42 mmol, yield: 71%. mp: 182–184 °C. R_f = 0.38 (CH/EtOAc 1:1). $[\alpha]_D^{20}$ = –18 (c = 5 in DCM). ^{1}H NMR: (300 MHz, $CDCl_3$) δ = 7.85–7.77 (m, 2H), 7.47–7.24 (m, 10*H*), 7.01 (d, J = 8.6 Hz, 2H), 6.79 (d, J = 8.6 Hz, 2H), 5.37 (t, J = 6.9 Hz, 1H), 4.95 (d, J = 1.2 Hz, 2H), 3.99 (s, 3H), 3.89 (s, 3H), 3.28 (d, J = 6.9 Hz, 2H) ppm. ^{13}C NMR: (75 MHz, $CDCl_3$) δ = 170.6, 167.8, 158.1, 157.4, 149.8, 148.0, 141.6, 137.0, 133.4, 132.2, 130.4, 128.7, 128.7, 128.1, 127.8, 127.6, 127.4, 123.0, 115.2, 103.3, 102.9, 70.0, 56.5, 56.3, 55.4, 37.5 ppm.

(*S*)-Benzyl 3-benzamido-4-((5,6-dimethoxybenzo[*d*]thiazol-2-yl)amino)-4-oxobutanoat (11b): 286 mg, 0.51 mmol, yield: 76%. mp: 191–192 °C. R_f = 0.28 (CH/EtOAc 1:1). $[\alpha]_D^{20}$ = –6 (c = 10 in DCM). ^{1}H NMR: (300 MHz, $CDCl_3$) δ = 7.81 (d, J = 7.2 Hz, 2H), 7.56–7.48 (m, 1H), 7.47–7.38 (m, 2H), 7.37–7.29 (m, 5H), 7.27 (s, 1H), 7.20 (s, 1H), 5.40–5.29 (m, 1H), 5.19 (s, 2H), 3.94 (s, 3H), 3.91 (s, 3H), 3.27 (dd, J = 17.0, 4.5 Hz, 1H), 2.95 (dd, J = 17.0, 5.8 Hz, 1H) ppm. ^{13}C NMR: (75 MHz, $CDCl_3$) δ = 171.9, 168.7, 168.0, 156.1, 149.6, 147.8, 142.2, 135.2, 132.6, 128.9, 128.8, 128.7, 128.5, 128.3, 127.5, 123.7, 103.5, 102.7, 70.0, 67.5, 56.5, 56.2, 50.2, 35.1 ppm.

***N*-(3-((5,6-dimethoxybenzo[*d*]thiazol-2-yl)amino)-3-oxopropyl)benzamide (16)**: 120 mg, 0.31 mmol, yield: 40%. mp: 124–127 °C. R_f = 0.28 (CH/EtOAc 1:1). ^{1}H NMR: (300 MHz, DMSO-d_6) δ = 7.88–7.80 (m, 2H), 7.53 (s, 1H), 7.52–7.39 (m, 3H), 7.28 (s, 1H), 3.82 (s, 3H), 3.80 (s, 3H), 3.59 (dt, J = 6.6, 5.5 Hz, 2H), 2.79 (t, J = 6.6 Hz, 2H) ppm. ^{13}C NMR: (75 MHz, DMSO-d_6) δ = 170.5, 166.8, 156.8, 149.3, 147.3, 143.0, 134.8, 131.6, 128.7, 127.6, 123.3, 104.1, 103.9, 56.4, 56.2, 35.9, 35.6 ppm.

***N*-(5,6-Dimethoxybenzo[*d*]thiazol-2-yl)-benzamide (24a)**: 326 mg, 1.04 mmol, yield: 72%. mp: 190–195 °C, R_f = 0.39 (CH/EtOAc 1:1). ^{1}H NMR: (300 MHz, $CDCl_3$) δ = 8.13–8.01 (m, 2H), 7.60–7.48 (m, 1H), 7.45–7.34 (m, 2H), 7.24 (s, 1H), 6.57 (s, 1H), 3.94 (s, 3H), 3.51 (s, 3H) ppm. ^{13}C NMR: (75 MHz, $CDCl_3$) δ = 165.8, 159.2, 149.1, 147.6, 140.7, 133.1, 131.9, 129.1, 128.4, 122.9, 102.5, 102.5, 56.3, 55.7 ppm.

(*S*)-3-benzamido-4-((5,6-dimethoxybenzo[*d*]thiazol-2-yl)amino)-4-oxobutanoic acid (18): **11b** (2.19 g, 4.22 mmol, 1 eq.) was dissolved in THF and LiOH (1.01 g, 41.29 mmol, 10 eq.), dissolved in water, was added. After stirring for 1 h, the organic solvent was removed under reduced pressure. The aqueous phase was acidified with HCl and extracted with ethyl acetate three times. The combined organic phases were washed with water and brine, dried with Mg_2SO_4 and the solvent was evaporated to yield the **18** (1.77 g, 4.12 mmol, yield: 98%). mp: 210–211 °C. R_f = 0.34 (CH/EtOAc 1:2). $[\alpha]_D^{20}$ = +39 (c = 10 in DMF). ^{1}H NMR: (300 MHz, DMSO-d_6) δ = 7.99–7.84 (m, 2H), 7.64–7.41 (m, 4H), 7.29 (s, 1H), 5.14–4.89 (m, 1H), 3.82 (s, 3H), 3.80 (s, 3H), 3.01–2.75 (m, 2H) ppm. ^{13}C NMR: (75 MHz, DMSO-d_6) δ = 171.8, 170.7, 166.9, 156.8, 149.4, 147.4, 143.0, 134.1, 132.0, 128.7, 128.0, 123.4, 104.1, 104.0, 56.4, 56.2, 51.1, 35.9 ppm.

4.8. General procedure for the deprotection of methoxy groups by BBr_3

At –78 °C, the respective aryl ether (1.0 eq.) was dissolved in DCM and BBr_3 (1 M in DCM, 8.0 eq.) was added dropwise. The cooling bath was removed after 30 min and stirring was continued for 16 h at r.t. While cooling with an ice-water bath, DCM (20 mL) was added, followed by 2 mL of MeOH. The product was obtained by filtration or the solvent was evaporated under reduced pressure and the residue was purified by

silica column chromatography.

(*S*)-2-Amino-*N*-(5,6-dihydroxybenzo[*d*]thiazol-2-yl)propionamide hydrobromide (7a): 292 mg, 0.78 mmol, yield: 66%. mp: 148–152 °C. $[\alpha]_D^{20} = 0$ ($c = 10$ in DMF). ^{1}H NMR: (300 MHz, DMSO-d_6) $\delta = 7.27$ (s, 1H), 7.13 (s, 1H), 4.23–4.08 (m, 1H), 1.48 (d, $J = 7.0$ Hz, 3H) ppm. ^{13}C NMR: (75 MHz, DMSO-d_6) $\delta = 169.3$, 155.5, 144.7, 144.0, 142.3, 122.2, 107.0, 106.3, 49.1, 17.2 ppm.

(*R*)-2-Amino-*N*-(5,6-dihydroxybenzo[*d*]thiazol-2-yl)propionamide hydrobromide (7b): 326 mg, 0.98 mmol, yield: 93%. mp: 149–153 °C. $[\alpha]_D^{20} = 0$ ($c = 10$ in DMF. ^{1}H NMR: (300 MHz, DMSO-d_6) $\delta = 7.27$ (s, 1H), 7.13 (s, 1H), 4.23–4.08 (m, 1H), 1.48 (d, $J = 7.0$ Hz, 3H) ppm. ^{13}C NMR: (75 MHz, DMSO-d_6) $\delta = 169.3$, 155.5, 144.7, 144.0, 142.3, 122.2, 107.0, 106.3, 49.1, 17.2 ppm.

(*S,S*)-2-Amino-*N*-(5,6-dihydroxybenzo[*d*]thiazol-2-yl)-3-methylpentoicamide hydrobromide (7c): 308 mg, 0.82 mmol, yield: 99%. mp: 281–283 °C. $[\alpha]_D^{20} = +29$ ($c = 10$ in DMF). ^{1}H NMR: (300 MHz, DMSO-d_6) $\delta = 7.26$ (s, 1H), 7.13 (s, 1H), 4.06–3.86 (m, 1H), 2.04–1.90 (m, 1H), 1.66–1.45 (m, 1H), 1.26–1.05 (m, 1H), 0.99–0.81 (m, 6H) ppm. ^{13}C NMR: (75 MHz, DMSO-d_6) $\delta = 167.6$, 154.8, 146.4, 145.9, 144.4, 121.9, 106.6, 106.5, 56.8, 36.3, 24.1, 14.7, 11.1 ppm.

(*S*)-2-Amino-*N*-(5,6-dihydroxybenzo[*d*]thiazol-2-yl)-3,3-dimethylbutyricamide hydrobromide (7d): 292 mg, 0.78 mmol, yield: 66%. mp: 140–150 °C. $[\alpha]_D^{20} = +34$ ($c = 10$ in MeOH). ^{1}H NMR: (300 MHz, DMSO-d_6) $\delta = 7.27$ (s, 1H), 7.14 (s, 1H), 3.97–3.79 (m, 1H), 1.03 (s, 9H) ppm. ^{13}C NMR: (75 MHz, DMSO-d_6) $\delta = 170.5$, 166.9, 145.9, 144.4, 143.7, 121.8, 106.5, 106.5, 60.4, 33.5, 26.2 ppm.

(*S*)-2-Amino-*N*-(5,6-dihydroxybenzo[*d*]thiazol-2-yl)-3-phenylpropionamide hydrobromide (7e): 231 mg, 0.56 mmol, yield: 86%. mp: 254–256 °C. $[\alpha]_D^{20} = +13$ ($c = 10$ in DMF). ^{1}H NMR: (300 MHz, DMSO-d_6) $\delta = 7.35$–7.21 (m, 6H), 7.11 (s, 1H), 4.41–4.27 (m, 1H), 3.27–3.08 (m, 2H) ppm. ^{13}C NMR: (75 MHz, DMSO-d_6) $\delta = 167.4$, 146.3, 145.9, 144.6, 144.4, 134.4, 129.6, 128.7, 127.5, 121.9, 106.6, 106.5, 53.9, 36.8 ppm.

(*S*)-2-amino-3-(benzylthio)-*N*-(5,6-dihydroxybenzo[*d*]thiazol-2-yl)propanamide (7f): 120 mg, 0.26 mmol, yield: 99%. mp: 180 °C. $[\alpha]_D^{20} = +88$ ($c = 5$ in MeOH). ^{1}H NMR: (300 MHz, DMSO-d_6) $\delta = 8.69$ (s, 3H), 8.60 (s 2H), 7.37–7.14 (m, 6H), 7.13 (s, 1H), 4.67 (s, 1H), 4.01 (s, 2H), 3.15 (s, 2H) ppm. ^{13}C NMR: (75 MHz, DMSO-d_6) $\delta = 166.0$, 154.4, 147.6, 145.0, 144.1, 138.0, 129.4, 128.9, 127.6, 122.4, 105.7, 102.7, 55.4, 49.0, 35.5 ppm.

(*S*)-*N*-(1-(5,6-dihydroxybenzo[*d*]thiazol-2-ylamino)-3-(4-hydroxyphenyl)-1-oxopropan-2-yl)benzamide (12a): 92 mg, 0.20 mmol, yield: 77%. mp: 121–125 °C. $R_f = 0.49$ (CH/EtOAc 1:1). $[\alpha]_D^{20} = +9$ ($c = 10$ in MeOH). ^{1}H NMR: (300 MHz, DMSO-d_6) $\delta = 8.74$ (d, $J = 7.7$ Hz, 1H), 7.90–7.75 (m, 2H), 7.58–7.39 (m, 3H), 7.23 (s, 1H), 7.20 (d, $J = 8.3$ Hz, 2H), 7.12 (s, 1H), 6.65 (d, $J = 8.3$ Hz, 2H), 4.91–4.78 (m, 1H), 3.15–2.90 (m, 2H) ppm. ^{13}C NMR: (75 MHz, DMSO-d_6) $\delta = 171.3$, 167.0, 156.0, 146.1, 145.7, 144.1, 143.4, 141.6, 140.6, 140.4, 133.7, 131.6, 130.3, 128.3, 127.8, 127.6, 115.0, 106.4, 105.2, 55.8, 36.0 ppm. MS (ESI) m/z [M + H$^+$] calcd for $C_{23}H_{19}N_3O_5S$ 450.14 (100%), 451.12 (24.9%), 452.10 (4.5%), found 450.14 (100%), 451.09 (24.2%), 452.08 (4.6%); purity (HPLC) = 95%.

(*S*)-3-Benzamido-4-((5,6-dihydroxybenzo[*d*]thiazol-2-yl)amino)-4-oxobutanoic acid (12b): $AlCl_3$ (257 mg, 1.92 mmol, 10.0 eq.) was stirred in ethanethiol (1 mL) for 15 min while cooling with an ice-water bath. A solution of **11b** (100 mg, 0.19 mmol, 1.0 eq.) in dichloromethane was added, the ice bath was removed, and the suspension was stirred for 16 h at r.t. Concentrated HCl (2 mL) was added under ice-cooling and after stirring for 30 min, **12b** (67 mg, 0.17 mmol, yield: 87%) was collected by filtration as a colorless solid. mp: 175–178 °C. $R_f = 0.28$ (CH/EtOAc 1:1). $[\alpha]_D^{20} = +5$ ($c = 10$ in MeOH). ^{1}H NMR: (300 MHz, DMSO-d_6) $\delta = 8.89$ (d, $J = 7.0$ Hz, 1H), 7.99–7.80 (m, 2H), 7.62–7.42 (m, 4H), 7.11 (s, 1H), 5.07–4.91 (m, 1H), 3.00–2.72 (m, 2H) ppm. ^{13}C NMR: (75 MHz, DMSO-d_6) $\delta = 171.4$, 170.3, 166.5, 156.4, 148.9, 147.0, 142.5, 133.6, 131.6, 128.3, 127.6, 122.9, 103.7, 103.5, 50.6, 35.5 ppm. MS (ESI) m/z [M + H$^+$] calcd for $C_{18}H_{15}N_3O_6S$ 402.07 (100%), 403.07 (19.5%), 404.06 (4.5%), found 402.13 (100%), 403.14 (21.9%), 404.14 (6.8%); purity (HPLC) = 95%.

***N*-(3-((5,6-dihydroxybenzo[*d*]thiazol-2-yl)amino)-3-oxopropyl)benzamide (17)**: 58 mg, 0.16 mmol, yield: 87%. mp: 118–120 °C. $R_f = 0.26$ (CH/EtOAc 1:1). ^{1}H NMR: (300 MHz, DMSO-d_6) $\delta = 12.55$ (d, $J = 38.6$ Hz, 1H), 8.63 (d, $J = 5.7$ Hz, 1H), 7.82 (d, $J = 7.1$ Hz, 2H), 7.55–7.39 (m, 3H), 7.32–7.04 (m, 1H), 3.65–3.50 (m, 2H), 2.84–2.68 (m, 2H) ppm. ^{13}C NMR: (75 MHz, DMSO-d_6) $\delta = 170.4$, 166.5, 156.0, 146.1, 144.0, 143.3, 134.4, 131.3, 128.4, 127.3, 121.7, 105.9, 105.2, 35.5, 35.2 ppm. MS (ESI) m/z [M + H$^+$] calcd for $C_{17}H_{15}N_3O_4S$ 358.08 (100%), 359.08 (18.4%), 360.09 (4.5%), found 358.08 (100%), 359.08 (18.4%), 360.09 (5.0%); purity (HPLC) = 95%.

(*S*)-2-Benzamido-N^1-(5,6-dihydroxybenzo[*d*]thiazol-2-yl)-N^4,N^4-diethylsuccinamide (20a): 41 mg, 0.09 mmol, yield: 44%. mp: 162–164 °C. $R_f = 0.22$ (CH/EtOAc 1:2). $[\alpha]_D^{20} = +3$ ($c = 10$ in MeOH). ^{1}H NMR: (300 MHz, DMSO-d_6) $\delta = 12.14$ (s, 1H), 9.18 (s, 2H), 8.77 (d, $J = 7.2$ Hz, 1H), 7.98–7.79 (m, 2H), 7.59–7.42 (m, 3H), 7.23 (s, 1H), 7.11 (s, 1H), 5.17–4.98 (m, 1H), 3.35–3.19 (m, 4H), 3.07–2.84 (m, 2H), 1.13 (t, $J = 7.0$ Hz, 3H), 0.99 (t, $J = 7.0$ Hz, 3H) ppm. ^{13}C NMR: (75 MHz, DMSO-d_6) $\delta = 170.4$, 168.1, 166.3, 155.6, 145.5, 143.8, 142.0, 133.8, 131.5, 128.2, 127.5, 121.9, 106.5, 106.3, 50.8, 41.3, 34.0, 14.0, 13.0 ppm. MS (ESI) m/z [M + H$^+$] calcd for $C_{22}H_{24}N_4O_5S$ 457.15 (100%), 458.15 (23.8%), 459.14 (4.5%), found 457.12 (100%), 458.04 (26.1%), 459.14 (4.0%); purity (HPLC) = 95%.

(*S*)-2-Benzamido-N^1-(5,6-dihydroxybenzo[*d*]thiazol-2-yl)-N^4-phenylsuccinamide (20b): 62 mg, 0.13 mmol, yield: 85%. mp: 209–211 °C. $R_f = 0.40$ (CH/EtOAc 1:2). $[\alpha]_D^{20} = +8$ ($c = 10$ in MeOH). ^{1}H NMR: (300 MHz, DMSO-d_6) $\delta = 10.27$ (s, 1H), 8.89 (d, $J = 7.0$ Hz, 1H), 7.91 (d, $J = 6.8$ Hz, 2H), 7.63 (d, $J = 7.4$ Hz, 2H), 7.57–7.41 (m, 3H), 7.36–6.98 (m, 5H), 3.81 (d, $J = 7.8$ Hz, 1H), 3.08 (d, $J = 6.8$ Hz, 2H) ppm. ^{13}C NMR: (75 MHz, DMSO-d_6) $\delta = 169.5$, 168.5, 166.4, 155.3, 145.5, 143.8, 141.3, 138.9, 133.8, 131.4, 128.6, 128.2, 127.5, 123.3, 121.5, 119.3, 106.3, 105.6, 51.0, 37.0 ppm. MS (ESI) m/z [M + H$^+$] calcd for $C_{24}H_{20}N_4O_5S$ 477.12 (100%), 478.12 (26.0%), 479.11 (4.5%), found 477.09 (100%), 478.06 (25.8%), 479.11 (3.8%); purity (HPLC) = 99%.

(2-((5,6-Dihydroxybenzo[*d*]thiazol-2-yl)amino)-2-oxoethyl)-*N*-phenylbenzamide (23a): 54 mg, 0.13 mmol, yield: 50%. mp: 266 °C. $R_f = 0.41$ (CH/EtOAc 1:3). ^{1}H NMR: (300 MHz, DMSO-d_6) $\delta = 7.36$–7.03 (m, 12H), 4.75 (s, 2H) ppm. ^{13}C NMR: (75 MHz, DMSO-d_6) $\delta = 169.7$, 167.4, 155.2, 145.6, 143.9, 143.8, 141.8, 135.4, 129.7, 129.0, 128.3, 127.8, 127.5, 126.6, 121.8, 106.5, 106.3, 53.0 ppm. MS (ESI) m/z [M + H$^+$] calcd for $C_{22}H_{17}N_3O_4S$ 420.09 (100%), 421.10 (23.8%), 422.09 (4.5%), found 420.22 (100%), 421.20 (19.6%), 422.19 (5.1%); purity (HPLC) = 99%.

***N*-(5,6-Dihydroxybenzo[*d*]thiazol-2-yl)-2,2-diphenylacetamide (23b)**: 75 mg, 0.19 mmol, yield: 53%. mp: 251 °C. $R_f = 0.43$ (CH/EtOAc 1:1). ^{1}H NMR: (300 MHz, DMSO-d_6) $\delta = 12.56$ (s, 1H), 7.44–7.19 (m, 11*H*), 7.09 (s, 1H), 5.36 (s, 1H) ppm. ^{13}C NMR: (75 MHz, DMSO-d_6) $\delta = 170.2$, 155.2, 145.6, 144.0, 141.7, 139.0, 128.5, 127.1, 121.8, 106.5, 106.3, 56.1 ppm. MS (ESI) m/z [M + H$^+$] calcd for $C_{21}H_{16}N_2O_3S$ 377.09 (100%), 378.09 (22.7%), 379.08 (4.5%), found 377.08 (100%), 378.00 (25.0%), 379.06 (4.3%); purity (HPLC) = 98%.

***N*-(5,6-Dihydroxybenzo[*d*]thiazol-2-yl)-2,2-bis-(4-hydroxyphenyl)acetamide (23c)**: 59 mg, 0.14 mmol, yield: 85%. mp: 261 °C. $R_f = 0.25$ (CH/EtOAc 1:1). ^{1}H NMR: (300 MHz, DMSO-d_6) $\delta = 12.37$ (s, 1H), 7.21 (s, 1H), 7.10 (s, 5H), 6.72 (d, $J = 8.3$ Hz, 4H), 5.12 (s, 1H) ppm. ^{13}C NMR: (75 MHz, DMSO-d_6) $\delta = 171.0$, 156.2, 155.3, 145.4, 143.8, 141.7, 129.7, 129.4, 121.7, 115.0, 106.4, 106.2, 54.5 ppm. MS (ESI) m/z [M + H$^+$] calcd for $C_{21}H_{16}N_2O_5S$ 409.08 (100%), 410.08 (22.7%), 411.07 (4.5%), found 409.07 (100%), 410.01 (23.2%), 411.01 (4.1%); purity (HPLC) = 97%.

***N*-(5,6-Dihydroxybenzo[*d*]thiazol-2-yl)-2,2-bis-(4-chlorophenyl)acetamide (23d)**: 103 mg, 0.23 mmol, yield: 70%. mp: 273 °C. $R_f = 0.52$ (CH/EtOAc 1:1). ^{1}H NMR: (300 MHz, DMSO-d_6) $\delta = 12.60$ (s, 1H), 9.17 (s, 2H), 7.42 (d, $J = 8.3$ Hz, 4H), 7.34 (d, $J = 8.3$ Hz,

5H), 7.22 (s, 1H), 7.09 (s, 1H), 5.36 (s, 1H) ppm. ^{13}C NMR: (75 MHz, DMSO-d_6) δ = 169.5, 155.1, 145.6, 144.0, 137.5, 132.0, 130.3, 128.6, 121.8, 106.5, 106.3, 54.6 ppm. MS (ESI) *m/z* [M + H$^+$] calcd for $C_{22}H_{14}Cl_2N_2O_3S$ 445.01 (100%), 446.01 (22.7%), 447.01 (63.9%), found 444.98 (100%), 445.98 (27.6%), 446.96 (75.2%); purity (HPLC) = 95%.

***N*-(5,6-Dihydroxybenzo[*d*]thiazol-2-yl)benzamide (25a)**: 105 mg, 0.37 mmol, yield: 99%. mp: 253–260 °C, R_f = 0.38 (DCM/MeOH 9:1). ^{1}H NMR: (300 MHz, DMSO-d_6) δ = 11.73 (s, 1H), 8.32 (s, 2H), 8.20–8.04 (m, 2H), 7.68–7.59 (m, 1H), 7.59–7.45 (m, 2H), 7.27 (s, 1H), 7.16 (s, 1H) ppm. ^{13}C NMR: (75 MHz, DMSO-d_6) δ = 165.4, 156.3, 145.7, 144.1, 141.7, 132.6, 132.3, 128.6, 128.2, 122.0, 106.5, 106.4 ppm. MS (ESI) *m/z* [M + H$^+$] calcd for $C_{14}H_{10}N_2O_3S$ 287.04 (100%), 288.04 (15.1%), 289.04 (4.5%), found 287.11 (100%), 288.10 (16.3%), 289.09 (4.2%); purity (HPLC) = 99%.

***N*-(5,6-Dihydroxybenzo[*d*]thiazol-2-yl)-4-iodobenzamide (25b)**: 40 mg, 0.01 mmol, yield: 29%. mp: 228 °C. R_f = 0.31 (CH/EtOAc 1:3). ^{1}H NMR: (300 MHz, DMSO-d_6) δ = 8.20–8.07 (m, 2H), 7.70–7.56 (m, 2H), 7.26 (s, 1H), 7.14 (s, 1H) ppm. ^{13}C NMR: (75 MHz, DMSO-d_6) δ = 168.0, 145.7, 144.1, 137.4, 131.2, 130.1, 128.7, 121.7, 117.7, 106.4, 105.8 ppm. MS (ESI) *m/z* [M + H$^+$] calcd for $C_{14}H_9IN_2O_3S$ 412.94 (100%), 413.94 (15.1%), 414.93 (4.5%), found 413.03 (100%), 414.01 (20.0%), 415.00 (3.0%); purity (HPLC) = 99%.

4-Chloro-*N*-(5,6-dihydroxybenzo[*d*]thiazol-2-yl)benzamide (25c): 29 mg, 0.09 mmol, yield: 32%. mp: 293 °C. R_f = 0.36 (DCM/MeOH 49:1). ^{1}H NMR: (300 MHz, DMSO-d_6): δ = 7.87 (d, *J* = 8.2 Hz, 2H), 7.37 (d, *J* = 8.2 Hz, 2H), 7.01 (s, 1H). 6.89 (s, 1H) ppm. ^{13}C NMR: (75 MHz, DMSO-d_6): δ = 164.7, 158.1, 145.7, 144.1, 137.5, 131.2, 130.1, 128.7, 121.7, 106.4, 106.0 ppm. MS (ESI) *m/z* [M + H$^+$] calcd for $C_{14}H_9ClN_2O_3S$ 321.00 (100%), 322.01 (15.1%), 323.00 (32.0%), found 321.04 (100%), 322.03 (15.9%), 323.02 (35.9%); purity (HPLC) = 98%.

4-Methyl-*N*-(5,6-dihydroxybenzothiazol-2-yl)benzamide (25d): 135 mg, 0.45 mmol, yield: 99%. mp: 331 °C. R_f = 0.57 (DCM/MeOH 19:1). ^{1}H NMR: (300 MHz, DMSO-d_6): δ = 8.00 (d, *J* = 8.0 Hz, 2H), 7.34 (d, *J* = 8.0 Hz, 2H), 7.26 (s, 1H), 7.14 (s, 1H), 2.38 (s, 3H) ppm. ^{13}C NMR: (75 MHz, DMSO-d_6): δ = 165.3, 156.6, 145.7, 144.1, 143.0, 129.2, 128.3, 121.8, 106.4, 106.2, 21.1 ppm. MS (ESI) *m/z* [M + H$^+$] calcd for $C_{15}H_{12}N_2O_3S$ 301.06 (100%), 302.06 (16.2%), 303.05 (4.5%), found 301.06 (100%), 302.06 (10.0%), 303.05 (2.8%); purity (HPLC) = 99%.

***N*-(5,6-dihydroxybenzo[*d*]thiazol-2-yl)-[1,1′-biphenyl]-4-carboxamide (25e)**: 163 mg, 0.45 mmol, yield: 94%. mp: 273 °C. R_f = 0.36 (CH/EtOAc 1:2). ^{1}H NMR: (600 MHz, DMSO-d_6) δ = 8.21 (d, *J* = 8.4 Hz, 2H), 7.86 (d, *J* = 8.4 Hz, 2H), 7.78 (d, *J* = 7.3 Hz, 2H), 7.51 (t, *J* = 7.7 Hz, 2H), 7.43 (t, *J* = 7.3 Hz, 1H), 7.27 (s, 1H), 7.14 (s, 1H) ppm. ^{13}C NMR: (151 MHz, DMSO-d_6) δ = 158.4, 158.2, 145.7, 144.0, 144.0, 138.9, 129.1, 128.9, 128.4, 127.0, 126.8, 106.4 ppm. MS (ESI) *m/z* [M + H$^+$] calcd for $C_{20}H_{14}N_2O_3S$ 363.07 (100%), 364.08 (21.6%), 365.07 (4.5%), found 363.05 (100%), 364.03 (20.7%), 365.03 (4.2%); purity (HPLC) = 99%.

3,4-Dichloro-*N*-(5,6-dihydroxybenzo[*d*]thiazol-2-yl)benzamide (25f): 36 mg, 0.10 mmol, yield: 52%. mp: 272 °C. R_f = 0.53 (DCM/MeOH 19:1). ^{1}H NMR: (300 MHz, DMSO-d_6): δ = 8.41–8.31 (m, 1H), 8.05 (d, *J* = 8.4 Hz, 1H), 7.81 (d, *J* = 8.6 Hz, 1H), 7.36–7.24 (m, 1H), 7.21–7.09 (m, 1H) ppm. ^{13}C NMR: (75 MHz, DMSO-d_6): δ = 164.0, 163.4, 156.3, 146.3, 145.8, 144.4, 144.2, 143.5, 141.8, 135.6, 135.3, 133.1, 132.3, 131.5, 130.9, 130.2, 128.4, 122.0, 121.4, 106.6, 105.7, 105.0 ppm. MS (ESI) *m/z* [M + H$^+$] calcd for $C_{14}H_8Cl_2N_2O_3S$ 354.96 (100%), 355.97 (15.1%), 356.96 (63.9%), found 355.01 (100%), 356.02 (15.6%), 356.96 (69.9%); purity (HPLC) = 98%.

5,6-Dihydroxy-*N*-phenylbenzo[*d*]thiazole-2-carboxamide (34a): 90 mg, 0.31 mmol, yield: 97%. mp: 297–299 °C. R_f = 0.47 (CH/EtOAc 1:2 + 0.1% TFA). ^{1}H NMR: (300 MHz, MeOD-d_4): δ = 7.76 (d, *J* = 7.9 Hz, 2H), 7.51 (s, 1H), 7.41–7.33 (m, 3H), 7.16 (t, *J* = 7.9 Hz, 1H) ppm. ^{13}C NMR: (75 MHz, MeOD-d_4): δ = 161.5, 160.2, 149.0, 148.4, 148.2, 138.8, 131.3, 130.6, 129.9, 125.9, 121.7, 109.3, 106.7 ppm. MS (ESI) *m/z* [M + H$^+$] calcd for $C_{14}H_{10}N_2O_3S$ 287.04 (100%), 288.04 (15.1%), 289.04 (4.5%), found 287.11 (100%), 288.08 (17.3%), 289.07 (4.0%); purity (HPLC) = 99%.

6-Hydroxy-*N*-phenylbenzo[*d*]thiazole-2-carboxamide (34b): 20 mg, 0.07 mmol, yield: 20%. decomp. > 225 °C. R_f = 0.62 (DCM/MeOH 19:1 + 0.1% TFA). ^{1}H NMR: (600 MHz, DMSO-d_6): δ = 10.96 (s, 1H), 10.24 (s, 1H), 8.01 (d, *J* = 8.9 Hz, 1H), 7.89 (d, *J* = 7.6 Hz, 2H), 7.51 (d, *J* = 2.4 Hz, 1H), 7.41–7.35 (m, 2H), 7.17–7.09 (m, 2H). ^{13}C NMR: (151 MHz, DMSO-d_6): δ = 160.7, 158.4, 157.2, 146.2, 138.3, 138.1, 128.8, 125.0, 124.4, 120.7, 117.4, 107.0 ppm. MS (ESI) *m/z* [M + H$^+$] calcd for $C_{14}H_{10}N_2O_2S$ 271.05 (100%), 272.05 (15.1%), 273.05 (4.5%), found 271.12 (100%), 272.10 (17.3%), 273.09 (3.8%); purity (HPLC) = 97%.

5,6-Dihydroxy-*N*-phenyl-1*H*-indole-2-carboxamide (34c): 40 mg, 0.15 mmol, yield: 44%. mp: 207–209 °C. R_f = 0.18 (DCM/MeOH 19:1 + 0.1% TFA). ^{1}H NMR: (300 MHz, DMSO-d_6): δ = 11.11 (s, 1H), 9.91 (s, 1H), 9.05 (s, 1H), 8.50 (s, 1H), 7.82–7.70 (m, 2H), 7.41–7.28 (m, 2H), 7.17 (s, 1H), 7.11–7.00 (m, 1H), 6.90 (s, 1H), 6.83 (s, 1H) ppm. ^{13}C NMR: (75 MHz, DMSO-d_6): δ = 159.9, 145.6, 141.9, 139.3, 132.2, 129.1, 128.6, 123.1, 120.0, 119.9, 104.9, 103.7, 97.1 ppm. MS (ESI) *m/z* [M + H$^+$] calcd for $C_{15}H_{12}N_2O_3$ 269.08 (100%), 270.09 (16.2%), 271.09 (1.2%), found 269.15 (100%), 270.13 (15.8%), 271.10 (0.8%); purity (HPLC) = 96%.

5,6-Dihydroxy-*N*-phenylbenzo[*b*]thiophene-2-carboxamide (34d): 90 mg, 0.32 mmol, yield: 99%. decomp. > 215 °C. R_f = 0.24 (DCM/MeOH 14:1 + 0.1% TFA). ^{1}H NMR: (300 MHz, DMSO-d_6): δ = 10.25 (s, 1H), 9.69 (s, 1H), 9.33 (s, 1H), 8.08 (s, 1H), 7.74 (d, *J* = 7.7 Hz, 2H), 7.35 (t, *J* = 7.7 Hz, 2H), 7.30–7.22 (m, 2H), 7.09 (t, *J* = 7.7 Hz, 1H) ppm. ^{13}C NMR: (75 MHz, DMSO-d_6): δ = 160.7, 147.5, 145.4, 138.9, 136.2, 133.2, 132.2, 128.7, 125.5, 123.7, 120.2, 109.5, 107.2 ppm. MS (ESI) *m/z* [M + H$^+$] calcd for $C_{15}H_{11}NO_3S$ 286.05 (100%), 287.05 (16.2%), 288.04 (4.5%), found 286.00 (100%), 286.97 (18.8%), 288.00 (4.3%); purity (HPLC) = 99%.

5,6-Dihydroxy-*N*-phenylbenzofuran-2-carboxamide (34e): 80 mg, 0.30 mmol, yield: 88%. mp: 180–182 °C. R_f = 0.18 (DCM/MeOH 14:1 + 0.1% TFA). ^{1}H NMR: (300 MHz, DMSO-d_6): δ = 10.27–10.14 (m, 1H), 7.86–7.75 (m, 2H), 7.59–7.50 (m, 1H), 7.34 (t, *J* = 7.9 Hz, 2H), 7.16–6.92 (m, 3H) ppm. ^{13}C NMR: (75 MHz, DMSO-d_6): δ = 156.9, 149.5, 147.4, 147.1, 143.9, 138.7, 128.7, 123.8, 120.4, 118.7, 111.2, 106.1, 97.7 ppm. MS (ESI) *m/z* [M + H$^+$] calcd for $C_{15}H_{11}NO_4$ 270.07 (100%), 271.07 (16.2%), 272.08 (1.2%), found 270.14 (100%), 271.12 (17.5%), 272.10 (0.8%); purity (HPLC) = 99%.

6,7-Dihydroxy-*N*-phenylquinoline-3-carboxamide (34f): 30 mg, 0.10 mmol, yield: 29%. mp: 224–226 °C. R_f = 0.24 (DCM/MeOH 14:1 + 0.1% TFA). ^{1}H NMR: (300 MHz, DMSO-d_6/TFA): δ = 9.32 (s, 2H), 8.11–6.74 (m, 9H) ppm. ^{13}C NMR: (75 MHz, DMSO-d_6/TFA): δ = 161.7, 157.6, 151.0, 141.6, 139.3, 138.8, 136.2, 129.0, 125.7, 124.6, 124.4, 120.8, 110.5, 102.5 ppm. MS (ESI) *m/z* [M + H$^+$] calcd for $C_{16}H_{12}N_2O_3$ 281.08 (100%), 282.09 (17.3%), 283.09 (1.4%), found 281.15 (100%), 282.14 (18.4%), 283.10 (0.9%); purity (HPLC) = 98%.

5-Hydroxy-*N*-phenylbenzofuran-2-carboxamide (34g): 40 mg, 0.16 mmol, yield: 42%. mp: 229–231 °C. R_f = 0.26 (CH/EtOAc 4:1 + 0.1% TFA). ^{1}H NMR: (300 MHz, DMSO-d_6) δ = 10.43 (s, 1H), 9.45 (s, 1H), 7.86–7.76 (m, 2H), 7.64–7.58 (m, 2H), 7.51 (d, *J* = 8.9 Hz, 1H), 7.42–7.30 (m, 2H), 7.18–7.11 (m, 1H), 7.08 (d, *J* = 2.5 Hz, 1H), 6.96 (dd, *J* = 8.9, 2.5 Hz, 1H) ppm. ^{13}C NMR: (75 MHz, DMSO-d_6) δ = 156.8, 154.0, 149.2, 148.8, 138.4, 128.7, 128.0, 124.0, 120.5, 116.5, 112.3, 110.6, 106.4 ppm. MS (ESI) *m/z* [M + H$^+$] calcd for $C_{15}H_{11}NO_3$ 254.07 (100%), 255.08 (16.2%), 256.08 (1.2%), found 254.13 (100%), 255.10 (16.0%), 256.09 (1.0%); purity (HPLC) = 99%.

6-Hydroxy-*N*-phenylbenzofuran-2-carboxamide (34h): 40 mg, 0.16 mmol, yield: 42%. mp: 237–239 °C. R_f = 0.3 (CH/EtOAc 2:1 + 0.1% TFA) ^{1}H NMR: (300 MHz, DMSO-d_6) δ = 10.31 (s, 1H), 9.99 (s, 1H), 7.80 (d, *J* = 7.7 Hz, 2H), 7.64 (s, 1H), 7.59 (d, *J* = 8.5 Hz, 1H), 7.35 (t, *J* = 7.9 Hz, 2H), 7.11 (t, *J* = 7.4 Hz, 1H), 7.02 (s, 1H), 6.86 (dd, *J* = 8.5, 2.1 Hz, 1H) ppm. ^{13}C NMR: (75 MHz, DMSO-d_6) δ = 157.9, 156.8, 156.0, 147.4, 138.5, 128.7, 123.9, 123.2, 120.4, 119.2, 113.9, 111.1,

97.6 ppm. MS (ESI) *m/z* [M + H^+] calcd for $C_{15}H_{11}NO_3$ 254.07 (100%), 255.08 (16.2%), 256.08 (1.2%), found 254.12 (100%), 255.16 (15.9%), 256.13 (1.1%); purity (HPLC) = 99%.

4,6-Dihydroxy-*N*-phenylbenzofuran-2-carboxamide (34i): 25 mg, 0.09 mmol, yield: 27%. decomp. > 270 °C. R_f = 0.34 (DCM/MeOH 19:1 + 0.1% TFA).[1] ^{1}H NMR: (300 MHz, DMSO-d_6) δ = 10.27 (s, 1H), 10.20 (s, 1H), 9.79 (s, 1H), 7.78 (d, J = 7.9 Hz, 2H), 7.64 (s, 1H), 7.34 (t, J = 7.7 Hz, 2H), 7.09 (t, J = 7.3 Hz, 1H), 6.48 (s, 1H), 6.25 (s, 1H) ppm. ^{13}C NMR: (75 MHz, DMSO-d_6) δ = 159.1, 157.2, 156.8, 152.6, 145.5, 138.7, 128.7, 123.7, 120.3, 109.6, 109.0, 98.4, 89.4 ppm. MS (ESI) *m/z* [M + H^+] calcd for $C_{15}H_{11}NO_4$ 270.07 (100%), 271.07 (16.2%), 272.08 (1.2%), found 270.10 (100%), 271.13 (14.5%), 272.10 (0.7%); purity (HPLC) = 98%.

6-Hydroxy-5-nitro-*N*-phenylbenzofuran-2-carboxamide (34j): 610 mg, 2.00 mmol, yield: 86%. decomp. > 230 °C. R_f = 0.60 (CH/EtOAc 2:1). ^{1}H NMR: (300 MHz, DMSO-d_6): δ = 11.32 (s, 1H), 10.49 (s, 1H), 8.43 (s, 1H), 7.83–7.73 (m, 3H), 7.41–7.31 (m, 3H), 7.13 (t, J = 7.3 Hz, 1H) ppm. ^{13}C NMR: (75 MHz, DMSO-d_6): δ = 157.1, 156.1, 152.0, 150.0, 138.2, 136.2, 128.7, 124.2, 120.5, 120.5, 119.2, 111.1, 100.3 ppm. MS (ESI) *m/z* [M + H^+] calcd for $C_{15}H_{10}N_2O_5$ 299.06 (100%), 300.06 (16.2%), 301.07 (1.2%), found 299.06 (100%), 300.04 (16.9%), 301.02 (0.7%); purity (HPLC) = 98%.

5,6-Dihydroxy-*N*-(4-iodophenyl)benzo [*d*] thiazole-2-carboxamide (34k): 30 mg, 0.07 mmol, yield: 31%. decomp. > 140 °C. R_f = 0.26 (DCM/MeOH 49:1 + 0.1% TFA). ^{1}H NMR: (300 MHz, DMSO-d_6): δ = 10.91 (s, 1H), 9.94 (s, 1H), 9.65 (s, 1H), 7.85–7.59 (m, 4H), 7.49 (s, 1H), 7.44 (s, 1H) ppm. ^{13}C NMR: (75 MHz, DMSO-d_6): δ = 160.2, 158.6, 147.7, 147.1, 146.7, 138.0, 137.4, 128.4, 122.8, 108.4, 106.4, 88.2 ppm. MS (ESI) *m/z* [M + H^+] calcd for $C_{14}H_9IN_2O_3S$ 412.95 (100.0%), 413.95 (15.1%), 414.94 (4.5%), found 412.88 (100.0%), 413.85 (14.0%), 414.90 (5.9%); purity (HPLC) = 99%.

6-Amino-5-hydroxy-*N*-phenylbenzofuran-2-carboxamide (34l): **34j** (0.59 g, 1.98 mmol, 1.0 eq.) and tin(II)chloride dihydrate (2.23 g, 9.89 mmol, 5.0 eq.) were dissolved in ethanol (8 mL) and HCl (2 mL) was added. After heating for 2 h at 70 °C, the reaction mixture was cooled to r.t. and poured into iced water. The pH was adjusted to 6.5 with 1 M NaOH. The remaining ethanol was removed under reduced pressure and the residue was extracted with ethyl acetate. Combined organic extracts were washed with brine, dried over Na_2SO_4 and the solvent was evaporated *in vacuo*. The crude product was purified by silica column chromatography to yield **34k** (30 mg, 1.1 mmol, yield: 56%). decomp > 250 °C. R_f = 0.08 (DCM/MeOH 10:1). ^{1}H NMR: (600 MHz, DMSO-d_6) δ = 10.37 (s, 1H), 7.79 (d, J = 7.5 Hz, 2H), 7.68 (s, 1H), 7.52 (s, 1H), 7.40–7.32 (m, 2H), 7.22 (s, 1H), 7.12 (t, J = 7.5 Hz, 1H) ppm. ^{13}C NMR: (151 MHz, DMSO-d_6) δ = 156.6, 153.1, 150.0, 148.1, 138.5, 128.8, 124.0, 120.5, 119.0, 111.1, 98.2 ppm. MS (ESI) *m/z* [M + H^+] calcd for $C_{15}H_{12}N_2O_3$ 269.08 (100%), 270.09 (16.2%), 271.09 (1.2%), found 268.99 (100%), 269.95 (17.1%), 271.00 (1.1%); purity (HPLC) = 97%.

(*S*)-1-(5,6-Dihydroxybenzo [*d*] thiazole-2-carbonyl)-*N*-phenylpyrrolidine-2-carboxamide (36a): 10 mg, 0.03 mmol, yield: 13%. mp: 112–114 °C. R_f = 0.30 (DCM/MeOH 14:1 + 0,1% TFA). $[\alpha]_D^{20}$ = –36 (*c* = 5 in MeOH). ^{1}H NMR: (300 MHz, DMSO-d_6): δ = 10.16 (d, J = 13.8 Hz, 1H), 10.02–9.29 (m, 2H), 7.65–7.57 (m, 1H), 7.56–7.49 (m, 1H), 7.45–7.35 (m, 1H), 7.34–7.19 (m, 3H), 7.11–6.95 (m, 1H), 5.56–5.23 (m, 1H), 4.74–4.44 (m, 1H), 4.37–4.12 (m, 1H), 3.94–3.81 (m, 1H), 3.80–3.59 (m, 1H), 2.47–2.16 (m, 2H) ppm. ^{13}C NMR: (75 MHz, DMSO-d_6): δ = 171.0, 170.0, 161.1, 159.1, 147.6, 147.5, 147.1, 146.9, 146.5, 139.3, 128.7, 128.7, 127.3, 123.3, 123.1, 119.3, 119.2, 108.7, 108.6, 106.0, 62.1, 32.2, 29.0, 25.0, 21.6 ppm. MS (ESI) *m/z* [M + H^+] calcd for $C_{19}H_{17}N_3O_4S$ 384.09 (100%), 385.10 (20.5%), 386.09 (4.5%), found 384.14 (100%), 385.12 (21.0%), 386.10 (3.5%); purity (HPLC) = 95%.

(*S*)-1-(6-Hydroxybenzo [*d*] thiazole-2-carbonyl)-*N*-phenylpyrrolidine-2-carboxamide (36b): 40 mg, 0.11 mmol, yield: 42%. decomp > 145 °C. R_f = 0.36 (DCM/MeOH 14:1 + 0.1% TFA). $[\alpha]_D^{20}$ = –104 (*c* = 5 in MeOH). ^{1}H NMR: (300 MHz, DMSO-d_6): δ = 10.18 (d, J = 12.9 Hz, 2H), 8.01–6.94 (m, 8H), 5.52–4.67 (m, 1H), 4.33–4.18 (m, 1H), 3.80–3.66 (m, 1H), 2.46–1.85 (m, 4H) ppm. ^{13}C NMR: (75 MHz, DMSO-d_6): δ = 170.9, 169.9, 161.3, 161.1, 159.1, 158.7, 157.1, 157.0, 146.7, 146.4, 139.3, 139.1, 137.5, 137.4, 128.7, 128.7, 125.4, 125.0, 123.3, 123.1, 119.3, 119.2, 117.1, 117.0, 106.5, 62.1, 49.6, 48.7, 32.1, 29.0, 24.9, 21.7 ppm. MS (ESI) *m/z* [M + H^+] calcd for $C_{19}H_{17}N_3O_3S$ 368.10 (100%), 369.10 (20.5%), 370.09 (4.5%), found 368.14 (100%), 369.18 (27.2%), 370.14 (2.4%); purity (HPLC) = 99%.

(*S*)-1-(5,6-Dihydroxy-1*H*-indole-2-carbonyl)-*N*-phenylpyrrolidine-2-carboxamide (36c): 30 mg, 0.08 mmol, yield: 32%. decomp > 230 °C. R_f = 0.24 (DCM/MeOH 14:1 + 0.1% TFA). $[\alpha]_D^{20}$ = –84 (*c* = 5 in MeOH). ^{1}H NMR: (300 MHz, DMSO-d_6): δ = 11.15–10.79 (m, 1H), 9.06–8.35 (m, 1H), 7.64–7.24 (m, 5H), 7.08–6.49 (m, 4H), 4.96–4.55 (m, 1H), 4.08–3.82 (m, 2H), 2.43–1.98 (m, 4H) ppm. ^{13}C NMR: (75 MHz, DMSO-d_6): δ = 170.8, 161.1, 148.1, 145.9, 141.9, 141.7, 136.4, 131.7, 128.7, 128.3, 127.2, 127.0, 120.3, 119.9, 119.2, 105.0, 96.9, 60.5, 48.7, 40.3, 40.0, 39.8, 39.5, 39.2, 38.9, 38.6, 29.0, 25.3 ppm. MS (ESI) *m/z* [M + H^+] calcd for $C_{20}H_{19}N_3O_4$ 366.14 (100%), 367.14 (20.5%), 368.14 (4.5%), found 366.28 (100%), 367.19 (23.7%), 368.10 (0.9%); purity (HPLC) = 99%.

(*S*)-1-(5,6-Dihydroxybenzo [*b*] thiophene-2-carbonyl)-*N*-phenylpyrrolidine-2-carboxamide (36d): 40 mg, 0.10 mmol, yield: 42%. mp: 150–152 °C. R_f = 0.24 (DCM/MeOH 14:1 + 0.1% TFA). $[\alpha]_D^{20}$ = –12 (*c* = 5 in MeOH). ^{1}H NMR: (300 MHz, DMSO-d_6): δ = 10.06 (s, 1H), 7.78 (s, 1H), 7.65–7.56 (m, 2H), 7.34–7.19 (m, 3H), 7.08–6.99 (m, 2H), 4.67–4.56 (m, 1H), 4.05–3.87 (m, 2H), 2.32–1.86 (m, 4H) ppm. ^{13}C NMR: (75 MHz, DMSO-d_6): δ = 171.4, 160.7, 151.8, 146.0, 139.9, 136.4, 134.3, 133.3, 129.5, 129.3, 124.1, 120.0, 110.5, 100.7, 62.8, 50.2, 26.0 ppm. MS (ESI) *m/z* [M + H^+] calcd for $C_{20}H_{18}N_2O_4S$ 383.10 (100%), 384.10 (21.6%), 385.09 (4.5%), found 383.14 (100%), 384.14 (23.2%), 385.14 (4.2%); purity (HPLC) = 99%.

(*S*)-1-(5,6-dihydroxybenzofuran-2-carbonyl)-*N*-phenylpyrrolidine-2-carboxamide (36e): 80 mg, 0.22 mmol, yield: 88%. mp: 146–148 °C. R_f = 0.21 (DCM/MeOH 14:1 + 0.1% TFA). $[\alpha]_D^{20}$ = –2 (*c* = 5 in MeOH). ^{1}H NMR: (300 MHz, DMSO-d_6): δ = 10.36–9.97 (m, 1H), 7.71–7.44 (m, 2H), 7.46–7.19 (m, 3H), 7.15–6.54 (m, 3H), 4.13–3.49 (m, 2H), 2.44–1.68 (m, 4H) ppm.[13] ^{13}C NMR: (75 MHz, DMSO-d_6): δ = 164.3, 158.0, 149.2, 147.2, 143.7, 139.2, 128.8, 123.3, 119.5, 119.2, 106.0, 97.8, 61.6, 48.7, 29.1, 25.1 ppm. MS (ESI) *m/z* [M + H^+] calcd for $C_{20}H_{18}N_2O_5$ 367.12 (100%), 368.12 (21.6%), 369.13 (2.2%), found 367.06 (100%), 368.05 (19.5%), 369.05 (1.4%); purity (HPLC) = 98%.

(*S*)-1-(6,7-Dihydroxyquinoline-3-carbonyl)-*N*-phenylpyrrolidine-2-carboxamide (36f): 90 mg, 0.24 mmol, yield: 96%. mp: 116–118 °C. R_f = 0.22 (DCM/MeOH 19:1 + 0.1% TFA). ^{1}H NMR: (300 MHz, DMSO-d_6/TFA): δ = 10.29–9.76 (m, 1H), 9.33–8.26 (m, 2H), 7.84–6.75 (m, 7H), 4.90–4.38 (m, 1H), 3.97–3.43 (m, 2H), 2.31 (s, 1H), 2.11–1.61 (m, 3H) ppm. ^{13}C NMR: (75 MHz, DMSO-d_6/TFA): δ = 171.1, 170.9, 151.5, 145.0, 139.8, 135.6, 129.3, 129.1, 128.0, 127.1, 124.1, 122.8, 120.3, 110.8, 104.7, 102.8, 62.2, 50.9, 30.6, 25.8 ppm. MS (ESI) *m/z* [M + H^+] calcd for $C_{21}H_{19}N_3O_4$ 378.14 (100%), 379.14 (22.7%), 380.14 (2.5%), found 378.24 (100%), 379.22 (24.4%), 380.20 (1.4%); purity (HPLC) = 98%.

(*S*)-1-(4,6-Dihydroxybenzofuran-2-carbonyl)-*N*-phenylpyrrolidine-2-carboxamide (36i): 100 mg, 0.2 mmol, yield: 81%. mp: 80–85C. R_f = 0.11 (DCM/MeOH 19:1 + 0.1% TFA). $[\alpha]_D^{20}$ = –32 (*c* = 5 in MeOH). ^{1}H NMR: (300 MHz, DMSO-d_6): δ = 10.27–10.07 (m, 1H), 7.74–7.23 (m, 5H), 7.19–6.91 (m, 1H), 6.55–5.97 (m, 2H), 5.16–4.59 (m, 1H), 4.04–3.91 (m, 1H), 2.46–1.79 (m, 4H) ppm. ^{13}C NMR: (75 MHz, DMSO-d_6): δ = 170.5, 158.9, 156.9, 152.5, 145.6, 139.2, 128.7, 123.2, 119.5, 119.2, 110.2, 109.3, 98.3, 89.2, 61.6, 49.0, 29.4, 25.5 ppm. MS (ESI) *m/z* [M + Na^+] calcd for $C_{20}H_{18}N_2O_5$ 389.11 (100%), 390.11 (21.6%), 391.12 (2.2%), found 398.09 (100%), 390.09 (21.3%), 391.10 (1.2%); purity (HPLC) = 95%

(*S*)-1-(6,7-Dihydroxy-2-naphthoyl)-*N*-phenylpyrrolidine-2-carboxamide (36m): 90 mg, 0.24 mmol, yield: 96%. mp: 200–202 °C. R_f =

0.50 (DCM/MeOH 19:1 + 0.1% TFA). $[\alpha]_D^{20}$ = –40 (*c* = 5 in MeOH). ^{1}H NMR: (300 MHz, DMSO-d_6): δ = 10.29–9.89 (m, 1H), 8.20–6.95 (m, 11*H*), 3.75–3.53 (m, 2H), 2.38–2.15 (m, 1H), 2.04–1.79 (m, 3H) ppm.^{13}C NMR: (75 MHz, DMSO-d_6): δ = 170.8, 169.0, 148.2, 147.5, 139.3, 129.5 128.8, 127.7, 125.4, 125,1, 123.2, 121.8, 119.3, 110.3, 109.4, 60.9, 50.2, 29.8, 25.2 ppm. MS (ESI) *m/z* [M + H^+] calcd for $C_{22}H_{20}N_2O_4$ 377.14 (100%), 378.15 (23.8%), 379.15 (2.7%), found 377.13 (100%), 378.13 (20.8%), 379.12 (1.4%) and [M−$C_6H_6N^{+\cdot}$] 284.11; purity (HPLC) = 99%

(*S*)-1-(5,6-Dihydroxybenzofuran-2-carbonyl)-*N*-phenylpiperidine-2-carboxamide (36n): 60 mg, 0.16 mmol, yield: 64%. mp: 81–83 °C. R_f = 0.13 (DCM/MeOH 19:1 + 0.1% TFA). $[\alpha]_D^{20}$ = +94 (*c* = 5 in MeOH). ^{1}H NMR: (300 MHz, DMSO-d_6): δ = 9.99 (s, 1H), 9.46 (s, 1H), 9.06 (s, 1H), 7.65–7.54 (m, 2H), 7.32 (t, *J* = 7.6 Hz, 2H), 7.19 (s, 1H), 7.06 (t, *J* = 7.6 Hz, 1H), 6.99 (s, 1H), 6.92 (s, 1H), 5.18–5.09 (m, 1H), 4.41–4.26 (m, 1H), 2.27–2.15 (m, 1H), 1.84–1.64 (m, 3H), 1.58–1.40 (m, 2H), 1.28–1.10 (m, 1H) ppm. ^{13}C NMR: (75 MHz, DMSO-d_6): δ = 169.9, 160.7, 148.8, 146.8, 143.7, 138.9, 128.7, 123.5, 119.7, 118.0, 111.9, 105.8, 97.7, 20.2 ppm. MS (ESI) *m/z* [M + Na^+] calcd for $C_{21}H_{20}N_2O_5$ 403.13 (100%), 404.13 (22.7%), 405.13 (2.5%), found 403.22 (100%), 404.22 (22.1%), 405.20 (1.9%); purity (HPLC) = 97%

4.9. *General procedure for the formation of sulfonamides*

The respective amine educt (1.0 eq.) was dissolved in pyridine and the corresponding sulfonyl chloride (1.0 eq.) was added portion-wise at room temperature. After stirring for 16 h, the solvent was removed, and the residue was purified by silica column chromatography.

(*R*)-*N*-(5,6-Dihydroxybenzo[*d*]thiazol-2-yl)-1-tosylpyrrolidine-2-carboxamide (1b): 86 mg, 0.20 mmol, yield: 71%. mp: 205–209 °C. R_f = 0.25 (CH/EtOAc 1:1). $[\alpha]_D^{20}$ = +113 (*c* = 10 in MeOH). ^{1}H NMR: (300 MHz, MeOD-d_4) δ = 8.69 (d, *J* = 8.1 Hz, 2H), 8.31 (d, *J* = 8.1 Hz, 2H), 8.18–8.03 (m, 2H), 5.37–5.19 (m, 1H), 4.99 (q, *J* = 7.1 Hz, 1H), 4.62–4.41 (m, 1H), 4.32–4.10 (m, 2H), 3.04–2.76 (m, 4H), 2.66–2.44 (m, 1H) ppm. ^{13}C NMR: (75 MHz, MeOD-d_4) δ = 172.5, 147.4, 145.8, 141.5, 134.9, 131.1, 128.9, 123.5, 107.0, 106.7, 63.1, 50.6, 32.0, 25.7, 21.5 ppm. MS (ESI) *m/z* [M + H^+] calcd for $C_{19}H_{19}N_3O_5S_2$ 434.08 (100%), 435.08 (20.5%), 436.07 (9.0%), found 434.07 (100%), 435.03 (24.1%), 436.05 (12.7%); purity (HPLC) = 98%.

(*S*)-*N*-(5,6-Dihydroxybenzo[*d*]thiazol-2-yl)-2-(4-methylphenylsulfonamido)propionamide (8a): 35 mg, 0.09 mmol, yield: 29%. mp: 185–190 °C. R_f = 0.45 (CH/EtOAc 1:1). $[\alpha]_D^{20}$ = –32 (*c* = 5 in MeOH). ^{1}H NMR: (300 MHz, DMSO-d_6) δ = 11.97 (s, 1H), 9.21 (s, 2H), 8.17 (d, *J* = 8.2 Hz, 1H), 7.65 (d, *J* = 8.1 Hz, 2H), 7.27 (d, *J* = 8.1 Hz, 2H), 7.20 (s, 1H), 7.09 (s, 1H), 4.16–3.99 (m, 1H), 2.22 (s, 3H), 1.18 (d, *J* = 7.0 Hz, 3H) ppm. ^{13}C NMR: (75 MHz, DMSO-d_6) δ = 170.4, 158.1, 157.7, 145.6, 143.9, 142.7, 137.8, 129.4, 126.5, 121.9, 106.5, 106.3, 51.6, 20.8, 18.6 ppm. MS (ESI) *m/z* [M + H^+] calcd for $C_{17}H_{17}N_3O_5S_2$ 408.06 (100%), 409.06 (18.4%), 410.06 (9.0%), found 408.07 (100%), 409.06 (22.7%), 410.06 (10.6%); purity (HPLC) = 99%.

(*R*)-*N*-(5,6-Dihydroxybenzo[*d*]thiazol-2-yl)-2-(4-methylphenylsulfonamido)propionamide (8b): 85 mg, 0.21 mmol, yield: 70%. mp: 196–199 °C. R_f = 0.45 (CH/EtOAc 1:1). $[\alpha]_D^{20}$ = +30 (*c* = 5 in MeOH). ^{1}H NMR: (300 MHz, DMSO-d_6) δ = 7.69–7.59 (m, 2H), 7.27 (d, *J* = 8.1 Hz, 2H), 7.20 (s, 1H), 7.08 (s, 1H), 4.07 (q, *J* = 7.0 Hz, 1H), 2.21 (s, 3H), 1.17 (d, *J* = 7.0 Hz, 3H) ppm. ^{13}C NMR: (75 MHz, DMSO-d_6) δ = 172.1, 170.4, 155.0, 145.5, 143.9, 142.7, 141.7, 137.8, 129.4, 126.5, 121.9, 106.4, 106.3, 51.5, 21.1, 18.7 ppm. MS (ESI) *m/z* [M + H^+] calcd for $C_{17}H_{17}N_3O_5S_2$ 408.06 (100%), 409.06 (18.4%), 410.06 (9.0%), found 408.15 (100%), 409.08 (20.6%), 410.14 (10.6%); purity (HPLC) = 99%.

(*S,S*)-*N*-(5,6-Dihydroxybenzo[*d*]thiazol-2-yl)-3-methyl-2-(4-methylphenylsulfonylamido)pentanoicamid (8c): 47 mg, 0.10 mmol, yield: 39%. mp: 253–256 °C. R_f = 0.35 (CH/EtOAc 1:1). $[\alpha]_D^{20}$ = –30 (*c* = 5 in MeOH). ^{1}H NMR: (300 MHz, DMSO-d_6) δ = 11.93 (s, 1H), 9.14 (s, 2H), 8.05 (d, *J* = 9.2 Hz, 1H), 7.62 (d, *J* = 8.2 Hz, 2H), 7.21–7.12 (m, 3H), 7.08 (s, 1H), 3.92–3.72 (m, 1H), 2.07 (s, 3H), 1.73–1.62 (m, 1H), 1.56–1.39 (m, 1H), 1.15–0.97 (m, 1H), 0.83–0.63 (m, 6H) ppm. ^{13}C NMR: (75 MHz, DMSO-d_6) δ = 169.6, 154.7, 145.5, 143.9, 142.5, 141.8, 137.7, 129.2, 126.6, 122.0, 106.5, 106.2, 60.1, 36.7, 24.2, 20.7, 14.9, 10.2 ppm. MS (ESI) *m/z* [M + H^+] calcd for $C_{20}H_{23}N_3O_5S_2$ 450.11 (100%), 451.11 (21.6%), 452.10 (9.0%), found 450.22 (100%), 451.10 (22.7%), 452.17 (12.0%); purity (HPLC) = 96%.

(*S*)-*N*-(5,6-Dihydroxybenzo[*d*]thiazol-2-yl)-3,3-dimethyl-2-(4-methylphenylsulfonamido)butyricamide (8d): 80 mg, 0.18 mmol, yield: 34%. mp: 254–256 °C. R_f = 0.43 (CH/EtOAc 1:1). $[\alpha]_D^{20}$ = –29 (*c* = 10 in MeOH). ^{1}H NMR: (300 MHz, DMSO-d_6) δ = 11.83 (s, 1H), 9.13 (s. 2H), 7.92 (s. 1H), 7.63 (d, *J* = 8.1 Hz, 2H), 7.17 (s, 1H), 7.11 (d, *J* = 8.1 Hz, 2H), 7.07 (s, 1H), 3.80 (s, 1H), 1.95 (s, 3H), 0.89 (s, 9H) ppm. ^{13}C NMR: (75 MHz, DMSO-d_6) δ = 168.4, 165.6, 145.5, 143.8, 142.5, 141.8, 137.4, 129.0, 126.8, 121.9, 106.4, 106.2, 63.6, 34.3, 26.2, 20.6 ppm. MS (ESI) *m/z* [M + H^+] calcd for $C_{20}H_{23}N_3O_5S_2$ 450.11 (100%), 451.11 (21.6%), 452.10 (9.0%), found 450.10 (100%), 451.07 (23.7%), 452.10 (11.5%); purity (HPLC) = 98%.

(*S*)-*N*-(5,6-Dihydroxybenzo[*d*]thiazol-2-yl)-2-(4-methylphenylsulfonamido)-3-phenylpropionamide (8e): 40 mg, 0.09 mmol, yield: 35%. mp: 209–213 °C. R_f = 0.28 (CH/EtOAc 1:1). $[\alpha]_D^{20}$ = +8 (*c* = 5 in MeOH). ^{1}H NMR: (300 MHz, DMSO-d_6) δ = 12.10 (s, 1H), 8.32 (d, *J* = 9.2 Hz, 1H), 7.41 (d, *J* = 8.2 Hz, 2H), 7.23–7.12 (m, 6H), 7.12–7.05 (m, 3H), 4.42–4.20 (m, 1H), 3.02–2.87 (m, 1H), 2.81–2.68 (m, 1H), 2.13 (s, 3H) ppm.^{13}C NMR: (75 MHz, DMSO-d_6) δ = 169.6, 154.9, 145.6, 144.0, 142.4, 141.8, 137.7, 136.5, 129.3, 129.2, 128.1, 126.6, 126.4, 122.0, 106.5, 106.3, 57.4, 38.1, 20.8 ppm. MS (ESI) *m/z* [M + H^+] calcd for $C_{23}H_{21}N_3O_5S_2$ 484.09 (100%), 485.10 (24.9%), 486.09 (9.0%), found 484.22 (100%), 485.10 (26.3%), 486.17 (13.2%); purity (HPLC) = 97%.

(*S*)-3-(Benzylthio)-*N*-(5,6-dihydroxybenzo[*d*]thiazol-2-yl)-2-(4-methylphenylsulfonamido)propionamide (8f): 30 mg, 0.05 mmol, yield: 32%. mp: 137 °C. R_f = 0.26 (CH/EtOAc 1:3). $[\alpha]_D^{20}$ = –96 (*c* = 1 in MeOH). ^{1}H NMR: (300 MHz, DMSO-d_6) δ = 8.39 (d, *J* = 8.4 Hz, 1H), 7.68 (d, *J* = 7.7 Hz, 2H), 7.35–7.18 (m, 5H), 7.13 (dd, *J* = 7.7, 2.1 Hz, 4H), 4.32–4.19 (m, 1H), 4.08–3.92 (m, 1H), 3.68 (s, 2H), 3.19 (s, 1H), 2.44 (s, 3H), 2.17 (s, 1H) ppm. ^{13}C NMR: (75 MHz, DMSO-d_6) δ = 174.2, 168.6, 164.5, 154.7, 153.3, 145.5, 144.6, 144.0, 142.9, 142.7, 137.7, 129.3, 128.8, 128.3, 126.9, 126.6, 126.1, 121.9, 106.8, 106.3, 58.0, 55.2, 34.4, 20.8. ppm. MS (ESI) *m/z* [M + H^+] calcd for $C_{24}H_{23}N_3O_5S_3$ 530.08 (100%), 531.08 (26.0%), 532.08 (9.0%), found 530.08 (100%), 531.08 (29.6%), 532.08 (17.6%); purity (HPLC) = 99%.

Declaration of Competing Interest

The authors declare that they have no known competing financial interests or personal relationships that could have appeared to influence the work reported in this paper.

Acknowledgements

We thank Janina Metzler, Nabil Farooq, and Jan Kwasnicki for their assistance during the syntheses of the inhibitors.

Appendix A. Supplementary material

Supplementary data to this article can be found online at https://doi.org/10.1016/j.bmc.2021.116392.

References

1 Stanaway JD, Shepard DS, Undurraga EA, et al. The Global Burden of Dengue: An Analysis from the Global Burden of Disease Study 2013. *Lancet Infect. Dis.* 2016;16(6):712–723. https://doi.org/10.1016/S1473-3099(16)00026-8.

2 Bhatt S, Gething PW, Brady OJ, et al. The Global Distribution and Burden of Dengue. *Nature.* 2013;496(7446):504–507. https://doi.org/10.1038/nature12060.

3 Coluccia A, Puxeddu M, Nalli M, et al. Discovery of Zika Virus NS2B/NS3 Inhibitors That Prevent Mice from Life-Threatening Infection and Brain Damage. *ACS Med. Chem. Lett.* 2020;11(10):1869–1874. https://doi.org/10.1021/acsmedchemlett.9b00405.

4 Lowe R, Barcellos C, Brasil P, et al. The Zika Virus Epidemic in Brazil: From Discovery to Future Implications. *Int. J. Environ. Res. Public Health.* 2018;15(1):96. https://doi.org/10.3390/ijerph15010096.

5 Kraemer MUG, Reiner RC, Brady OJ, et al. Past and Future Spread of the Arbovirus Vectors Aedes Aegypti and Aedes Albopictus. *Nat. Microbiol.* 2019;4(5):854–863. https://doi.org/10.1038/s41564-019-0376-y.

6 Bonizzoni M, Gasperi G, Chen X, James AA. The Invasive Mosquito Species Aedes Albopictus: Current Knowledge and Future Perspectives. *Trends Parasitol.* 2013;29(9):460–468. https://doi.org/10.1016/j.pt.2013.07.003.

7 Rogers DJ, Suk JE, Semenza JC. Using Global Maps to Predict the Risk of Dengue in Europe. *Acta Trop.* 2014;129(1):1–14. https://doi.org/10.1016/j.actatropica.2013.08.008.

8 Gjenero-Margan, I.; Aleraj, B.; Krajcar, D.; Lesnikar, V.; Klobučar, A.; Pem-Novosel, I.; Kurečić-Filipović, S.; Komparak, S.; Martić, R.; Duričić, S.; Betica-Radić, L.; Okmadžić, J.; Vilibić-Čavlek, T.; Babić-Erceg, A.; Turković, B.; Avšić-Županc, T.; Radić, I.; Ljubić, M.; Šarac, K.; Benić, N.; Mlinarić-Galinović, G. Autochthonous Dengue Fever in Croatia, August- September 2010. Eurosurveillance 2011, 16 (9), 1–4. https://doi.org/10.2807/ese.16.09.19805-en.

9 La Ruche, G.; Souarès, Y.; Armengaud, A.; Peloux-Petiot, F.; Delaunay, P.; Desprès, P.; Lenglet, A.; Jourdain, F.; Leparc-Goffart, I.; Charlet, F.; Ollier, L.; Mantey, K.; Mollet, T.; Fournier, J. P.; Torrents, R.; Leitmeyer, K.; Hilairet, P.; Zeller, H.; Van Bortel, W.; Dejour-Salamanca, D.; Grandadam, M.; Gastellu-Etchegorry, M. First Two Autochthonous Dengue Virus Infections in Metropolitan France, September 2010. Eurosurveillance 2010, 15 (39), 1–5. https://doi.org/10.2807/ese.15.39.19676-en.

10 ECDC (European Centre for Disease Prevention and Control). Dengue Outbreak in Madeira, Portugal, October-November 2012.; 2014. https://doi.org/10.2900/75830.

11 Counotte MJ, Kim CR, Wang J, et al. Sexual Transmission of Zika Virus and Other Flaviviruses: A Living Systematic Review. *PLoS Med.* 2018;15(7):e1002611. https://doi.org/10.1371/journal.pmed.1002611.

12 Mlakar J, Korva M, Tul N, et al. Zika Virus Associated with Microcephaly. *N. Engl. J. Med.* 2016;374(10):951–958. https://doi.org/10.1056/NEJMoa1600651.

13 Cao-Lormeau V, Blake A, Mons S, et al. Guillain-Barré Syndrome Outbreak Caused by ZIKA Virus Infection in French Polynesia. *Lancet*. 2016;387(10027):1531–1539. https://doi.org/10.1016/S0140-6736(16)00562-6.

14 Duffy MR, Chen T-H, Hancock WT, et al. Zika Virus Outbreak on Yap Island, Federated States of Micronesia. *N. Engl. J. Med.* 2009;360(24):2536–2543. https://doi.org/10.1056/NEJMoa0805715.

15 Aubry M, Teissier A, Huart M, et al. Zika Virus Seroprevalence, French Polynesia, 2014–2015 Maite. *Emerg. Infect. Dis.* 2017;23(4):669–672. https://doi.org/10.3201/eid2304.161549.

16 Kirkpatrick, B. D.; Whitehead, S. S.; Pierce, K. K.; Tibery, C. M.; Grier, P. L.; Hynes, N. A.; Larsson, C. J.; Sabundayo, B. P.; Talaat, K. R.; Janiak, A.; Carmolli, M. P.; Luke, C. J.; Diehl, S. A.; Durbin, A. P. The Live Attenuated Dengue Vaccine TV003 Elicits Complete Protection against Dengue in a Human Challenge Model. Sci. Transl. Med. 2016, 8 (330), 1–8. https://doi.org/10.1126/scitranslmed.aaf1517.

17 Yauch LE, Shresta S. Dengue Virus Vaccine Development. *Adv. Virus Res.* 2014;88:315–372. https://doi.org/10.1016/B978-0-12-800098-4.00007-6.

18 Katzelnick LC, Gresh L, Halloran ME, et al. Antibody-Dependent Enhancement of Severe Dengue Disease in Humans. *Science*. 2017;358(6365):929–932. https://doi.org/10.1126/science.aan6836.

19 WHO. Dengue and severe dengue https://www.who.int/news-room/fact-sheets/detail/dengue-and-severe-dengue.

20 Mustafa MS, Rasotgi V, Jain S, Gupta V. Discovery of Fifth Serotype of Dengue Virus (DENV-5): A New Public Health Dilemma in Dengue Control. *Med. J. Armed Forces India*. 2015;71(1):67–70. https://doi.org/10.1016/j.mjafi.2014.09.011.

21 Normile, D. Surprising New Dengue Virus Throws A Spanner in Disease Control Efforts. Science 2013, 342 (6157), 415. https://doi.org/10.1126/science.342.6157.415.

22 Preugschat F, Yao CW, Strauss JH. In Vitro Processing of Dengue Virus Type 2 Nonstructural Proteins NS2A, NS2B, and NS3. *J. Virol.* 1990;64(9):4364–4374. https://doi.org/10.1128/jvi.64.9.4364-4374.1990.

23 Falgout B, Markoff L. Evidence That Flavivirus NS1-NS2A Cleavage Is Mediated by a Membrane-Bound Host Protease in the Endoplasmic Reticulum. *J. Virol.* 1995;69(11):7232–7243. https://doi.org/10.1128/jvi.69.11.7232-7243.1995.

24 Chambers TJ, Hahn CS, Galler R, Rice CM. Flavivirus Genome Organization, Expression and Replication. *Annu. Rev. Microbiol.* 1990;44(1):649–688. https://doi.org/10.1146/annurev.mi.44.100190.003245.

25 Stadler K, Allison SL, Schalich J, Heinz FX. Proteolytic Activation of Tick-Borne Encephalitis Virus by Furin. *J. Virol.* 1997;71(11):8475–8481. https://doi.org/10.1128/jvi.71.11.8475-8481.1997.

26 Yamshchikov VF, Compans RW. Processing of the Intracellular Form of the West Nile Virus Capsid Protein by the Viral NS2B-NS3 Protease: An in Vitro Study. *J. Virol.* 1994;68(9):5765–5771. https://doi.org/10.1128/jvi.68.9.5765-5771.1994.

27 Aguirre S, Maestre AM, Pagni S, et al. DENV Inhibits Type I IFN Production in Infected Cells by Cleaving Human STING. *PLoS Pathog.* 2012;8(10):e1002934. https://doi.org/10.1371/journal.ppat.1002934.

28 Luo D, Vasudevan SG, Lescar J. The Flavivirus NS2B-NS3 Protease-Helicase as a Target for Antiviral Drug Development. *Antiviral Res.* June 2015;2015(118):148–158. https://doi.org/10.1016/j.antiviral.2015.03.014.

29 Nitsche C, Holloway S, Schirmeister T, Klein CD. Biochemistry and Medicinal Chemistry of the Dengue Virus Protease. *Chem. Rev.* 2014;114(22):11348–11381. https://doi.org/10.1021/cr500233q.

30 da Silva Rodrigues, É. E.; Maus, H.; Hammerschmidt, S. J.; Ruggieri, A.; dos Santos, E. C.; Bassi, Ê. J.; Anderson, L.; Aquino, P. G. V.; de Araújo-Júnior, J. X.; Wei, F.; Liu, X.; Zhan, P.; Schirmeister, T.; da Silva-Júnior, E. F. The Medicinal Chemistry of Zika Virus. In Human Viruses: Diseases, Treatments and Vaccines; Ahmad, S. I., Ed.; Springer International Publishing, 2021; pp 233–295. https://doi.org/10.1007/978-3-030-71165-8_13.

31 Silva-Júnior EF, Schirmeister T, Araújo-Júnior JX. Recent Advances in Inhibitors of Flavivirus NS2B-NS3 Protease from Dengue, Zika, and West Nile Viruses. *Vector-Borne Dis. Treat.* 2018;No. November:1–25.

32 Noble CG, Seh CC, Chao AT, Shi PY. Ligand-Bound Structures of the Dengue Virus Protease Reveal the Active Conformation. *J. Virol.* 2012;86(1):438–446. https://doi.org/10.1128/JVI.06225-11.

33 Hill ME, Yildiz M, Hardy JA. Cysteine Disulfide Traps Reveal Distinct Conformational Ensembles in Dengue Virus NS2B-NS3 Protease. *Biochemistry*. 2019;58(6):776–787. https://doi.org/10.1021/acs.biochem.8b00978.

34 Yusof R, Clum S, Wetzel M, Murthy HMK, Padmanabhan R. Purified NS2B/NS3 Serine Protease of Dengue Virus Type 2 Exhibits Cofactor NS2B Dependence for Cleavage of Substrates with Dibasic Amino Acids in Vitro. *J. Biol. Chem.* 2000;275(14):9963–9969. https://doi.org/10.1074/jbc.275.14.9963.

35 Erbel P, Schiering N, D'Arcy A, et al. Structural Basis for the Activation of Flaviviral NS3 Proteases from Dengue and West Nile Virus. *Nat. Struct. Mol. Biol.* 2006;13(4):372–373. https://doi.org/10.1038/nsmb1073.

36 Lei J, Hansen G, Nitsche C, Klein CD, Zhang L, Hilgenfeld R. Crystal Structure of Zika Virus Ns2b-Ns3 Protease in Complex with a Boronate Inhibitor. *Science*. 2016;353(6298):503–505. https://doi.org/10.1126/science.aag2419.

37 Millies B, von Hammerstein F, Gellert A, et al. Proline-Based Allosteric Inhibitors of Zika and Dengue Virus NS2B/NS3 Proteases. *J. Med. Chem.* 2019;62(24):11359–11382. https://doi.org/10.1021/acs.jmedchem.9b01697.

38 Yildiz M, Ghosh S, Bell JA, Sherman W, Hardy JA. Allosteric Inhibition of the NS2B-NS3 Protease from Dengue Virus. *ACS Chem. Biol.* 2013;8(12):2744–2752. https://doi.org/10.1021/cb400612h.

39 Nitsche C, Zhang L, Weigel LF, et al. Peptide-Boronic Acid Inhibitors of Flaviviral Proteases: Medicinal Chemistry and Structural Biology. *J. Med. Chem.* 2017;60(1):511–516. https://doi.org/10.1021/acs.jmedchem.6b01021.

40 Lee H, Ren J, Nocadello S, et al. Identification of Novel Small Molecule Inhibitors against NS2B/NS3 Serine Protease from Zika Virus. *Antiviral Res.* 2017;139:49–58. https://doi.org/10.1016/j.antiviral.2016.12.016.

41 Behnam MAM, Graf D, Bartenschlager R, Zlotos DP, Klein CD. Discovery of Nanomolar Dengue and West Nile Virus Protease Inhibitors Containing a 4-Benzyloxyphenylglycine Residue. *J. Med. Chem.* 2015;58(23):9354–9370. https://doi.org/10.1021/acs.jmedchem.5b01441.

42 Gruba N, Rodriguez Martinez JI, Grzywa R, et al. Substrate Profiling of Zika Virus NS2B-NS3 Protease. *FEBS Lett.* 2016;590(20):3459–3468. https://doi.org/10.1002/1873-3468.12443.

43 Kühl N, Graf D, Bock J, Behnam MAM, Leuthold M-M, Klein CD. A New Class of Dengue and West Nile Virus Protease Inhibitors with Submicromolar Activity in Reporter Gene DENV-2 Protease and Viral Replication Assays. *J. Med. Chem.* 2020;63(15):8179–8197. https://doi.org/10.1021/acs.jmedchem.0c00413.

44 Kühl N, Leuthold MM, Behnam MAM, Klein CD. Beyond Basicity: Discovery of Nonbasic DENV-2 Protease Inhibitors with Potent Activity in Cell Culture. *J. Med. Chem.* 2021;64(8):4567–4587. https://doi.org/10.1021/acs.jmedchem.0c02042.

45 Chen X, Yang K, Wu C, et al. Mechanisms of Activation and Inhibition of Zika Virus NS2B-NS3 Protease. *Cell Res.* 2016;26(11):1260–1263. https://doi.org/10.1038/cr.2016.116.

46 Wu H, Bock S, Snitko M, et al. Novel Dengue Virus NS2B/NS3 Protease Inhibitors. *Antimicrob. Agents Chemother.* 2015;59(2):1100–1109. https://doi.org/10.1128/AAC.03543-14.

47 Abd-Allah WH, Aboutabl ME, Aboul-Enein MN, El-Azzouny AAS. Synthesis, Molecular Modeling Studies and Anticonvulsant Activity of Certain (1-(Benzyl (Aryl) Amino) Cyclohexyl) Methyl Esters. *Bioorg. Chem.* April 2017;2017(71):135–145. https://doi.org/10.1016/j.bioorg.2017.01.021.

48 Sandeep, Venugopalan P, Kumar A. Metal Free, Direct and Selective Deoxygenation of α-Hydroxy Carbonyl Compounds: Access to α, α-Diaryl Carbonyl Compounds. *European. J. Org. Chem.* 2020;2020(17):2530–2536. https://doi.org/10.1002/ejoc.202000142.

49 Moore DL, Denton AE, Kohinke RM, Craig BR, Brenzovich WE. Silica Sulfuric Acid as a Highly Efficient Catalyst for the Synthesis of Diarylacetic Acids. *Synth. Commun.* 2016;46(7):604–612. https://doi.org/10.1080/00397911.2016.1158269.

50 Gbilimou A, Darmanin T, Godeau G, Guittard F. A Templateless Electropolymerization Approach to Nanorings Using Substituted 3,4-Naphthalenedioxythiophene (NaPhDOT) Monomers. *ChemNanoMat.* 2018;4(1):140–147. https://doi.org/10.1002/cnma.201700269.

51 Göksu S, Kazaz C, Sütbeyaz Y, Seçen H. A Concise Synthesis of 2-Amino-1,2,3,4-Tetrahydronaphthalene-6,7-Diol ('6,7-ADTN') from Naphthalene-2,3-Diol. *Helv. Chim. Acta*. 2003;86(10):3310–3313. https://doi.org/10.1002/hlca.200390272.

52 Zhao S, Zhao L, Zhang X, et al. Design, Synthesis, and Structure-Activity Relationship Studies of Benzothiazole Derivatives as Antifungal Agents. *Eur. J. Med. Chem.* 2016;123:514–522. https://doi.org/10.1016/j.ejmech.2016.07.067.

53 Boger, D. L. CBI Analogues of the Duocarmycins and CC-1065. US 2005/0026987 A1, 2003.

54 Wang S, Jia K, Cheng J, Chen Y, Yuan Y. Dual Roles of Substituted Thiourea as Reductant and Ligand in CuAAC Reaction. *Tetrahedron Lett.* 2017;58(38):3717–3721. https://doi.org/10.1016/j.tetlet.2017.08.029.

55 Jakkaraj SR, Young VG, Georg GI. Syntheses of PDE3A Inhibitor ORG9935 and Determination of the Absolute Stereochemistries of Its Enantiomers by X-Ray

Crystallography. *Tetrahedron*. 2018;74(22):2769–2774. https://doi.org/10.1016/j.tet.2018.04.045.
56 Laplace DR, Verbraeken B, Van Hecke K, Winne JM. Total Synthesis of (+/-)-Frondosin B and (+/-)-5-Epi-Liphagal by Using a Concise (4+3) Cycloaddition Approach. *Chem. - A Eur. J.* 2014;20(1):253–262. https://doi.org/10.1002/chem.201303273.
57 Tew, D. G.; Thompson, S. K.; Veber, D. F. WO20/17924 A1, 2002.
58 Santangelo F, Casagrande C, Miragoli G, Vecchietti V. Synthesis and Positive Inotropic Effect of 1-Alkyl- and 1-Acyl-6,7-Dimethoxy-3-Dimethylamino-1,2,3,4-Tetrahydroquinolines. *Eur. J. Med. Chem.* 1994;29(11):877–882. https://doi.org/10.1016/0223-5234(94)90110-4.
59 Gavara L, Boisse T, Hénichart JP, Daïch A, Rigo B, Gautret P. Toward New Camptothecins. Part 6: Synthesis of Crucial Ketones and Their Use in Friedländer Reaction. *Tetrahedron*. 2010;66(38):7544–7561. https://doi.org/10.1016/j.tet.2010.07.048.
60 Gryko D, Lipiński R. Asymmetric Direct Aldol Reaction Catalysed by L-Prolinethioamides. *European J. Org. Chem.* 2006;2006(17):3864–3876. https://doi.org/10.1002/ejoc.200600219.
61 von Hammerstein F, Lauth LM, Hammerschmidt S, Wagner A, Schirmeister T, Hellmich UA. Cis Autocatalytic Cleavage of Glycine-Linked Zika Virus NS2B-NS3 Protease Constructs. *FEBS Lett.* 2019;593(16):2204–2213. https://doi.org/10.1002/1873-3468.13507.
62 Steuer C, Heinonen KH, Kattner L, Klein CD. Optimization of Assay Conditions for Dengue Virus Protease: Effect of Various Polyols and Nonionic Detergents. *J. Biomol. Screen.* 2009;14(9):1102–1108. https://doi.org/10.1177/1087057109344115.
63 Maier GP, Bernt CM, Butler A. Catechol Oxidation: Considerations in the Design of Wet Adhesive Materials. *Biomater. Sci.* 2018;6(2):332–339. https://doi.org/10.1039/c7bm00884h.
64 Brecher M, Li Z, Liu B, et al. A Conformational Switch High-Throughput Screening Assay and Allosteric Inhibition of the Flavivirus NS2B-NS3 Protease. *PLoS Pathog.* 2017;13(5):e1006411. https://doi.org/10.1371/journal.ppat.1006411.
65 Othman R, Kiat TS, Khalid N, et al. Docking of Noncompetitive Inhibitors into Dengue Virus Type 2 Protease: Understanding the Interactions with Allosteric Binding Sites. *J. Chem. Inf. Model.* 2008;48(8):1582–1591. https://doi.org/10.1021/ci700388k.
66 BioSolveIT GmbH. LeadIT Version 2.3.2; BioSolveIT GmbH, Sankt Augustin, Germany, 2017, Www.Biosolveit.de/LeadIT. BioSolveIT GmbH: Sankt Augustin, Germany.
67 Zimmermann MO, Lange A, Zahn S, Exner TE, Boeckler FM. Using Surface Scans for the Evaluation of Halogen Bonds toward the Side Chains of Aspartate, Asparagine, Glutamate, and Glutamine. *J. Chem. Inf. Model.* 2016;56(7):1373–1383. https://doi.org/10.1021/acs.jcim.6b00075.
68 Kumar A, Buhler S, Selisko B, et al. Nuclear Localization of Dengue Virus Nonstructural Protein 5 Does Not Strictly Correlate with Efficient Viral RNA Replication and Inhibition of Type I Interferon Signaling. *J. Virol.* 2013;87(8):4545–4557. https://doi.org/10.1128/JVI.03083-12.
69 Münster M, Płaszczyca A, Cortese M, et al. A Reverse Genetics System for Zika Virus Based on a Simple Molecular Cloning Strategy. *Viruses*. 2018;10(7):368. https://doi.org/10.3390/v10070368.
70 Cortese M, Goellner S, Acosta EG, et al. Ultrastructural Characterization of Zika Virus Replication Factories. *Cell Rep.* 2017;18(9):2113–2123. https://doi.org/10.1016/j.celrep.2017.02.014.
71 Johansson M, Brooks AJ, Jans DA, Vasudevan SG. A Small Region of the Dengue Virus-Encoded RNA-Dependent RNA Polymerase, NS5, Confers Interaction with Both the Nuclear Transport Receptor Importin-β and the Viral Helicase, NS3. *J. Gen. Virol.* 2001;82(4):735–745. https://doi.org/10.1099/0022-1317-82-4-735.
72 Baronti C, Piorkowski G, Charrel RN, Boubis L, Leparc-Goffart I, de Lamballerie X. Complete Coding Sequence of Zika Virus from a French Polynesia Outbreak in 2013. *Genome Announc.* 2014;2(3):e00500–e514. https://doi.org/10.1128/genomeA.00500-14.
73 Rarey M, Kramer B, Lengauer T. Multiple Automatic Base Selection: Protein-Ligand Docking Based on Incremental Construction without Manual Intervention. *J. Comput. Aided. Mol. Des.* 1997;11(4):369–384. https://doi.org/10.1023/A:1007913026166.
74 Halgren TA. Merck Molecular Force Field. I. Basis, Form, Scope, Parameterization, and Performance of MMFF94*. *J. Comput. Chem.* 1996;17(5–6):490–519. https://doi.org/10.1002/(SICI)1096-987X(199604)17:5/6<490::AID-JCC1>3.0.CO;2-P.
75 Leatherbarrow RJ. *GraFit 6*. Erithacus Software Limited: East Grinstead, West Sussex, UK; 2007.
76 Ludewig S, Kossner M, Schiller M, Baumann K, Schirmeister T. Enzyme Kinetics and Hit Validation in Fluorimetric Protease Assays. *Curr. Top. Med. Chem.* 2010;10(3):368–382. https://doi.org/10.2174/156802610790725498.
77 Klein P, Barthels F, Johe P, et al. Naphthoquinones as Covalent Reversible Inhibitors of Cysteine Proteases—Studies on Inhibition Mechanism and Kinetics. *Molecules*. 2020;25(9):2064. https://doi.org/10.3390/molecules25092064.
78 Amendola G, Ettari R, Previti S, et al. Lead Discovery of SARS-CoV-2 Main Protease Inhibitors through Covalent Docking-Based Virtual Screening. *J. Chem. Inf. Model.* 2021;61(4):2062–2073. https://doi.org/10.1021/acs.jcim.1c00184.
79 Angelini A, Cendron L, Chen S, et al. Bicyclic Peptide Inhibitor Reveals Large Contact Interface with a Protease Target. *ACS Chem. Biol.* 2012;7(5):817–821. https://doi.org/10.1021/cb200478t.
80 Barthels F, Marincola G, Marciniak T, et al. Asymmetric Disulfanylbenzamides as Irreversible and Selective Inhibitors of Staphylococcus Aureus Sortase A. *ChemMedChem*. 2020;15(10):839–850. https://doi.org/10.1002/cmdc.201900687.
81 Poreba M, Szalek A, Rut W, et al. Highly Sensitive and Adaptable Fluorescence-Quenched Pair Discloses the Substrate Specificity Profiles in Diverse Protease Families. *Sci. Rep.* 2017;7(1). https://doi.org/10.1038/srep43135.
82 van den Hoff, M. J. B.; Christoffels, V. M.; Labruyère, W. T.; Moorman, A. F. M.; Lamers, W. H. Electrotransfection with "Intracellular" Buffer. In Animal Cell Electroporation and Electrofusion Protocols; Nickoloff, J. A., Ed.; Humana Press, 1995; Vol. 48, pp 185–197. https://doi.org/10.1385/0-89603-304-X:185.
83 GraphPad Prism 7.0.4 for Windows. GraphPad Software: San Diego, California USA.
84 Trapani G, Franco M, Latrofa A, Reho A, Liso G. Synthesis, in Vitro and in Vivo Cytotoxicity, and Prediction of the Intestinal Absorption of Substituted 2-Ethoxycarbonyl-Imidazo[2,1-b]Benzothiazoles. *Eur. J. Pharm. Sci.* 2001;14(3):209–216. https://doi.org/10.1016/S0928-0987(01)00173-7.
85 Maolanon AR, Risgaard R, Wang S-Y, et al. Subtype-Specific Agonists for NMDA Receptor Glycine Binding Sites. *ACS Chem. Neurosci.* 2017;8(8):1681–1687. https://doi.org/10.1021/acschemneuro.7b00117.
86 Götz C, Hinze A, Gellert A, et al. Conformational dynamics of the Dengue virus protease revealed by fluorescence correlation and single-molecule FRET studies. *J. Phys. Chem. Part B*. 2021;125:6837–6846. https://doi.org/10.1021/acs.jpcb.1c01797.